uOttawa

L'Université canadienne
Canada's university

FACULTÉ DES ÉTUDES SUPÉRIEURES ET POSTOCTORALES

uOttawa

L'Université canadienne
Canada's university

FACULTY OF GRADUATE AND POSDOCTORAL STUDIES

Tuncer Baykas

AUTEUR DE LA THÈSE / AUTHOR OF THESIS

Ph.D. (Electrical Engineering)

GRADE / DEGREE

School of Information Technology and Engineering

FACULTÉ, ÉCOLE, DÉPARTEMENT / FACULTY, SCHOOL, DEPARTMENT

Discrete-Time RAKE Receivers with Applications

TITRE DE LA THÈSE / TITLE OF THESIS

Abbas Yongacoglu

DIRECTEUR (DIRECTRICE) DE LA THÈSE / THESIS SUPERVISOR

CO-DIRECTEUR (CO-DIRECTRICE) DE LA THÈSE / THESIS CO-SUPERVISOR

EXAMINATEURS (EXAMINATRICES) DE LA THÈSE / THESIS EXAMINERS

Jean-Yves Chouinard

Kemal Tepe

Claude D'Amours

Roshdy Hafez

Gary W. Slater

Le Doyen de la Faculté des études supérieures et postdoctorales / Dean of the Faculty of Graduate and Postdoctoral Studies

Discrete-Time RAKE Receivers with Applications

by

Tuncer Baykas

Thesis submitted to the
Faculty of Graduate and Postdoctoral Studies
In partial fulfillment of the requirements
For the Ph.D. degree in
Electrical and Computer Engineering

School of Information Technology and Engineering
Faculty of Engineering
University of Ottawa

Your file Votre référence
ISBN: 978-0-494-41603-7
Our file Notre référence
ISBN: 978-0-494-41603-7

Abstract

Wireless channels are often multipath channels. In a multipath channel, a path can be defined as a copy of the transmitted signal arriving at the receiver with a particular delay and amplitude. If the multipaths are resolvable, RAKE receivers can collect the energy of distinct paths. DS-CDMA systems, with their low auto-correlation spreading sequences, enable resolving of the multipaths and therefore the use of RAKE reception. Each RAKE finger, the elementary receiver in RAKE reception, is associated with one of the strongest incoming paths. The outputs of those fingers are combined together to detect the transmitted symbols. The conventional RAKE receivers have several weaknesses. This thesis focuses on the major weaknesses of sensitivity to interference and channel estimation error. It introduces a receiver model to cope with both of them for both single and multi antenna (MIMO) systems. We propose a new RAKE reception method, which is called the generalized decorrelating RAKE receiver (GD-RAKE). GD-RAKE is obtained by the combination of two advanced RAKE receivers: the decorrelating discrete time RAKE receiver (D-DTR) and the generalized RAKE receiver (G-RAKE). The method enables robust performance in the presence of channel estimation errors and colored noise plus interference with the help of statistics on the channel, noise and interference. Additionally the performance of the new receiver is tested in MIMO channels.

Soon to be commercialized ultra wideband (UWB) systems use more than 500 MHz bandwidth. Such a high bandwidth results in many resolvable multipaths and as such the employment of RAKE receivers is very suitable. We tested the performance of a G-RAKE receiver with decision feedback equalizers and showed that it can be used to improve overall performance of the system.

Acknowledgements

I would like to express my gratitude for many kindnesses I have received in the preparation and completion of this thesis. First of all many thanks to my supervisor Dr. Abbas Yongaçoğlu for believing in me and giving me the opportunity to work with him and our trips to many countries, to be an outstanding advisor and mentor. I am grateful to Dr. Mohamed Siala, the unofficial co-supervisor of this thesis, for his help, advice and our long fruitful conversations. I should also mention Dr. Halim Yanıkömeroğlu. I have learned a great deal from him for past 6 years. I am deeply indebted to my committee members, Dr. Claude D'Amours, Dr. Kemal Tepe, Dr. Roshdy Hafez, Dr. Jean-Yves Chouinard, for their time and effort in reviewing this work and their valuable suggestions throughout the research.

4 yıl, 4 ay, 4 gün önce başlayan felsefe doktoru ünvanına yolculuğumun son kilometre taşında bugüne kadar bana emeği geçmiş herkese şükranlarımı sunmak istiyorum. Kızarkadaşım Ebru'ya bana benden cok inandığı, bana verdiği sonsuz destek için minnetarım. Her olmayacak dediğim de, meleğim nasıl yaptıysa beni ikna etti ve tezi bitirtti. Ottawa ki yoldaşım İstemi'ye diyorum ki ölümüne kankayız ve gün gelecek seni winning eleven 25'te yeneceğim. Çiğdem ve Murat, geç oldu belki kaynaşmamız ama iyi ki oldu. Buralardan gidersem karşılıksız dostluğunuzu çok özleyeceğim. Emre, Serra, Işıl, Cevat, Frederic, Nava, Ali, Serdar, Çağrı hepinize tekrar çok teşekkürler. Türkiye'den sırdaşım, dostum ve aslan kardeşim Turgut bir gün bile beni yalnız bırakmadı. Tarık ve Faruk Paşalar internetten, sahibü's-seyf ve'l kalem ve'l kelam Sedat Paşamsa buralara kadar gelerek yaşam tecrübelerini benimle paylaştı. Bir de canım anneannemin, Bursa'dan yukarıyla kurduğu bağlantı sayesinde, her şey çok kolay oldu. :)

Bu tezi canımdan çok sevdiğim anneme ve babama, bizim iyi yetişmemiz iyi insanlar olmamız için verdikleri çabalara ufak bir şükran ifadesi olarak ithaf ediyorum.

Contents

List of Tables

List of Figures

Nomenclature

First appeared on page:

*	Complex conjugate,	9
^{H}	Hermitian transpose,	12
$\hat{}$	denotes that the value is estimated in general,	23
$a_{i,j}$	The (i,j)th element of $\mathbf{A}$,	37
$a_{k,i}$	For UMTS downlink part, spreading waveform of kth users ith symbol,	61
$a_{k,i}(\tau)$	Spreading waveform of the ith user's kth symbol,	9
$b_{i,j}$	The (i,j)th element of $\mathbf{B}$,	36
$c_{k,i,n}$	For UMTS downlink part, nth chip of the $a_{k,i}$,	61
$C_{k,i}$	For UMTS downlink part, crosscorrelation function between complex spreading sequences of $a_{k,i}(t)$ and $a_{0,0}(t)$,	62
d_0	Reference delay of a discrete system,	22
d_l	Delay applied to the lth RAKE finger,	11
$\mathbf{e}$	Vector of the channel estimation errors,	23

List of Abbreviations

First appeared on page:

GD-RAKE: Generalized Decorrelating RAKE Receiver, ... ii

ISI: Inter-Symbol Interference, ... 9

JD-GRAKE: Jointly Decoding Generalized Rake Receiver, ... 3

KLT: Karhunen-Loeve Transform, ... 3

LOS: Line of Sight, ... 94

MAP: Maximum a Posteriori, ... 2

MIMO: Multi Input Multi Output, ... ii

MMSE-GRAKE: Minimum Mean Square Error Generalized Rake Receiver, ... 3

MMSE: Minimum Mean Square Error, ... 15

NLOS: No Line of Sight, ... 94

QPSK: Quadrature Phase Shift Keying, ... 12

rms: root mean square, ... 42

UMTS WCDMA: Universal Mobile Telecommunications System Wideband CDMA, 3

UWB: Ultra Wideband, ... ii

WPAN: Wireless Personal Area Network, ... 91

Chapter 1

Introduction

Wireless communication is now a part of our daily life with our cellular phones and wireless Internet connections. One wireless communication technique, namely the spread spectrum, is quite popular, because of its compelling advantages. For example, it is robust against interference and it enables spectrum sharing among multiple users without any time or frequency division multiplexing. Among the spread spectrum systems, the DS-CDMA uses RAKE receivers to collect energy from the multipath wireless channels. In a multipath channel, reception of multiple, possibly interfering copies of the same signal is observed. A conventional RAKE receiver is a combination of elementary receivers called RAKE fingers. Each finger is associated with one path of the multipath signal. The outputs of the RAKE fingers are combined to detect the transmitted symbols.

The conventional RAKE receivers have several drawbacks. For example, conventional RAKE receivers assume that the interference is uncorrelated and correlated (colored) interference could be a major source of degradation in system performance. Bottomley *et al.* proposed a generalized RAKE receiver in order to have correlated interference suppression [2]. The weakness of the G-RAKE is the nonrealistic assumption of having

a perfect channel state information at the receiver.

For the conventional RAKE receiver another drawback arises from the time-varying nature of the wireless channels. Conventional RAKE receivers use an acquisition system (or searcher) to detect new paths with significant power, and a tracking system to follow the continuously time-varying delays of the paths [3, 4]. The acquisition and tracking systems have two main weaknesses. First, the assumption that the multipaths are resolvable is often unrealistic [4]. Secondly, the acquisition and tracking systems can neither distinguish nor follow paths separated by less then a chip period [5, 6]. To eliminate the need for complex acquisition and tracking devices and to avoid their drawbacks, the conventional discrete-time RAKE receiver (C-DTR) has been proposed in [7]. It is obtained by sampling a transmit filtered version of the channel impulse response. The main drawback of the C-DTR is its sensitivity to channel estimation errors. Furthermore, some paths taken into consideration are mainly due to noise, and they reduce the overall performance of the C-DTR. To cope with these weaknesses of the C-DTR, several intuitive methods have been presented in [7]. Whereas the derivation of an optimum structure of the discrete-time RAKE receiver, complying with the maximum a posteriori (MAP) criterion, has been made in [4]. This optimum structure, referred to as the decorrelating discrete-time RAKE (D-DTR), exploits the covariance matrix of the channel values at RAKE fingers to obtain robustness against channel estimation errors. The D-DTR is designed with the assumption that both thermal noise samples and the interference samples are uncorrelated. As mentioned above, this assumption is invalid for many cases.

The system we are proposing, the generalized decorrelating RAKE (GD-RAKE), combines the complementary advantages of the G-RAKE and the D-DTR. It could suppress the interference, and it takes into consideration the channel estimation errors. In this work, we simulate the discrete-time versions of the G-RAKE and the GD-RAKE and

therefore we use the abbreviations G-DTR (Generalized Discrete-Time RAKE) and GD-DTR (Generalized Decorrelating Discrete-Time RAKE).

For the optimum performance of the GD-RAKE, we require the eigenvalues and eigenvectors of the covariances matrices of the channel and noise plus interference. Usually those matrices are estimated and then the eigenvalues and eigenvectors are obtained by Karhunen-Loeve Transform (KLT). KLT increases the system complexity, especially when the number of fingers is high. In this work, we evaluate through simulations the effect of the estimation errors of those matrices. Furthermore we implement a method, which estimates the eigenvalues and eigenvectors directly from data to reduce the overall complexity of the system.

The performance simulations of the receivers are done in a system loosely based on the uplink of UMTS WCDMA (Universal mobile telecommunications system Wideband CDMA), one of the 3G wireless communication systems. Our simulation results show that the GD-RAKE and the D-DTR improve the performance compared to the conventional RAKE receiver, whereas the G-RAKE can cause performance degradations under certain conditions.

Another area we are considering is multi input multi output (MIMO) systems. As a generalization of the G-RAKE principle to MIMO systems, Grant *et al.* have proposed two methods in [8], namely the JD-GRAKE and the MMSE-GRAKE . The JD-GRAKE jointly decodes the symbols spread by the same spreading code and transmitted from different antennas. The MMSE-GRAKE is an alternative system which is less complex than the JD-GRAKE. Instead of being jointly decoded, the symbols in the MMSE-GRAKE are decoded one by one, by treating the rest of the symbols as interference. Such a decoding decreases the complexity at the price of a decrease in performance. In this work we are proposing a MIMO D-DTR receiver. We also propose a MIMO GD-RAKE receiver, which is based on the combination of the discrete-time version of

the JD-RAKE receiver and MIMO D-DTR.

The G-RAKE receiver can be used in other communication systems as well. In our thesis, we selected ultrawideband (UWB) systems to test the performance of G-RAKE. UWB systems are originated from impulse radio systems and a high number of multipaths is observed in their associated channels. During the standardization process of ultrawideband systems for wireless personal area networks, one of the standard proposals for UWB was DS-UWB. Due to its use of DS-CDMA with short spreading codes at the transmission and the multipaths in the channel, interference has a major effect in its performance. Therefore we believe using G-RAKE system could improve the system performance.

1.1 Contributions

The main contribution of the thesis is the introduction of the GD-DTR receiver. Furthermore we did detailed simulations of the D-DTR, G-DTR and GD-DTR systems in diffuse multipath channels for both single and multi antenna systems. Our simulations show that the G-DTR receiver may degrade the system performance, whereas the GD-DTR improves it. Another contribution of the thesis is the study of the estimation methods of the covariance matrices of the channel and noise plus interference. We introduced a method which does not require KLT transform. We also studied the performance of G-RAKE system in UWB channels.

1.2 Outline

The outline of the thesis is as follows. Chapter 2 treats the properties of the basic multipath channel and different types of multipath channels and the theory behind the conventional RAKE receiver, the C-DTR, the D-DTR and the G-RAKE.

In **Chapter 3** the GD-RAKE is introduced for multipath channels with channel estimation errors and colored noise.

The performance of the receivers we introduced heavily depend on the estimation of channel statistics and noise statistics. In **Chapter 4** we study the methods to estimate and update those statistics.

Chapter 5 provides performance results of the RAKE receivers in different simulation scenarios with perfect and estimated statistics.

Chapter 6 covers the study of RAKE reception methods in MIMO systems, as well as includes the performances of the introduced systems.

Chapter 7, the final chapter of the thesis, is devoted to a summary of the results and future work.

Appendix A studies the UWB systems and the performance of G-RAKE in those systems.

Chapter 2

Multipath Wireless Channels and RAKE Reception Methods

2.1 Multipath Wireless Channels

In a communication system, channel is the medium that is used to transfer the information [9]. The characteristics of a channel could limit the performance of the system and most of the time they cannot be changed by the system designer. This statement is also valid for the wireless communication systems. Another definition of communication channel is, that it provides the connection between transmitters and receivers. Therefore not only free space or atmosphere between mobile users and base stations but every object that affects communication signals is a part of the channel. Examples of these objects are mountains, large buildings, homes and cars as seen in Figure 2.1, where we illustrated a wireless communication system, with base stations and mobile users.

In terms of their effect to the signals, the objects encountered can be divided into two groups as deflectors and scatterers. The deflectors are large far away objects from the

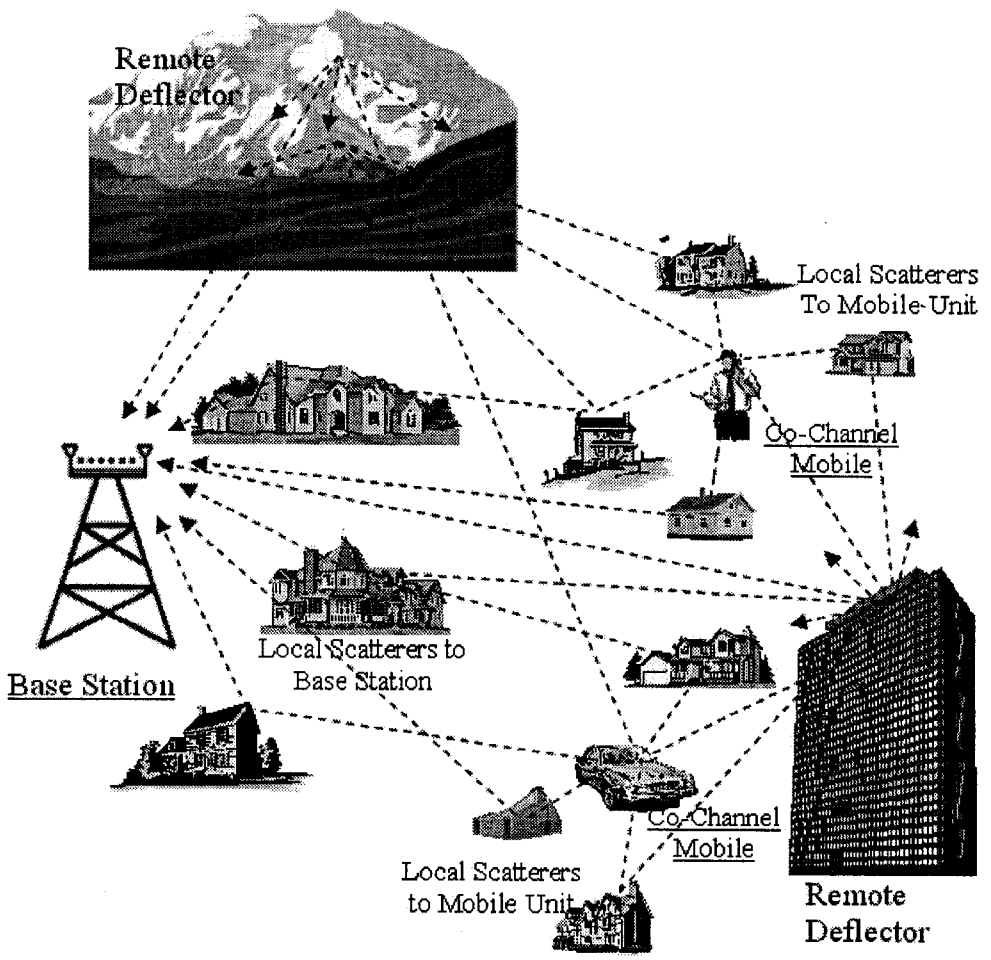

Figure 2.1: Time varying multipath fading channel for cellular wireless systems.

base stations and mobile units like mountains or skyscrapers, which reflect the signals like a mirror. Due to these reflections, the signals follow different paths to reach the antennas of receivers and in the literature every reflection is called a path or a multipath. Large differences in the arrival time of these multipaths cause the observation of specular multipath channel. In cellular wireless systems, the same frequency band can be used by different pairs of transceivers (channel reuse). The interference between these pairs is known as co-channel interference. Deflectors could increase this type of

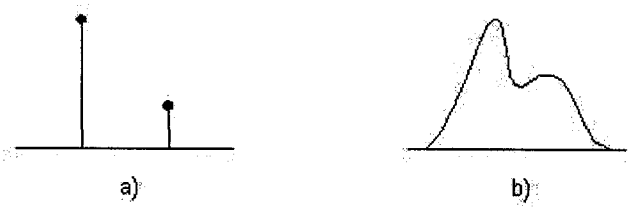

Figure 2.2: The impulse response of two path multipath channel model with specular paths (a), and the diffuse version of the channel due to scatterers (b).

interference as well, since the reflected signals could reach other antennas beside the aimed ones.

The scatterers, the second group of objects, are objects nearby of the antennas, which are relatively small such as houses or vehicles. They scatter the signal with different amplitudes and phases. Due to the short distance between the scatterers and antennas, the difference between the arrival time of the multipaths is small. Therefore the multipaths cannot be separated by the receiver and a diffuse channel is observed. In Figure 2.2 we present the impulse response of a specular multipath channel with two paths and its diffuse version due to scatterers.

For the specular channel, it is easy to locate the positions of the paths in time, but for the diffuse channel we observe a continuous impulse response and distinguishing any path is hard.

The effect of motion is also important in wireless channels. The relative motion between a base station and mobile antennas such as the motion of a user or the motion of scatterers changes the channel coefficients in time. Therefore the receivers use pilot symbols or other methods to update the channel estimates.

For the time being, we disregard the time varying nature of the channel and concentrate only on a specific time instant. Assume we have a specular channel at that time instant

with path delays τ_j and the complex path gain coefficients h_j, the impulse response of the channel can be written as

$$h(\tau) = \sum_{j=0}^{J-1} h_j \delta(\tau - \tau_j). \tag{2.1}$$

In (2.1), J and $\delta(\tau)$ denote the number of paths and the dirac delta function respectively. We have summarized the properties of the multipath channels and presented a channel impulse response. In the next section, we will explain, how a RAKE receiver collects energy from multipath channels.

2.2 Conventional RAKE receiver

DS-CDMA systems use RAKE receivers to collect energy from the multipath wireless channels. Hence, we choose a basic equivalent baseband DS-CDMA system model with RAKE reception, as shown in Figure 2.3.

In DS-CDMA, the spread spectrum is obtained by multiplying the symbol with a spreading sequence waveform. In our model the unit energy symbol $s_{k,i}$ is spread by the waveform $a_{k,i}(t)$. We assume that $a_{k,i}(t)$ has perfect correlation properties, i.e,

$$R_a(t) = \int_{-\infty}^{\infty} a_{k,i}(t+\tau) a_{k,i}^*(t) dt = \begin{cases} 1 & \text{if } \tau = 0 \\ 0 & \text{if } \tau \neq 0 \end{cases}. \tag{2.2}$$

If $a_{k,i}(t)$ is selected properly, this is a reasonable assumption and used by many researchers for example in [3],[7] and [10]. It allows the inter-symbol interference (ISI) to be neglected with respect to multiple access interference and thermal noise. We will later relax this assumption and consider spreading waveforms without perfect correlation in Chapter 6. After the spreading, the signal is transmitted through a multipath

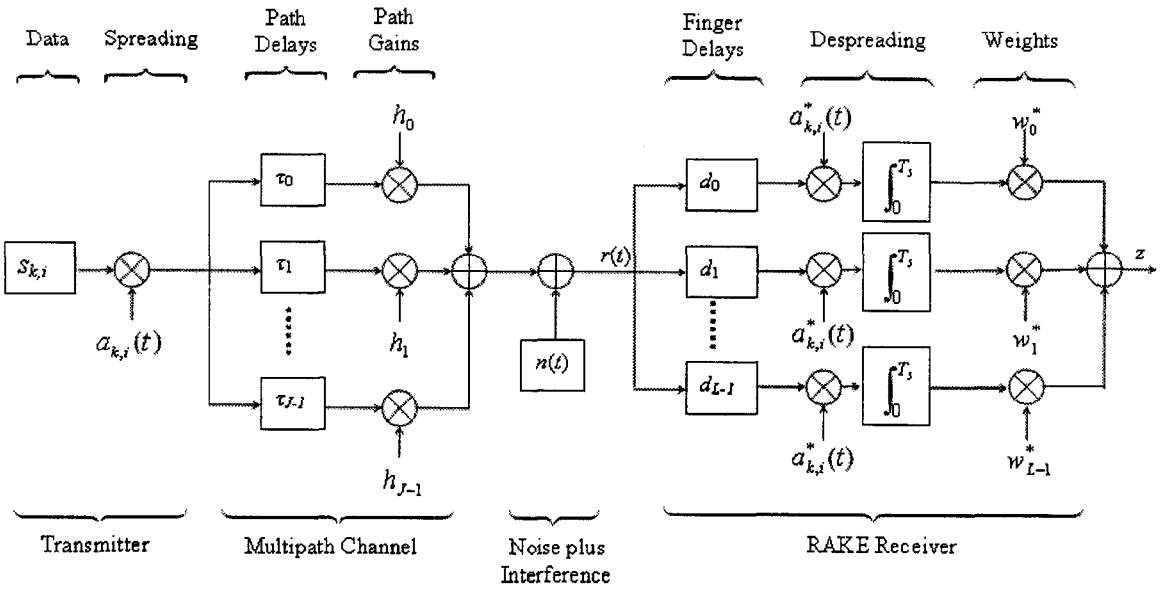

Figure 2.3: System model with RAKE reception.

channel. We assume that the channel is specular and has the impulse response given in (2.1). In Figure 2.3 we show each path separately. The signal is received after being corrupted by noise and interference. At the front end of the RAKE receiver, we have the signal $r(t)$

$$r(t) = h(t) \otimes (s_{k,i} a_{k,i}(t)) + n(t), \tag{2.3}$$

where $\otimes$ represents the convolution operator and $n(t)$ denotes the noise plus interference. The conventional RAKE receiver uses elementary receivers called the RAKE fingers. In our model we employ L RAKE fingers. Since the aim of the conventional RAKE receiver is collecting energy, the receiver matches the RAKE fingers to the most powerful L paths. The conventional RAKE receiver assumes $n(t)$ as additive white gaussian noise (AWGN) and therefore employs a form of matched filtering, which is

the optimum receiver under AWGN. From [9], the sampled output of a matched filter, matched to the jth path, can be written as:

$$z_j = \int_{\tau_j}^{T_s+\tau_j} r(t)(h_j a_{k,i}(t-\tau_j))^* dt, \tag{2.4}$$

where T_s denotes the symbol period. The integral starts at τ_j, since for the jth path the received signal is nonzero between τ_j and $T_s + \tau_j$. By manipulating (2.4) we can obtain

$$z_j = h_j^* \int_0^{T_s} r(t+\tau_j) a_{k,i}^*(t) dt. \tag{2.5}$$

The equation above shows the steps done in the RAKE fingers. In the first step the received signal should be delayed. Suppose the number of the paths and the fingers is equal (J=L), then each finger has a delay corresponding to one path such that,

$$d_l = \tau_l, \qquad l = 0, ..., J-1, \tag{2.6}$$

where d_l denotes the associated delay of lth finger. Then the signal should be despread by multiplying the delayed signal with the complex conjugate of $a_{k,i}(t)$ and integrating between 0 and T_s such that

$$y_l = \int_0^{T_s} r(t+d_l) a_{k,i}^*(t) dt. \tag{2.7}$$

The perfect correlation property of $a_{k,i}$ eliminates any effect from multipaths other than the matched one. Therefore y_l has a signal component if and only if d_l is equal to one of the path delays. The idea behind the RAKE reception was the combining each path separately and this is obtained.

For this section, we keep the perfect correlation property assumption and in the next

section, we will give an example how the channel gains are modified if there is correlation between the shifted versions of $a_{k,i}(t)$.

To detect the symbol $s_{k,i}$, we need to combine the outputs of the RAKE fingers. The weighting coefficients $\mathbf{w} = [w_0, w_1, ..., w_{L-1}]^T$ are used for this purpose and the decision statistic z is formed such that,

$$z = \sum_{l=0}^{L-1} w_l^* y_l = \mathbf{w}^H \mathbf{y}, \tag{2.8}$$

where $\mathbf{y} = [y_0, y_1..., y_{L-1}]^T$ is the vector of the finger outputs. From (2.5), the weights are equal to the channel coefficients, such that,

$$w_l = h_l, \qquad l = 0, ..., L-1. \tag{2.9}$$

The decision statistic z can be used to detect the symbols or bits. For example if gray-coded QPSK modulation is used, the hard decisions of in-phase and quadrature bits are obtained via $\text{sgn}(\Re(z))$ and $\text{sgn}(\Im(z))$. $\Re$ and $\Im$ denote the real and imaginary part operators respectively.

For a conventional RAKE receiver, if the number of available fingers is larger than the number of the multipaths ($L > J$), extra finger weights are equal to zero, since the corresponding channel coefficients are zero. Therefore extra fingers could not improve the performance of the conventional RAKE receiver.

In this section the conventional RAKE receiver has been treated. We made the assumptions:

1. The noise is AWGN. Therefore matched filtering is used.
2. The channel is specular, so that each path can be distinguished.
3. The channel gains are known at the receiver.

In the next section, we will change the first assumption and show how the generalized RAKE receiver can benefit from extra available fingers.

2.3 Generalized RAKE Receiver

The generalized RAKE receiver has the same structure shown in Figure 2.3, but it has different combining weights and delays. To explain the weights in the generalized RAKE receiver, we should write the vector of finger outputs more explicitly, such that,

$$\mathbf{y} = \mathbf{h}s_k + \mathbf{u}, \tag{2.10}$$

where $\mathbf{h}$ corresponds to the channel vector and $\mathbf{u}$ embraces the noise plus interference. We changed $\mathbf{u}$ being AWGN assumption to $\mathbf{u}$ being complex valued colored gaussian noise vector with covariance $\mathbf{R_u}$=E[$\mathbf{uu}^H$]. The coloration could be due to the interference from other users in the system, the pulse shaping filter or as we will see in later chapters imperfect autocorrelation property of the spreading code. For such a system, the maximum likelihood detector for s_k has the weight vector,

$$\mathbf{w} = \mathbf{R_u}^{-1}\mathbf{h}, \tag{2.11}$$

if $\mathbf{h}$ is given, i.e. the channel is known at the receiver [2]. We can check the optimality of the weights using a basic example. The probability density function (pdf) of the vector $\mathbf{u}$ can be written as:

$$p(\mathbf{u}) = \frac{1}{\pi^L|\mathbf{R_u}|}\exp(-\mathbf{u}^H\mathbf{R_u}^{-1}\mathbf{u}), \tag{2.12}$$

which is equal to:

$$p(\mathbf{y}-\mathbf{h}s_k) = \frac{1}{\pi^L|\mathbf{R_u}|}\exp(-(\mathbf{y}-\mathbf{h}s_k)^H\mathbf{R_u}^{-1}(\mathbf{y}-\mathbf{h}s_k)), \tag{2.13}$$

Since $\mathbf{h}$ is assumed to be known, we can write (2.13) as

$$p(\mathbf{y}|\mathbf{h},s_k) = \frac{1}{\pi^L|\mathbf{R_u}|}\exp(-(\mathbf{y}-\mathbf{h}s_k)^H\mathbf{R_u}^{-1}(\mathbf{y}-\mathbf{h}s_k)). \tag{2.14}$$

If the symbol values for s_k have equal probabilities, the detector chooses the symbol value which maximizes (2.14). For a more convenient way of detection we can take the logarithm of the above equation,

$$\ln p(\mathbf{y}|\mathbf{h},s_k) = \ln(\frac{1}{\pi^L|\mathbf{R_u}|}) - ((\mathbf{y}-\mathbf{h}s_k)^H\mathbf{R_u}^{-1}(\mathbf{y}-\mathbf{h}s_k)). \tag{2.15}$$

Maximizing (2.14) is equal to maximizing (2.15), since logarithm is a monotonically increasing function. If we disregard the constant terms of (2.15), we obtain,

$$-((\mathbf{y}-\mathbf{h}s_k)^H\mathbf{R_u}^{-1}(\mathbf{y}-\mathbf{h}s_k)), \tag{2.16}$$

which is equal to

$$2\Re(s_k\mathbf{h}^H\mathbf{R_u}^{-1}\mathbf{y}) - \mathbf{y}^H\mathbf{R_u}^{-1}\mathbf{y} - |s_k|^2\mathbf{h}^H\mathbf{R_u}^{-1}\mathbf{h}. \tag{2.17}$$

The last two terms of (2.17) are constant for BPSK, QPSK and 8PSK modulation schemes. Therefore a decision statistic for those modulations is equal to:

$$\Lambda(s_k) = \Re(s_k\mathbf{h}^H\mathbf{R_u}^{-1}\mathbf{y}) = \Re(s_k^*(\mathbf{R_u}^{-1}\mathbf{h})^H\mathbf{y}) = \Re(s_k^*\mathbf{w}^H\mathbf{y}) \tag{2.18}$$

Furthermore, if gray-coded QPSK modulation is used, the hard decisions of in-phase and quadrature bits are obtained via $\text{sgn}(\Re(\mathbf{w}^H\mathbf{y}))$ and $\text{sgn}(\Im(\mathbf{w}^H\mathbf{y}))$. Actually this combining scheme is well-known and used in antenna arrays to detect the symbols [11] and in linear MMSE equalizers [12]. We specified the combining scheme above, however we did not specify how to set the delays of the correlator. For this purpose we require the signal to noise ratio (SNR) at the output of the combiner. Assuming unit energy symbols, for any weight vector $\mathbf{w}$, SNR equation can be specified as:

$$SNR = \mathrm{E}\left[\frac{\mathbf{w}^H\mathbf{h}\mathbf{h}^H\mathbf{w}}{\mathbf{w}^H\mathbf{u}^H\mathbf{u}\mathbf{w}}\right] = \frac{\mathbf{w}^H\mathbf{h}\mathbf{h}^H\mathbf{w}}{\mathbf{w}^H\mathbf{R}_\mathbf{u}\mathbf{w}}. \tag{2.19}$$

In the above equation, since $\mathbf{w}$ and $\mathbf{h}$ vectors are constant, the expectation operation is done only on $\mathbf{u}$ vectors. If the weights of the G-RAKE are put in the equation, we obtain

$$SNR = \frac{\mathbf{h}^H(\mathbf{R_u}^{-1})^H\mathbf{h}\mathbf{h}^H\mathbf{R_u}^{-1}\mathbf{h}}{\mathbf{h}^H(\mathbf{R_u}^{-1})^H\mathbf{R_u}\mathbf{R_u}^{-1}\mathbf{h}}, \tag{2.20}$$

which is equal to

$$SNR = \frac{\mathbf{h}^H(\mathbf{R_u}^{-1})^H\mathbf{h}\mathbf{h}^H\mathbf{R_u}^{-1}\mathbf{h}}{\mathbf{h}^H(\mathbf{R_u}^{-1})^H\mathbf{h}} = \mathbf{h}^H\mathbf{R_u}^{-1}\mathbf{h}. \tag{2.21}$$

Therefore if L RAKE fingers are available, the G-RAKE chooses L paths which maximize the SNR [2]. The chosen paths do not necessarily correspond to paths with energy. They could as well be the paths with zero channel gain. Basically, paths chosen with zero gains are used for interference suppression, and the rest of the paths are for energy collection. The performance depends on choosing the optimum combination. We will show how the conventional RAKE and the G-RAKE work with a simple example.

2.3.1 Example: The Conventional RAKE and the G-RAKE Weights in a Multipath Channel

For this example, we have the channel shown in Figure 2.4. It is a two path channel with one strong and one weak path gain. The duration between the paths is arbitrary since G-RAKE is a continuous time receiver. We select real path gains to ease the demonstration. The strong path has the gain 1 and the weak path has the gain 0.5. We consider an extra finger location, where no signal is observed, to show the effect of the G-RAKE weighting. That finger location can be considered as a path with zero gain.

For the G-RAKE performance demonstration, we need the correlation coefficients between the noise plus interference values of the paths. They are shown in Figure 2.4 with arrows. Assuming the noise plus interference has unit energy at each finger, the diagonal elements of the matrix $\mathbf{R_u}$ (variance of the elements $\mathbf{u}$) will be 1. In Figure 2.4, the noise plus interference values of the zero path and the strong path have the correlation of 0.5, therefore the second element of the first row and first element of the second row of $\mathbf{R_u}$ should be 0.5. Using the other values in Figure 2.4, we can write $\mathbf{R_u}$ as,

$$\mathbf{R_u} = \begin{bmatrix} 1 & 0.5 & 0.1 \\ 0.5 & 1 & 0.2 \\ 0.1 & 0.2 & 1 \end{bmatrix}. \tag{2.22}$$

Let us find the SNR values for the conventional RAKE and the G-RAKE receivers with 2 fingers. For the optimum performance of the conventional RAKE receiver, the weight vector is equal to w=[1 0.5]. The SNR of the conventional RAKE is therefore,

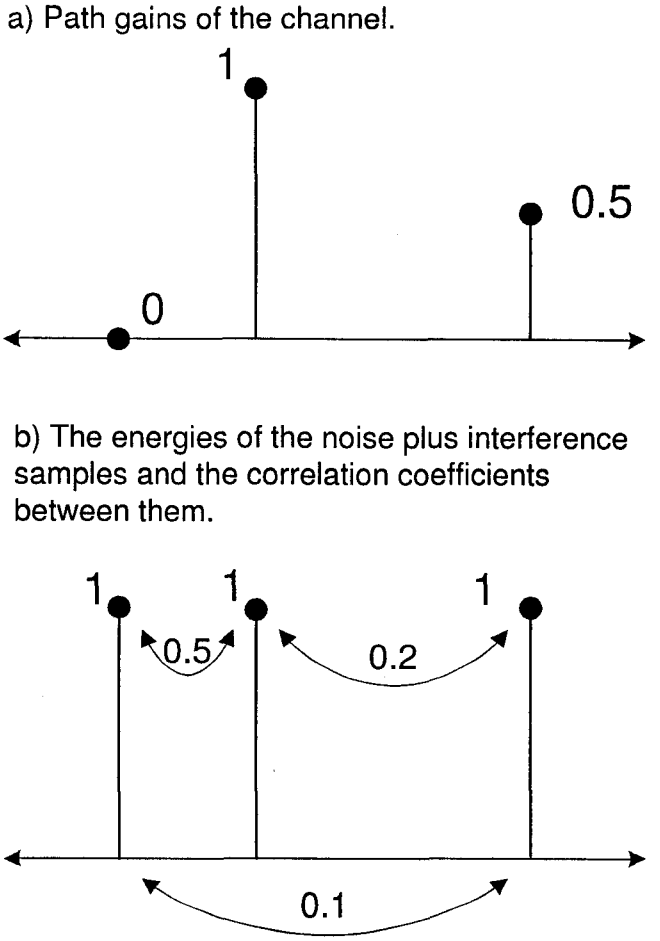

Figure 2.4: A simple channel model with real gains and colored noise plus interference. The correlation coefficients between noise plus interference values are shown with arrows.

$$SNR = \frac{\begin{bmatrix}1 & 0.5\end{bmatrix}\begin{bmatrix}1 & 0.5\\ 0.5 & 0.25\end{bmatrix}\begin{bmatrix}1\\ 0.5\end{bmatrix}}{\begin{bmatrix}1 & 0.5\end{bmatrix}\begin{bmatrix}1 & 0.2\\ 0.2 & 1\end{bmatrix}\begin{bmatrix}1\\ 0.5\end{bmatrix}} = 1.0775 \rightarrow 0.324\text{dB} \tag{2.23}$$

The weight vector of the G-RAKE receiver matched to the same paths will be

$$\mathbf{w} = \mathbf{R_u}^{-1}\mathbf{h} = \begin{bmatrix} 1 & 0.2 \\ 0.2 & 1 \end{bmatrix}^{-1} \begin{bmatrix} 1 \\ 0.5 \end{bmatrix} = \begin{bmatrix} 0.9375 \\ 0.3125 \end{bmatrix}. \tag{2.24}$$

As a consequence and using the equation (2.21), the SNR is equal to

$$SNR = \mathbf{h}^H\mathbf{R_u}^{-1}\mathbf{h} = \begin{bmatrix} 1 & 0.5 \end{bmatrix} \begin{bmatrix} 1 & 0.2 \\ 0.2 & 1 \end{bmatrix}^{-1} \begin{bmatrix} 1 \\ 0.5 \end{bmatrix} = 1.0937 \rightarrow 0.389\text{dB}. \tag{2.25}$$

For the G-RAKE, another option is choosing the strong path and the zero path. In this case, the weights are

$$\mathbf{w} = \mathbf{R_u}^{-1}\mathbf{h} = \begin{bmatrix} 1 & 0.5 \\ 0.5 & 1 \end{bmatrix}^{-1} \begin{bmatrix} 0 \\ 1 \end{bmatrix} = \begin{bmatrix} -0.6667 \\ 1.3333 \end{bmatrix}, \tag{2.26}$$

and the SNR ratio is,

$$SNR = 1.3335 \rightarrow 1.25\text{dB} \tag{2.27}$$

For the G-RAKE receiver, we increase the SNR around 0.85dB by choosing the RAKE finger containing a zero path instead of a nonzero path. For the above example, interference suppression is more important than collecting energy from a weak path. Even if we had a third finger, the SNR of the conventional RAKE receiver is the same, but for the G-RAKE we will have the weights

$$\mathbf{w} = \mathbf{R_u}^{-1}\mathbf{h} = \begin{bmatrix} 1 & 0.5 & 0.1 \\ 0.5 & 1 & 0.2 \\ 0.1 & 0.2 & 1 \end{bmatrix}^{-1} \begin{bmatrix} 0 \\ 1 \\ 0.5 \end{bmatrix} = \begin{bmatrix} -0.6667 \\ 1.2708 \\ 0.3125 \end{bmatrix}, \tag{2.28}$$

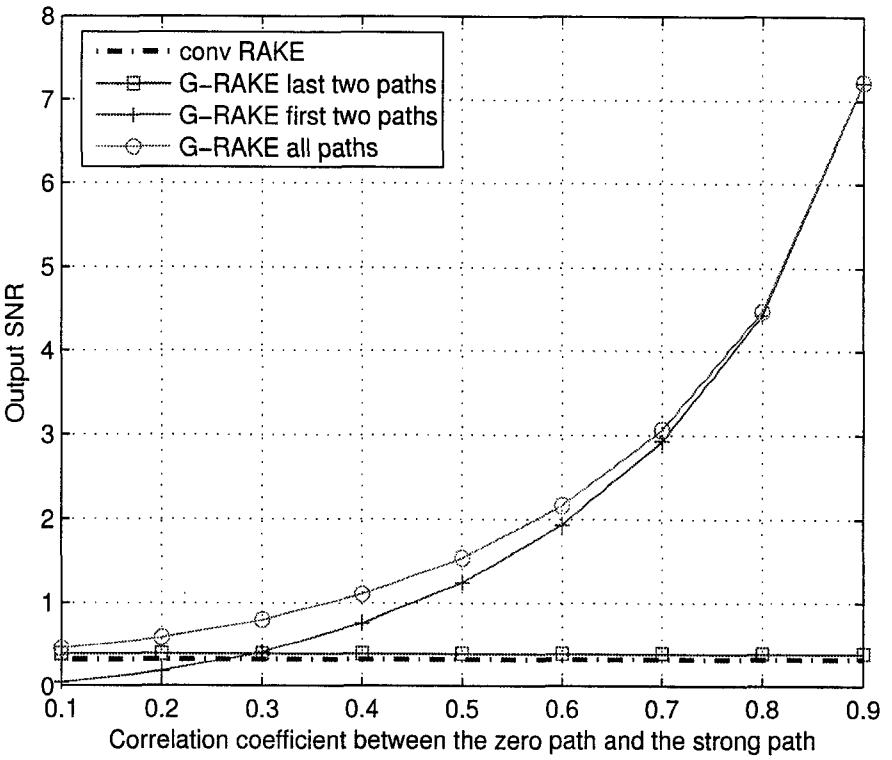

Figure 2.5: Output SNR values of the conventional RAKE and the G-RAKE receivers at different correlation coefficient values between the zero path and the strong path.

and the SNR,

$$SNR = 1.4256 \rightarrow 1.54\text{dB}. \tag{2.29}$$

In this case, the SNR is the maximum and it is 1.2 dB higher than the conventional RAKE receiver. In Figure 2.5, we present the effect of the correlation to the output SNR, by changing the correlation coefficient between the zero path and the strong path. After 0.3 correlation, the performance of the G-RAKE matched to the first two paths exceeds the performance of the G-RAKE matched to the last two paths. If the correlation coefficient is equal to 0.7, the gain of the 3 finger G-RAKE receiver is around

2.5 dB with respect to conventional RAKE receiver.

Another numerical example can be given from our simulations. The arbitrary channel coefficient vector $\mathbf{h}$ is from a simulation, in which there are 5 half chip spaced RAKE fingers and the channel has the rms delay spread value equal to 0.25 of the chip duration.

$$\mathbf{h} = \begin{bmatrix} -0.454 + 0.384i \\ -0.407 + 0.560i \\ 0.188 + 0.241i \\ 0.550 - 0.085i \\ 0.274 - 0.021i \end{bmatrix}, \tag{2.30}$$

Including the effect of the pulse shaping with root raised cosine filter with roll off factor $\alpha = 0.22$, the delay spread of the channel observed by the receiver is given in Figure 2.6.

In the next chapters we will explain the simulation parameters in detail. For this section we need only the given channel vector $\mathbf{h}$ and the matrix $\mathbf{R_u}$ during that simulation, which is equal to,

$$\mathbf{R_u} = \begin{bmatrix} 0.11 & 0.05 & 0 & -0.02 & 0 \\ 0.05 & 0.11 & 0.05 & 0 & -0.02 \\ 0 & 0.05 & 0.11 & 0.05 & 0 \\ -0.02 & 0 & 0.05 & 0.11 & 0.05 \\ 0 & -0.02 & 0 & 0.05 & 0.11 \end{bmatrix}. \tag{2.31}$$

The instantaneous SNR of the conventional RAKE receiver for the above values will be equal to 7.27 dB, whereas the G-RAKE will have an SNR of 7.86dB. If we had a 6 finger G-RAKE we would have an SNR equal to 8.03 dB and an 8 finger G-RAKE would have 8.05 dB SNR.

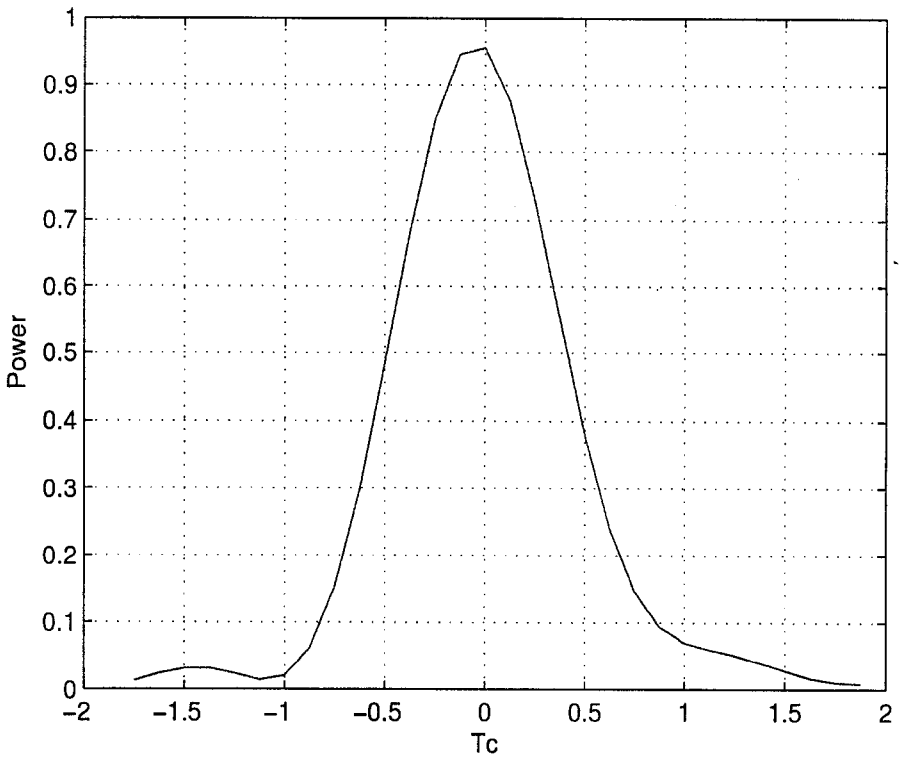

Figure 2.6: The observed power delay profile of the channel with rms delay spread value $0.25T_c$ including the effect of root raised cosine pulse shaping filter with rolloff factor equal to 0.22.

2.4 Conventional Discrete-Time RAKE Receiver

Before the D-DTR, we will explain the conventional discrete-time RAKE (C-DTR) receiver of [7]. We stated that the conventional RAKE receiver assumes that the channel has specular paths. However if the paths arrive in a short period of time (less than the chip period), we observe diffuse channels and it is hard to distinguish the paths. The C-DTR solves this problem by sampling the received signal $r(t)$ at twice the chip rate and processing the sampled version. The DTR can be seen as a conventional RAKE

receiver with L fingers, whose lth finger has the delay element $d_0 + lT_c/2$. Here d_0 is the reference delay of the system. In Figure 2.7, we present the equivalent system of the C-DTR.

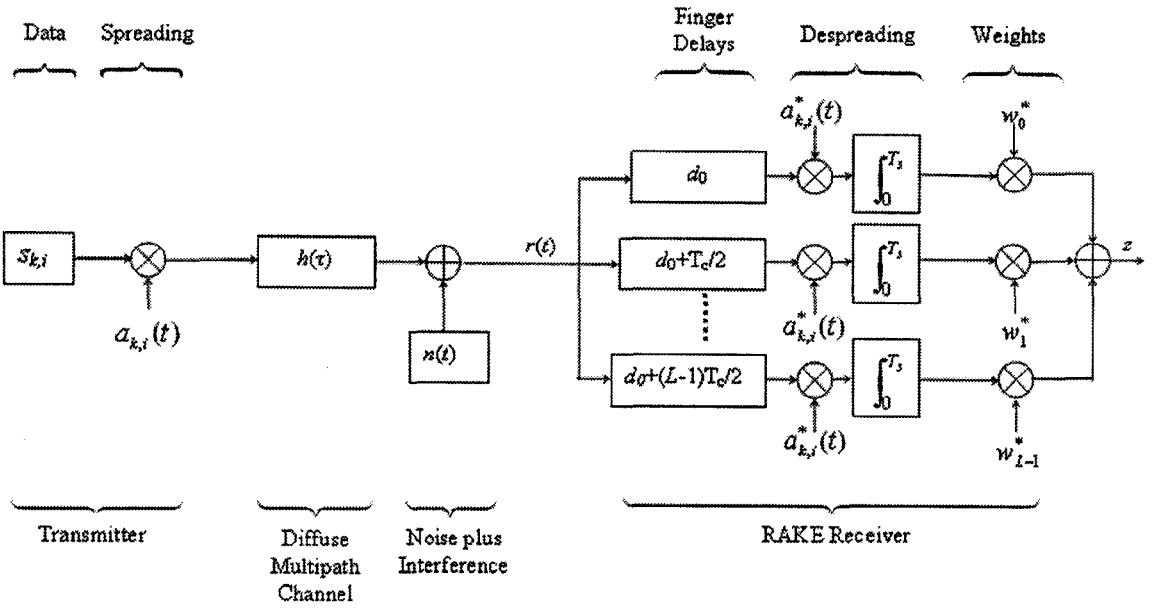

Figure 2.7: Equivalent system model of the C-DTR system.

Since the finger locations are set, the RAKE receiver does not need to locate every single path one by one but to set only the first delay element. The price paid by the C-DTR is increased sensitivity to channel estimation errors. We can explain this sensitivity with the sampled version of the simple channel used in the previous example as shown in Figure 2.8. Assume that the C-DTR starts sampling the channel at the strong gain and ends sampling at the weak gain. As seen in Figure 2.8, there are 3 zero channel gains between the strong and the weak paths. Since all the gains are estimated, the estimations of the zero channel gains will be due to only noise and thus will degrade the performance of the overall system. If perfect channel state information is available

then the weights of the C-DTR will be equal to the conventional RAKE receiver, i.e. the channel gains of the paths.

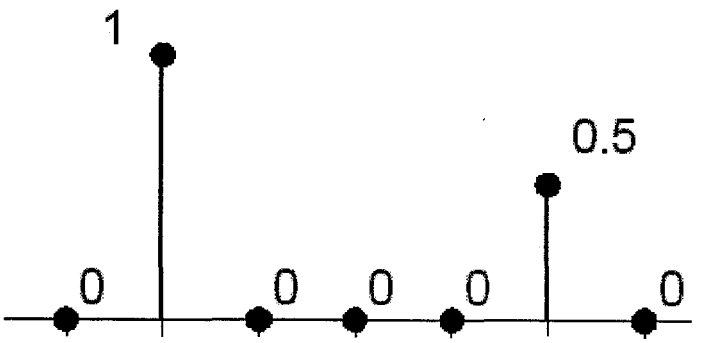

Figure 2.8: The sampled version of the simple channel model.

2.5 Decorrelating Discrete-Time RAKE Receiver

To improve the performance of the C-DTR, Siala proposed the D-DTR. But the way to obtain the combining weights in the D-DTR is also applicable to the conventional continuous time RAKE receiver with channel estimation errors.

In (2.10), the D-DTR assumes that $\mathbf{u}$ is made up of zero mean complex white gaussian noise samples with variance $\Sigma^2 = 2N_0/T_c$, where N_0 is the power spectral density of the complex noise before sampling. The D-DTR, unlike other receivers we mentioned, takes into consideration that only an estimate $\hat{\mathbf{h}}$ of the channel vector is available, such that

$$\hat{\mathbf{h}} = \mathbf{h} + \mathbf{e} \tag{2.32}$$

where $\hat{\mathbf{h}}$ is the estimated channel and $\mathbf{e}$ is the channel estimation error vector. We assume in this work that $\mathbf{h}$ is estimated with N_p pilot symbols and the estimated

channel vector is equal to:

$$\hat{\mathbf{h}} = \frac{1}{N_p E_p} \sum_{m=0}^{N_p-1} \mathbf{y_m} s_m^*, \tag{2.33}$$

where E_p is the energy of pilot symbols, $\mathbf{y}_m$ is the received vector of the mth pilot symbol and s_m's are the pilot symbols. We will treat separately the $\mathbf{y}$ and $\hat{\mathbf{h}}$ vectors to form the decision statistic z. Such an approach is helpful to understand the idea behind the D-DTR. The D-DTR starts by decorrelating the channel gains in the received vector $\mathbf{y}$, using the eigenvectors of the channel covariance matrix $\mathbf{R_h}$=E[$\mathbf{hh}^H$] such that,

$$\tilde{\mathbf{y}} = \mathbf{U}^H \mathbf{y}, \tag{2.34}$$

where $\mathbf{U}$ is the matrix consisting of the eigenvectors of $\mathbf{R_h}$. Decorrelating is applied to $\hat{\mathbf{h}}$ as well, since $\hat{\mathbf{h}}$ contains the correlated channel gains. As the third step, the weights matrix $\mathbf{W}$, a diagonal matrix with the lth diagonal entry being the weighting factor w_l, is computed. If the data and pilot symbols have the energy E_s, then w_l is equal to

$$w_l = \frac{1}{1 + \sigma^2(\frac{E_s}{\Sigma^2} + \frac{1}{\Gamma_l})}, \tag{2.35}$$

where σ^2=$\Sigma^2/(N_p E_s)$ and Γ_l is the eigenvalue corresponding to the lth eigenvector of $\mathbf{R_h}$. In [4], it is shown that the above weights are optimum under the assumptions of the D-DTR. In the last step, the D-DTR obtains the decision statistic z by,

$$z = (\mathbf{U}^H \hat{\mathbf{h}})^H \mathbf{W} \tilde{\mathbf{y}}. \tag{2.36}$$

In the previous sections, we had a weight vector $\mathbf{w}$ to combine the elements of $\mathbf{y}$ for both the conventional RAKE and the G-RAKE, so that $z = \mathbf{w}^H \mathbf{y}$. For the D-DTR, we can obtain such a vector by manipulating the equations (2.34) and (2.36) and it is

equal to:

$$\mathbf{w} = \mathbf{UWU}^H\hat{\mathbf{h}}. \tag{2.37}$$

The core of the weight vector is the matrix $\mathbf{W}$. Let us focus on the behavior of $\mathbf{W}$ at different values of N_p and Γ_l. First, we set N_p to infinity, to see the weights at perfect channel state information. From (2.35), $\mathbf{W}$ becomes identity matrix and since $\mathbf{U}$ is inverse of its hermitian transpose, $\mathbf{w}$ becomes

$$\mathbf{w} = \mathbf{UWU}^H\hat{\mathbf{h}} = \hat{\mathbf{h}} = \mathbf{h}, \tag{2.38}$$

which is equal to the weights of the conventional RAKE receiver. Now assuming N_p is given and we focus on Γ_l. For small values of Γ_l, the values of w_l are close to zero, whereas for large values of Γ_l, the values of w_l are close to $1/(1 + (1/N_p))$. Therefore we can conclude, the weak gains in the decorrelated channel are attenuated more than the strong gains. To maximize the recovered energy from the channel, the D-DTR sets the delays so that $\hat{\mathbf{h}}^H\mathbf{w}^H\mathbf{y}$ is maximized [4]. However since finger positioning is done usually per frame, instead $\hat{\mathbf{h}}^H\mathbf{w}^H\hat{\mathbf{h}}$ can be used. In the next subsection, we will give a numerical example on the weights of the D-DTR receiver.

2.5.1 Example: The D-DTR Weights in a Multipath Channel

In the previous section, we gave a two path channel with one strong and one weak path gain in Figure 2.4 and its sampled version in Figure 2.8. We decided to use the first version of the channel in this example, since the D-DTR weights are applicable in the conventional RAKE receivers too. Assume that the channel vector has the covariance matrix:

$$\mathbf{R_h} = \mathrm{E}[\mathbf{h}\mathbf{h}^H] = \begin{bmatrix} 0 & 0 & 0 \\ 0 & 1 & 0 \\ 0 & 0 & 0.25 \end{bmatrix}. \tag{2.39}$$

$\mathbf{R_h}$ shows that there is no correlation between the channel values and the corresponding eigenvalues are 0 for the 0 gain path, 1 for the strong path and 0.25 for the weak path. Assume that we use 4 pilot symbols to estimate the channel, then the weights of the D-DTR is equal to:

$$\mathbf{w} = \mathbf{W}\hat{\mathbf{h}} = \begin{bmatrix} 0 & 0 & 0 \\ 0 & \frac{1}{1+\frac{2}{4}} & 0 \\ 0 & 0 & \frac{1}{1+\frac{5}{4}} \end{bmatrix} \hat{\mathbf{h}} \tag{2.40}$$

Our comments regarding the weights are verified with the above example. The zero path will get zero weight, whatever the estimated value is and the estimated value for the weak path is attenuated more than the strong path. In the next section, we will introduce the Generalized Decorrelating RAKE Receiver.

2.6 Generalized Decorrelating RAKE Receiver

In the section of the conventional RAKE receiver we made the assumptions that:

1. The noise plus interference is not correlated.

2. The channel gains are known at the receiver.

Both of these assumptions are not valid in many realistic scenarios. As mentioned, interference could be correlated and pulse shaping correlates both the noise and interference. Therefore the validity of the first assumption is damaged. Due to the change of the channel gains in time and limited number of pilot symbols, only an estimate of

the channel gain is available at the receiver. The GD-RAKE is designed to operate in multipath channels with colored noise and estimated channel coefficients.

The structure of the GD-RAKE is the same of the conventional RAKE receiver which is shown in Figure 2.3. In conventional RAKE receiver, we had the $\mathbf{y}$ vector of RAKE finger outputs as

$$\mathbf{y} = \mathbf{h}s_k + \mathbf{u}, \tag{2.41}$$

For the GD-RAKE, we assume that $\mathbf{u}$, the vector of noise plus interference, has the covariance $\mathbf{R_u}$ like the G-RAKE. The assumptions about $\mathbf{h}$ are the same assumptions made in the D-DTR part: the channel vector $\mathbf{h}$ has the covariance $\mathbf{R_h}$, and only the estimate of $\mathbf{h}$, i.e. $\hat{\mathbf{h}}$, is available at the receiver. To explain the GD-RAKE, we treat $\mathbf{y}$ and $\hat{\mathbf{h}}$ separately, but at the end of the section, we will combine the processes and obtain one weight vector $\mathbf{w}$.

The GD-RAKE first decorrelates the colored noise $\mathbf{u}$ in $\mathbf{y}$ by using the eigenvectors and eigenvalues of the $\mathbf{R_u}^{-1}$ such that,

$$\mathbf{y}' = \Lambda\Omega^H\mathbf{y} = \Lambda\Omega^H(\mathbf{h}s_k + \mathbf{u}), \tag{2.42}$$

where Λ is the diagonal matrix of the square roots of the eigenvalues of $\mathbf{R_u}^{-1}$ and Ω is the eigenvector matrix of $\mathbf{R_u}^{-1}$. On the other hand, $\hat{\mathbf{h}}$ is multiplied with the same decorrelating matrix such that,

$$\hat{\mathbf{h}}' = \Lambda\Omega^H\hat{\mathbf{h}}. \tag{2.43}$$

The decorrelating of noise changes the covariance matrix $\mathbf{R_h}$ to $\mathbf{R'_h}$ as well,

$$\mathbf{R'_h} = \Lambda\Omega^H\mathbf{R_h}\Omega\Lambda. \tag{2.44}$$

At this point the system has white gaussian noise samples with unit energy (N_0=1), since we used the eigenvalues of the $\mathbf{R_u}^{-1}$ in the noise decorrelating process. Additionally, the channel vector has the new covariance matrix $\mathbf{R'_h}$. Since the above situation matches the assumptions of the D-DTR, that method can be applied directly.

$$z = (\mathbf{U'}\hat{\mathbf{h}}')^H\mathbf{W'U'y'}, \tag{2.45}$$

where $\mathbf{U'}$ consists of the eigenvectors of $\mathbf{R'_h}$ and $\mathbf{W'}$ is a diagonal matrix with the lth diagonal entry being the weighting factor w'_l, which is equal to

$$w'_l = \frac{1}{1+\frac{1}{N_p}(1+\frac{1}{\Gamma'_l}\frac{1}{E_s})}, \tag{2.46}$$

where Γ'_l is the lth eigenvalue of $\mathbf{R'_h}$. Again the whole process can be written in the form of $z = \mathbf{w}^H\mathbf{y}$, where the weight vector $\mathbf{w}$ is equal to

$$\mathbf{w} = \Omega\mathbf{\Lambda U'W'U'}^H\mathbf{\Lambda}\Omega^H\hat{\mathbf{h}} \tag{2.47}$$

The GD-RAKE chooses the delays so that $\mathbf{w}^H\mathbf{w}$ is maximized, due to the decorrelation of the noise, we need only to focus the energy recovered from the channel. To check the validity of the GD-RAKE approach, we set $N_p = \infty$ to find the weights of the GD-RAKE with perfect channel state information. In this case, the weight vector of the GD-RAKE should be equal to the weight vector of the G-RAKE. From (2.46) $\mathbf{W'}$ and therefore $\mathbf{U'W'U'}^H$ becomes the identity matrix if $N_p = \infty$. Remaining $\Omega\mathbf{\Lambda}^2\Omega^H$ is equal to $\mathbf{R_u}^{-1}$ by definition. Since the channel estimation error becomes 0, $\hat{\mathbf{h}}$ is equal to $\mathbf{h}$. As a result, the weight vector is equal to:

$$\mathbf{w} = \mathbf{R_u}^{-1}\mathbf{h}, \tag{2.48}$$

which is the weight vector of the G-RAKE, so our method is valid for no channel estimation error case. In this section we will obtain the theoretical performance of the GD-RAKE for QPSK modulation as well. We start by modifying (2.45) so that,

$$z = (\tilde{\mathbf{h}} + \tilde{\mathbf{e}})^H \mathbf{W}' \tilde{\mathbf{h}} s_k + \tilde{\mathbf{u}}, \tag{2.49}$$

where $\tilde{\mathbf{h}}$ and $\tilde{\mathbf{e}}$ are the channel and estimation error parts in $(\mathbf{U}'\hat{\mathbf{h}}')$ respectively and $\tilde{\mathbf{u}}$ is still a whitened noise plus interference vector with unit variance. Let the complex baseband symbols of QPSK be $\sqrt{E_s/2}(\pm 1 \pm j)$, assuming that $\sqrt{E_s/2}(1+j)$ is sent, the probability of error of the inphase component can be written as:

$$P_e = \mathrm{p}(\sqrt{E_s}\Re\{(\tilde{\mathbf{h}} + \tilde{\mathbf{e}})^H \mathbf{W}'(\tilde{\mathbf{h}}(1+j)\sqrt{E_s/2} + \tilde{\mathbf{u}}\}) < 0) \tag{2.50}$$

The scalar product in the above expression can be written as a summation such that,

$$\sqrt{E_s}\Re\left[(\tilde{\mathbf{h}} + \tilde{\mathbf{e}})^H \mathbf{W}'(\tilde{\mathbf{h}}(1+j)\sqrt{E_s/2} + \tilde{\mathbf{u}})\right] = \sum_{l=0}^{L-1} \chi_l, \tag{2.51}$$

where

$$\begin{aligned} \chi_l \;&= \tfrac{E_s w_l}{\sqrt{2}}|\tilde{h}_l|^2 + \tfrac{\sqrt{E_s}w'_l}{2}(\tilde{h}_l\tilde{u}_l^* + \tilde{h}_l^*\tilde{u}_l) + \tfrac{E_s w'_l}{2\sqrt{2}}(\tilde{e}_l^*\tilde{f}_l(1+j) + \\ &\quad \tilde{e}_l\tilde{h}_l^*(1-j)) + \tfrac{\sqrt{E_s}w'_l}{2}(\tilde{e}_l^*\tilde{u}_l + \tilde{e}_l\tilde{u}_l^*), \qquad \text{for } l = 0, 1, ..., L-1 \end{aligned} \tag{2.52}$$

The variables $\tilde{h}_l$, $\tilde{u}_l$ and $\tilde{e}_l$ are independent zero-mean complex Gaussian random variables with variances Γ'_l, 1 and $1/(N_p E_s)$, respectively. If we perform variable changes

$$\tilde{h}_l = \bar{h}_l \sqrt{\Gamma'_l}, \tag{2.53}$$

and

$$\tilde{e}_l = \bar{e}_l / \sqrt{N_p E_s}, \tag{2.54}$$

where $\bar{e}_l$ and $\bar{h}_l$ are Gaussian random variables with unit variances, we can write the random variable $2\chi_l / w'_l$ in a quadratic form, using the Hermitian matrix

$$\mathbf{K}_l = \eta_l \begin{bmatrix} 1 & \frac{1-j}{2\sqrt{N_p \eta_l}} & \frac{1}{\sqrt{\eta_l}} \\ \frac{1+j}{2\sqrt{N_p \eta_l}} & 0 & \frac{1}{\sqrt{N_p \eta_l}} \\ \frac{1}{\sqrt{\eta_l}} & \frac{1}{\sqrt{N_p \eta_l}} & 0 \end{bmatrix}, \tag{2.55}$$

where

$$\eta_l = E_s \Gamma'_l. \tag{2.56}$$

Two eigenvalues of $\mathbf{K}_l$, which are not equal to zero, are

$$\kappa_l^{\pm} = \frac{\eta_l}{\sqrt{2}} \left(1 \pm \sqrt{1 + 2(\frac{1}{\eta_l} + \frac{1}{N_p \eta_l} + \frac{1}{N_p \eta_l^2})} \right). \tag{2.57}$$

Assuming all the eigenvalues are distinct ($\kappa_l^{\pm}$ for l=0, .., $L-1$) and all κ_l^- are negative and all κ_l^+ are positive, we can write the probability of error as [4]

$$P_e = \sum_{l=0}^{L-1} \prod_{m=0}^{L-1} \frac{w'_l \kappa_l^-}{w'_l \kappa_l^- - w'_m \kappa_m^+} \prod_{m=0, m \neq l}^{L-1} \frac{w'_l \kappa_l^-}{w'_l \kappa_l^- - w'_m \kappa_m^-}. \tag{2.58}$$

In Chapter 4 we will compare the theoretical performance with the simulation results. Before concluding this chapter, we illustrate how to compute the weights of GD-RAKE receiver.

2.6.1 Example: The GD-RAKE Weights in a Multipath Channel

For the example the same two path channel with one strong and one weak path gain in Figure 2.4 is used. The noise plus interference has the covariance:

$$\mathbf{R_u} = \begin{bmatrix} 1 & 0.5 & 0.1 \\ 0.5 & 1 & 0.2 \\ 0.1 & 0.2 & 1 \end{bmatrix}. \tag{2.59}$$

The channel vector has the covariance matrix:

$$\mathbf{R_h} = \begin{bmatrix} 0 & 0 & 0 \\ 0 & 1 & 0 \\ 0 & 0 & 0.25 \end{bmatrix}. \tag{2.60}$$

To find the weights matrix of the GD-RAKE, we should obtain the $\mathbf{R'_h}$, which is equal to

$$\mathbf{R'_h} = \Lambda\Omega^H\mathbf{R_h}\Omega\Lambda = \begin{bmatrix} 0.3112 & -0.01086 & -0.5424 \\ -0.01086 & 0.2502 & -0.1982 \\ -0.5424 & -0.1982 & 1.074 \end{bmatrix}. \tag{2.61}$$

We assume, that 4 pilot symbols are used to estimate the channel. Using the eigenvalues of the $\mathbf{R'_h}$, i.e. (Γ'_l) and (2.46), we can obtain the diagonal weight matrix $\mathbf{W'}$.

$$\mathbf{W'} = \begin{bmatrix} 0.6990 & 0 & 0 \\ 0 & 0 & 0 \\ 0 & 0 & 0.4450 \end{bmatrix} \tag{2.62}$$

Then the weights of the GD-RAKE are equal to:

$$\mathbf{w} = \Omega\Lambda\mathbf{U}'\mathbf{W}'\mathbf{U}'^{H}\Lambda\Omega^{H}\hat{\mathbf{h}} = \begin{bmatrix} 0.2291 & -0.4645 & 0.0311 \\ -0.4645 & 0.9606 & -0.1573 \\ 0.0311 & -0.1573 & 0.4755 \end{bmatrix} \hat{\mathbf{h}} \tag{2.63}$$

To make a comparison, we compute $\mathbf{R_u}^{-1}$, which is used by the G-RAKE,

$$\mathbf{R_u}^{-1} = \begin{bmatrix} 1.3333 & -0.6666 & 0 \\ -0.6666 & 1.375 & -0.2083 \\ 0 & -0.2083 & 1.0417 \end{bmatrix} \tag{2.64}$$

Comparing the last coefficient of the matrices above, shows the difference between the GD-RAKE and the G-RAKE. That coefficient corresponds to the contribution of the weak path to the weight coefficient of itself. The GD-RAKE have the value 0.4755 whereas the G-RAKE has 1.0417. The reason is that the GD-RAKE tries to attenuate the contribution of weak paths, since they are more vulnerable to channel estimation errors.

2.7 Chapter Summary

In this chapter, we have introduced the GD-RAKE receiver and explained the G-RAKE and the D-DTR receivers. While the G-RAKE receiver improves the system performance by using the coloration in the noise plus interference vectors, the D-DTR increases the robustness to channel estimation errors and GD-RAKE combines the advantages to those receivers. The price for those improvements is increased complexity and the requirement of the channel statistics and/or the noise plus interference statistics. Beside giving weight examples for every receiver type, we have formulated raw bit error rate probability for the GD-RAKE receiver, if QPSK modulation is used. Next

chapter focuses on how to estimate those statistics.

Chapter 3

Estimation of the Channel and Noise Statistics

In the previous chapter, we explained how to construct the weights for the D-DTR and GD-RAKE receiver. During the calculation of the weights, we assumed that the channel and noise plus interference covariance matrices ($\mathbf{R_h}$ and $\mathbf{R_u}$) are known. However, in real life situations those matrices should be estimated from the incoming signals. In this chapter, we concentrate on this problem, starting with the estimation of $\mathbf{R_h}$ for D-DTR.

3.1 Estimation of the Channel Statistics for D-DTR

For the optimum weights of the D-DTR, we need to estimate the noise variance and eigenvalues and eigenvectors of the channel covariance matrix $\mathbf{R_h}$. In [4], Siala derived the maximum likelihood estimate for $\mathbf{R_h}$ for the case of $\mathbf{R_u}=\Sigma^2\mathbf{I}$ and assumed that Karhunen-Loeve transform is taken to form the eigenvalues and eigenvectors. In the previous chapters we assumed that for every channel realization we have N_p pilot

symbols and therefore N_p correlator output vectors ($\mathbf{y_n}$). If the correlator outputs and the channel estimate vectors for M channel realizations (time slots) are available, the D-DTR estimates Σ^2 and $\mathbf{R_h}$ by using the equations:

$$\hat{\Sigma}^2 = \frac{1}{(N_p-1)LM}\sum_{m=0}^{M-1}\left(\sum_{n=0}^{N_p-1}\mathbf{y}_{n,m}^H\mathbf{y}_{n,m} - N_pE_p\hat{\mathbf{h}}_m^H\hat{\mathbf{h}}_m\right) \tag{3.1}$$

$$\hat{\mathbf{R}}_\mathbf{h} = \frac{1}{M}\sum_{m=0}^{M-1}\hat{\mathbf{h}}_m\hat{\mathbf{h}}_m^H - \frac{\hat{\Sigma}^2}{N_pE_p}\mathbf{I} \tag{3.2}$$

In a realistic system, usually a forgetting factor ε is used to update the estimated values of $\hat{\mathbf{R}}_\mathbf{h}$ and $\hat{\Sigma}^2$, such that

$$\hat{\Sigma}_m^2 = (1-\varepsilon)\hat{\Sigma}_{m-1}^2 + \frac{\varepsilon}{(N_p-1)L}\left(\sum_{n=0}^{N_p-1}\mathbf{y}_{n,m}^H\mathbf{y}_{n,m} - N_pE_p\hat{\mathbf{h}}_m^H\hat{\mathbf{h}}_m\right) \tag{3.3}$$

$$\hat{\mathbf{R}}_\mathbf{h}^m = (1-\varepsilon)\hat{\mathbf{R}}_\mathbf{h}^{m-1} + \varepsilon(\hat{\mathbf{h}}_m\hat{\mathbf{h}}_m^H - \frac{\hat{\Sigma}^2}{N_pE_p}\mathbf{I}) \tag{3.4}$$

where $\hat{\mathbf{R}}_\mathbf{h}^m$ is the estimate for the mth time slot. Siala used the above update algorithm in [4]. In our simulations, we will call this algorithm as the KLT algorithm, since the algorithm we will present next does not require the KLT. In [13], Champagne presented three algorithms to estimate the eigenvalues and eigenvectors of a covariance matrix. In literature there exist more advanced versions of these algorithms (e.g [14], [15], [16]). However, our simulations indicate that the third and simplest algorithm of [13] is efficient enough to track both eigenvalues and eigenvectors. In [16], Willink, while extending the algorithm to track both left and right eigenvectors, simplified the notation. We will follow Willink's notation to explain the algorithm. It starts with the update equation in terms of the eigenvalues and eigenvectors of $\hat{\mathbf{R}}_\mathbf{h}$,

$$\hat{\mathbf{U}}_m\hat{\mathbf{\Gamma}}_m\hat{\mathbf{U}}_m^H = (1-\varepsilon)\hat{\mathbf{U}}_{m-1}\hat{\mathbf{\Gamma}}_{m-1}\hat{\mathbf{U}}_{m-1}^H + \varepsilon(\hat{\mathbf{h}}_m\hat{\mathbf{h}}_m^H - \frac{\hat{\Sigma}^2}{N_pE_p}\mathbf{I}). \tag{3.5}$$

In the above equation $\hat{\mathbf{U}}_m$ and $\hat{\mathbf{\Gamma}}_m$ denote the matrices consisting of the eigenvectors and eigenvalues of $\hat{\mathbf{R}}_{\mathbf{h}}^m$ respectively. Updated $\hat{\mathbf{R}}_{\mathbf{h}}^m$ can be written as a first order perturbation such that,

$$\hat{\mathbf{R}}_{\mathbf{h}}^m = \hat{\mathbf{R}}_{\mathbf{h}}^{m-1} + \mathbf{E} \tag{3.6}$$

where,

$$\mathbf{E} = \varepsilon(\hat{\mathbf{h}}_m\hat{\mathbf{h}}_m^H - \frac{\hat{\Sigma}^2}{N_pE_p}\mathbf{I} - \hat{\mathbf{R}}_{\mathbf{h}}^{m-1}). \tag{3.7}$$

Another way to write the perturbation equation is

$$\hat{\mathbf{R}}_{\mathbf{h}}^m = \hat{\mathbf{U}}_{m-1}(\hat{\mathbf{\Gamma}}_{m-1} + \mathbf{B})\hat{\mathbf{U}}_{m-1}^H \tag{3.8}$$

where $\mathbf{B} = \hat{\mathbf{U}}_{m-1}^H\mathbf{E}\hat{\mathbf{U}}_{m-1}$, i.e. from (3.7),

$$\mathbf{B} = \varepsilon(\hat{\mathbf{U}}_{m-1}^H\hat{\mathbf{h}}_m\hat{\mathbf{h}}_m^H\hat{\mathbf{U}}_{m-1} - \frac{\hat{\Sigma}^2}{N_pE_p}\mathbf{I} - \hat{\mathbf{\Gamma}}_{m-1}). \tag{3.9}$$

Denoting the ith column of $\hat{\mathbf{U}}_{m-1}$ by $\mu_{m-1,i}$, the (i,j)th element of $\mathbf{B}$ is given by

$$b_{i,j} = \mu_{m-1,i}^H\mathbf{E}\mu_{m-1,i}. \tag{3.10}$$

Using matrix perturbation theory, the eigenvalues of the perturbed matrix $\hat{\mathbf{R}}_{\mathbf{h}}^m$ can be approximated by

$$\Gamma_{m,i} \approx \Gamma_{m-1,i} + b_{i,i}, \tag{3.11}$$

Using the definition of $b_{i,j}$, we can write the update equation as

$$\Gamma_{m,i} = (1-\varepsilon)\Gamma_{m-1,i} + x_i x_i^* - \varepsilon\frac{\hat{\Sigma}^2}{N_p E_p}, \tag{3.12}$$

where $x_i = \sqrt{\varepsilon}\mu_{m-1,i}^H \mathbf{h}_m$. This ends the eigenvalue update part of the algorithm. The main equation to update the eigenvectors is

$$\hat{\mathbf{U}}_m = \hat{\mathbf{U}}_{m-1}(\mathbf{I}+\mathbf{A}), \tag{3.13}$$

where $\mathbf{A}$ is the update matrix. Since $\hat{\mathbf{U}}_{m-1}$ is unitary, up to a first order approximation

$$\mathbf{A} + \mathbf{A}^H = 0 \tag{3.14}$$

The (i,j)th element of $\mathbf{A}$ is $a_{i,j} = \mu_{m-1,i}^H \mu_{m,j}$ for $i \neq j$ and $a_{i,i} = 0$. Willink showed in [16] that $a_{i,j}$ can be approximated by

$$a_{j,i} \approx \frac{b_{j,i}}{\Gamma_{m-1,i}} = \frac{x_j x_i^*}{\Gamma_{m-1,i}} \quad i < j \tag{3.15}$$

and $a_{j,i}$=$-a_{i,j}^*$ from 3.14. Using the definition of $x(i)$ and the above approximation of $a_{j,i}$, we can write the update equation for the ith eigenvector as,

$$\mu_{m,i} = \mu_{m-1,i} + \sum_{j=i+1}^{L} \frac{x_i^* x_j}{\Gamma_{m-1,i}}\mu_{m-1,j} - \sum_{j=1}^{i-1} \frac{x_i^* x_j}{\Gamma_{m-1,j}}\mu_{m-1,j} \tag{3.16}$$

For an efficient update algorithm Willink introduced two vectors $\mathbf{p}_i$ and $\mathbf{q}_i$ with the following relationships

$$\mathbf{p}_0 = \sum_{j=1}^{L} x_j \mu_{m-1,j} = \sqrt{\varepsilon}\hat{\mathbf{h}}_m \tag{3.17}$$

$$\mathbf{p}_i = \sum_{j=i+1}^{L} x_j^* \mu_{m-1,j} = \mathbf{p}_{i-1} - x_i^* \mu_{m-1,i} \quad i = 1, ..., L \tag{3.18}$$

and $\mathbf{q}_1 = 0$,

$$\mathbf{q}_{i+1} = \sum_{j=1}^{i} \frac{x_i^* x_j}{\Gamma_{m-1,i}} \mu_{m-1,j} = \mathbf{q}_i + \frac{x_i}{\Gamma_{m-1,i}} \mu_{m-1,i} \quad i = 1, ..., L-1 \tag{3.19}$$

Using the definitions of $\mathbf{p}_i$ and $\mathbf{q}_i$ the update algorithm can be written as

$$\mu_{m,i} = \mu_{m-1,i} + x_i^* (\frac{\mathbf{p}_i}{\Gamma_{m,i}} - \mathbf{q}_i) \tag{3.20}$$

Following the update, the eigenvectors are normalized. The whole algorithm is shown in Table 3.1.

Table 3.1: The eigenvector and eigenvalue update algorithm for D-DTR.

Initialization
$\hat{\mathbf{h}}_m = \sqrt{\varepsilon}\hat{\mathbf{h}}_m$
$\mathbf{p} = \hat{\mathbf{h}}_m$
$\mathbf{q} = 0$
$i = 1$
Recursion
$x_i = \mu_{m-1,i}^H \hat{\mathbf{h}}_m$
$\mathbf{p} = \mathbf{p} - x_i \mu_{m-1}$
$\mu_m = \mu_{m-1} + x_i^* (\mathbf{p}/\Gamma_{m-1,i} - \mathbf{q})$
$\mathbf{q} = \mathbf{q} + (x_i/\Gamma_{m-1,i})\mu_{m-1}$
$\Gamma_{m,i} = (1-\varepsilon)\Gamma_{m-1,i} + x_i x_i^* - \varepsilon \frac{\hat{\Sigma}^2}{N_p E_p}$
$\mu_m = \mu_m / \sqrt{\mu_m^H \mu_m}$
$i = i + 1$

In our simulations we will call this algorithm as the update algorithm, since it updates the eigenvalues and eigenvectors rather than recalculating them, using the KLT. Coming section expands both KLT and update algorithms to the GD-DTR case by including the estimation of $\mathbf{R_u}$.

3.2 Estimation of the Channel and Noise Statistics for GD-RAKE

For the optimum weights of the GD-RAKE, we should estimate the covariance matrices $\mathbf{R_h}$ and $\mathbf{R_u}$. As mentioned in the previous section, in [4] Siala derived the ML estimate for $\mathbf{R_h}$ and $\mathbf{R_u}$ assuming that $\mathbf{R_u}=\Sigma^2\mathbf{I}$, where $\mathbf{I}$ is the identity matrix. We extend below the above estimations for any arbitrary $\mathbf{R_u}$,

$$\hat{\mathbf{R}}_\mathbf{u} = \frac{\sum_{m=0}^{M-1}\sum_{n=0}^{N_p-1}(\mathbf{y}_{n,m} - s_{n,m}\hat{\mathbf{h}}_{n,m})(\mathbf{y}_{n,m} - s_{n,m}\hat{\mathbf{h}}_{n,m})^H}{(N_p-1)M} \tag{3.21}$$

$$\hat{\mathbf{R}}_\mathbf{h} = \frac{1}{M}\sum_{m=0}^{M-1}\hat{\mathbf{h}}_m\hat{\mathbf{h}}_m^H - \frac{1}{N_pE_p}\hat{\mathbf{R}}_\mathbf{u} \tag{3.22}$$

If a forgetting factor ε is used to update the estimated $\hat{\mathbf{R}}_\mathbf{u}$ and $\hat{\mathbf{R}}_\mathbf{h}$, the equations will have the form:

$$\hat{\mathbf{R}}_\mathbf{u}^m = (1-\varepsilon)\hat{\mathbf{R}}_\mathbf{u}^{m-1} + \frac{\varepsilon\sum_{n=0}^{N_p-1}(\mathbf{y}_{n,m} - s_{n,m}\hat{\mathbf{h}}_{n,m})(\mathbf{y}_{n,m} - s_{n,m}\hat{\mathbf{h}}_{n,m})^H}{(N_p-1)} \tag{3.23}$$

$$\hat{\mathbf{R}}_\mathbf{h}^m = (1-\varepsilon)\hat{\mathbf{R}}_\mathbf{h}^{m-1} + \varepsilon(\hat{\mathbf{h}}_m\hat{\mathbf{h}}_m^H - \frac{1}{N_pE_p}\hat{\mathbf{R}}_\mathbf{u}^m) \tag{3.24}$$

where $\hat{\mathbf{R}}_\mathbf{u}^m$ and $\hat{\mathbf{R}}_\mathbf{h}^m$ are the estimates for the mth time slot. The KLT algorithm finds the eigenvector and eigenvalues of those matrices .

The update algorithm for GD-RAKE starts by the update equation in terms of the eigenvalues and eigenvectors of $\hat{\mathbf{R}}_\mathbf{u}$,

$$\hat{\mathbf{\Omega}}_m\hat{\mathbf{\Lambda}}_m\hat{\mathbf{\Omega}}_m^H = (1-\varepsilon)\hat{\mathbf{\Omega}}_{m-1}\hat{\mathbf{\Lambda}}_{m-1}\hat{\mathbf{\Omega}}_{m-1}^H + \varepsilon\frac{1}{(N_p-1)}\sum_{n=0}^{N_p-1}\hat{\mathbf{u}}_{n,m}\hat{\mathbf{u}}_{n,m}^H, \tag{3.25}$$

In the above equation $\hat{\mathbf{\Omega}}_m$ and $\hat{\mathbf{\Lambda}}_m$ denote the matrices consisting of the eigenvectors and eigenvalues of $\hat{\mathbf{R}}_{\mathbf{u}}^m$ respectively. The vector $\hat{\mathbf{u}}_{n,m}$ is equal to

$$\hat{\mathbf{u}}_{n,m} = \mathbf{y}_{n,m} - s_{n,m}\hat{\mathbf{h}}_{n,m}. \tag{3.26}$$

At this point, we are at the equivalent state of (3.5) and the update algorithm explained in the previous section is applied first to update $\hat{\mathbf{\Omega}}_m$ and $\hat{\mathbf{\Lambda}}_m$. Then, we need to use the eigenvectors Ψ and square root of eigenvalues Υ of $\mathbf{R_u}^{-1}$, which is necessary for the GD-RAKE algorithm. From the matrix theory,

$$\Omega = \Psi, \tag{3.27}$$

and

$$\Lambda^{-1} = \Upsilon\Upsilon. \tag{3.28}$$

Using above equations we obtain

$$\hat{\mathbf{h}}' = \Upsilon\Omega^H\hat{\mathbf{h}}. \tag{3.29}$$

The eigenvalues $\mathbf{\Gamma}$ and eigenvectors $\mathbf{U}$ of the covariance matrix $\mathbf{R'_h} = E[\mathbf{h'h'^H}]$ should be updated as well. For this purpose the algorithm is repeated with the parameters $\hat{\mathbf{h}}'$, $\mathbf{\Gamma}$ and $\mathbf{U}$. Then the weights can be computed and the system can obtain the decision variable. According to [16] the update algorithm has the complexity of order $O(L^2)$, since KLT transforms for the matrices, whose complexity is in the order of $18L^3$ to $30L^3$, if Jacobi transformations is used according to [17]. The update algorithm has an complexity advantage.

3.3 Chapter Summary

In this chapter, we extended the update algorithm of Siala for the channel statistics of D-DTR to the update algorithm of channel and noise statistics of the GD-RAKE. Siala's algorithm requires KLT transform to form the weights. We introduced another update scheme, which directly updates the eigenvectors and eigenvalues, which has a complexity advantage.

Chapter 4

Simulation Results

4.1 Introduction

In this chapter we will present the performances of the systems introduced in the previous chapters in a simple DS-CDMA system. Siala [4] obtained the performance of the D-DTR in a DS-CDMA system based on a diffuse channel model with the assumptions:

1. The channel is a quasi static diffuse multipath Rayleigh fading channel. The channel impulse response changes independently from one realization to another, but the multipath intensity profile of the channel does not change.

2. The multipath intensity profile of the channel $\phi_h(\tau)$ is exponentially decaying with the rms delay spread T_m such that

$$\phi_h(\tau) = \begin{cases} \phi_H(0;0)\frac{e^{-\tau/T_m}}{T_m}, & \tau \geq 0 \\ 0 & \tau < 0 \end{cases}, \tag{4.1}$$

   where $\phi_H(0;0)$ is the average channel power.

3. Transmit shaping filter is the square root raised cosine filter with the rolloff factor

$\alpha = 0.22$ with the impulse response $g(\tau)$.

The assumptions about the received signal were:

1. The received signal is first filtered by an antialiasing filter and then sampled at a rate of $T_c/2$ i.e. at twice the chip rate. Due to the sampling, we will have a discrete-time version of the GD-RAKE and therefore we changed its acronym to GD-DTR.

2. The vector $\mathbf{h}$ at the input of the RAKE receiver denotes the total effect of the channel and transmit shaping filter.

3. The elements of $\mathbf{R_h}$ (i.e covariance matrix of $\mathbf{h}$) are found by

$$\mathbf{R_h}(x,y) = \int_{-\infty}^{\infty} \phi_h(\tau) g(d_x - \tau) g^*(d_y - \tau) d\tau, \tag{4.2}$$

   where d_x and d_y are the delays of the fingers $l = x$ and $l = y$.

4. The spreading sequences assumed to have perfect correlation properties.

5. The noise is assumed to be AWGN with variance $\Sigma^2 = 2N_0/T_c$, due to sampling, where N_0 is the power spectral density of the complex noise and there are no intereference present in the system.

We use all the above assumptions of [4], except the last one. In our system, noise plus interference are accounted for. The noise plus interference vector $\mathbf{u}_k$ have the covariance matrix $\mathbf{R_u}$. In our system, the (x,y)th element of the $\mathbf{R_u}$ which corresponds to the covariance between the interference values of the correlators with discrete delays d_x and d_y can be approximated as:

$$R_u(x,y) = \Sigma^2 \delta_{x,y} + E_I \int_{-\infty}^{\infty} g(d_x - \tau) g^*(d_y - \tau) d\tau, \tag{4.3}$$

where E_I and $\delta_{x,y}$ denote the power spectral density of the interference and the Kronecker delta function, respectively. The number of interferers and the effectiveness of the power control could affect the values of E_I. The thermal noise contributes to the covariance matrix with $\Sigma^2\delta_{x,y}$. In our simulations, to set the power of the interference, we define a noise rise coefficient η, which is equal to

$$\eta = (E_I + N_0)/N_0. \tag{4.4}$$

The noise rise coefficient is also related to the system load x through $x = (\eta - 1)/\eta$. The system load shows the percentage of energy coming from interference sources to the total energy of noise plus interference in the system [18]. If the load is higher than a specific value, the system does not accept new users. This concludes the system properties and in the next section, we present the simulation results with known channel and noise statistics.

4.2 Simulations with Known Channel and Noise Statistics

To show the performance of the GD-DTR, the first channel we simulated has the rms delay spread of T_m=0.25T_c, which is observed in UMTS channels in [19] by Foo *et al.* Since we are going to simulate channels with T_m=0.5T_c and T_m=0.125T_c too, we are presenting all of the delay profiles of those channels in Fig 4.1.

The number of correlators L is equal to 9. This system collects %99 of the average received energy according to [4]. We assumed that, the number of data bits N_d and pilot symbols per channel realization N_p are 36 and 4 respectively. This assumption is

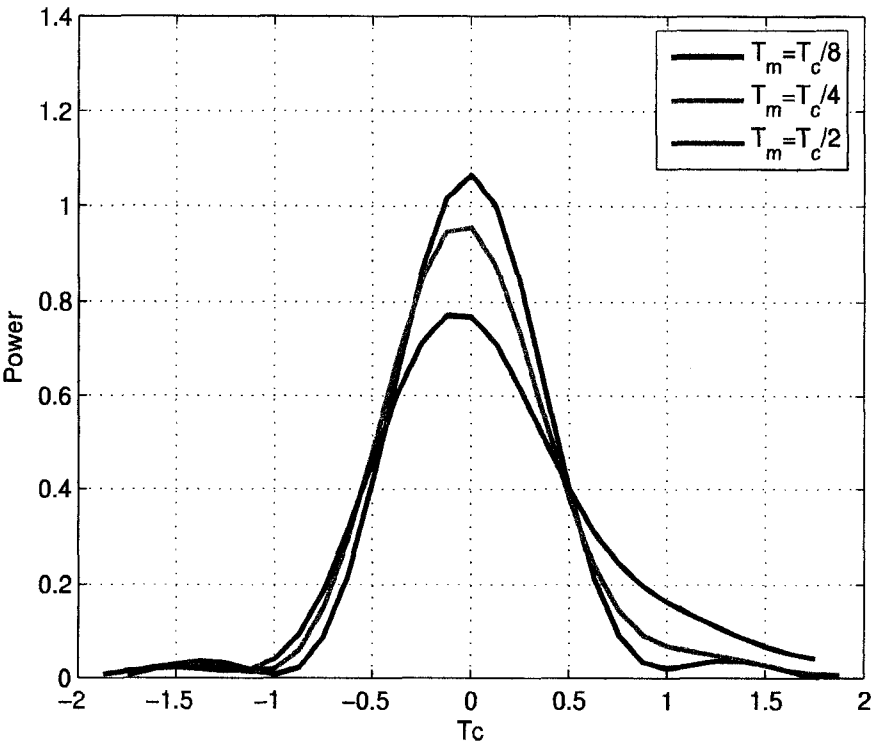

Figure 4.1: The observed power delay profiles of the channels with rms delay spread values 0.5Tc,0.25Tc and 0.125Tc including the effect of root raised cosine pulse shaping filter with rolloff equal to 0.22.

taken from UMTS specifications [20]. To simulate a highly loaded system we set η=10. The reason behind working in a heavily loaded system is that optimizations are mainly sought to increase the capacity for the same maximum load. The results for the systems are shown in Figure 4.2. In our work, all performance curves from top to bottom at the left edge follow the same order of the legend of their figure. As can be seen from Figure 4.2, the analytical and simulated performances of GD-DTR coincide and the gain of the GD-DTR compared to the C-DTR is about 0.7 dB at a bit error rate (BER) of 10^{-2}. Thus, employing the G-DTR causes a performance loss, whereas the D-DTR

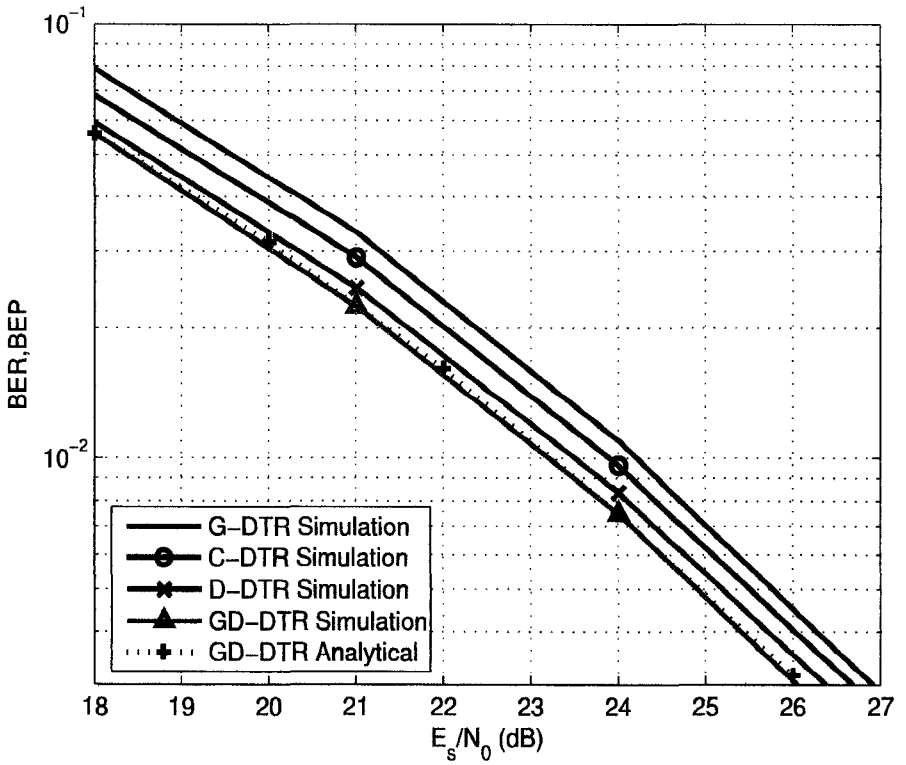

Figure 4.2: BER performances of G-DTR, C-DTR, D-DTR and GD-DTR, where L=9, N_p=4, α=0.22, T_m=0.25T_c, η = 10 and E_s denotes the average received symbol energy. (The performance curves from top to bottom follow the same order of the legend)

has almost 0.4 dB gain compared to the C-DTR. For the rest of our work, we will not show the analytical performance results of the GD-DTR for the clarity of presentation. We choose 10^{-2} BER for comparison because it is usually the target uncoded bit error rate.

In the second set of simulations, we changed the delay spread of the channel to T_m=0.5T_c. Such an increase in the delay spread increases the diversity order of the channel and therefore the performances of all the receivers (Figure 4.3) compared to the first simulation set (Figure 4.2). If we focus only on the results in the second set, we

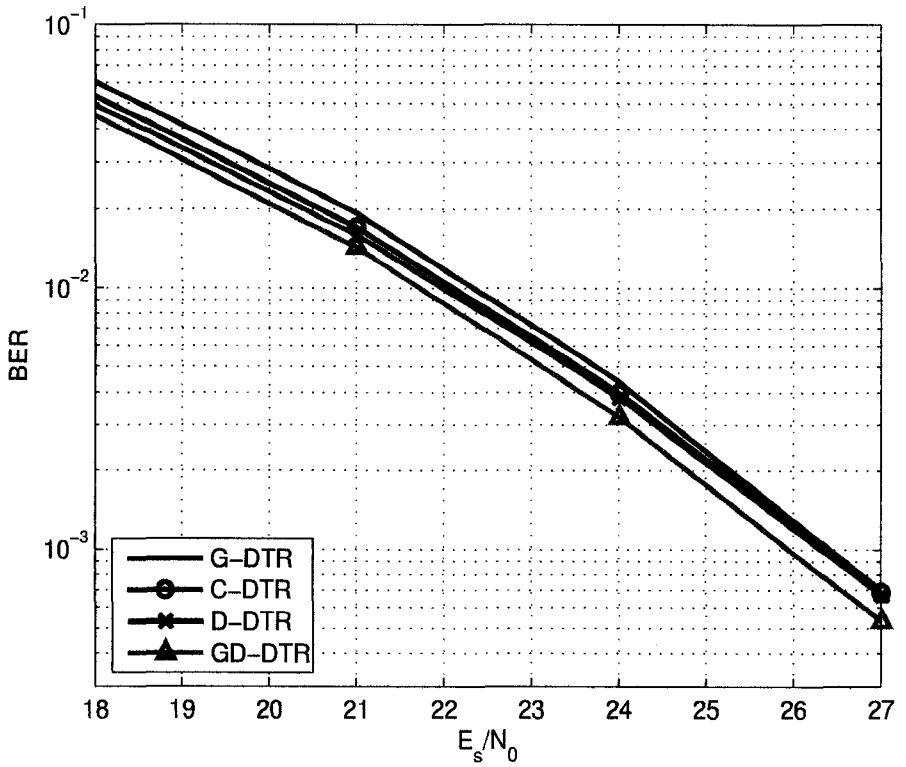

Figure 4.3: BER performances of G-DTR, C-DTR, D-DTR and GD-DTR, where L=9, N_p=4, T_m=0.5T_c.

observe that at a BER of 10^{-2} the performances of the C-DTR, the D-DTR are almost the same, whereas the GD-DTR has 0.4 dB gain compared to the C-DTR. Another observation is that higher SNR's improve the performance of the G-DTR the most, such that at 27 dB the G-DTR has the same performance of the C-DTR and D-DTR.

The third set of simulations shows the results for the delay spread value of the channel equal to T_m=0.125T_c. This decrease in the delay spread results in poorer performances of all receivers compared to the first and second simulation sets as seen in Figure 4.4, as expected. Additionally the performance gap between the GD-DTR and

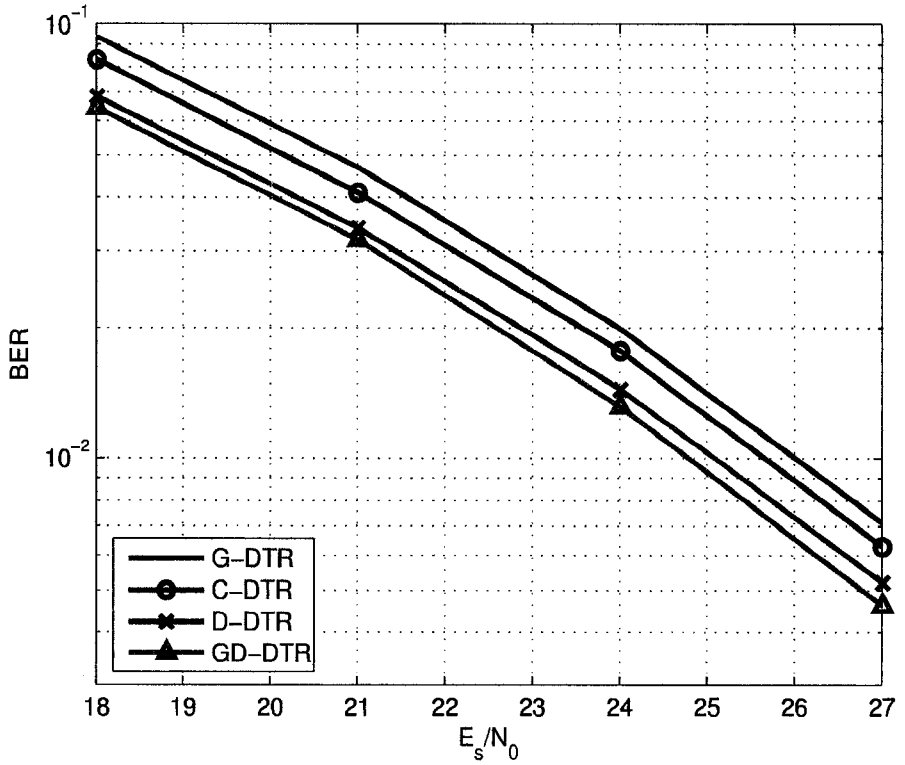

Figure 4.4: BER performances of G-DTR, C-DTR, D-DTR and GD-DTR, where L=9, N_p=4, T_m=0.125T_c.

C-DTR widens such that at a BER of 10^{-2} the GD-DTR has 0.9 dB gain compared to the C-DTR.

To study the effect of pulse shaping, we increased the roll off factor to α=0.5, while taking the T_m=0.25. As seen in Figure 4.5, the gain of the GD-DTR compared to the C-DTR increased with respect to Figure 4.2 and now is equal to 1 dB at a BER of 10^{-2}. The performance difference between the D-DTR and the C-DTR decrease. Such an effect was observed in [4] for uncorrelated noise as well. Although the increase of the rolloff factor decreases the correlation between the noise plus interference samples,

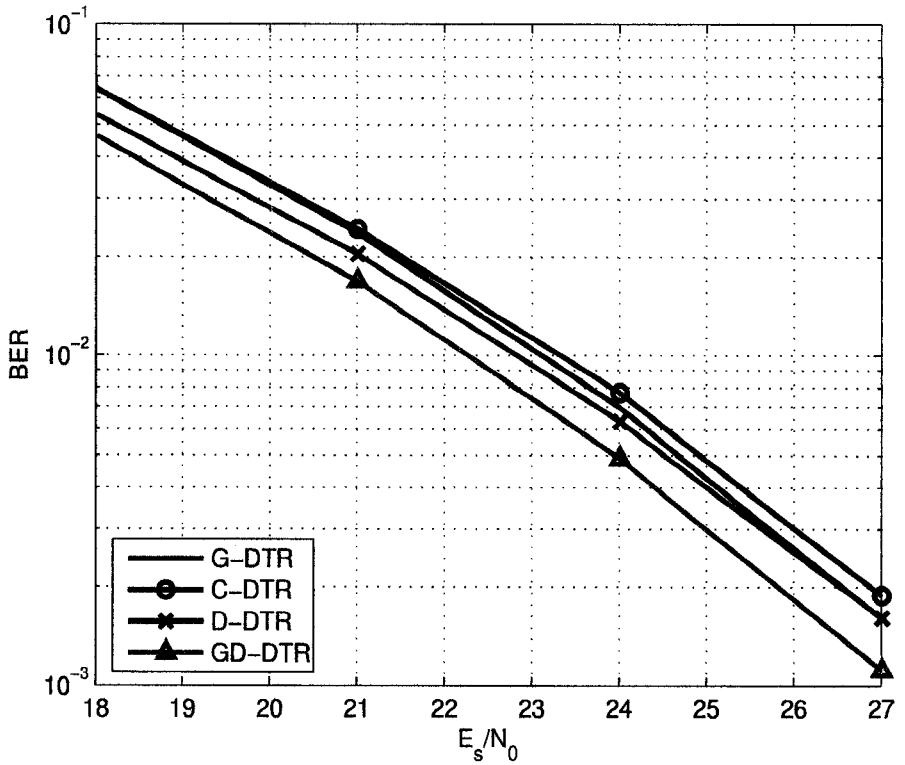

Figure 4.5: BER performances of (from top to bottom at 18dB SNR, in that order) G-DTR, C-DTR, D-DTR and GD-DTR, where L=9, N_p=4, α=0.5, T_m=0.25T_c.

it reduces the correlation of the channel samples as well. The G-DTR benefits from this reduction and has better performance than the C-DTR after 18.1 dB and at 27 dB the performance of the G-DTR is equal to the performance of the D-DTR.

The last set of simulation with QPSK modulation is designed to show the effect of the number of pilot symbols on the performance of different RAKE reception methods. We use the simulation parameters of the first simulation, i.e. L=9, T_m=0.25T_c. The SNR of the system is set to E_s/N_0=24dB. The number of pilot symbols changes from 1 to 8. As seen in Figure 4.6, for a BER of 10^{-2}, the GD-DTR needs only 2 pilot symbols whereas

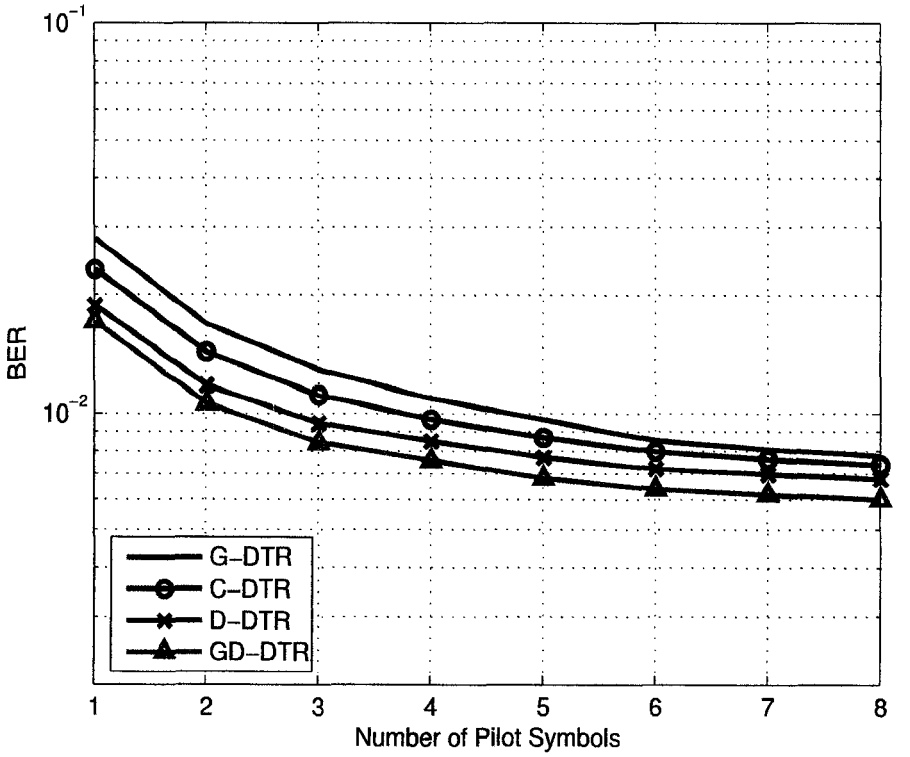

Figure 4.6: BER performances of G-DTR, C-DTR, D-DTR and GD-DTR, where L=9, T_m=0.25T_c, E_s/N_0=24dB.

the D-DTR and the C-DTR require 3 and 4 pilot symbols, respectively. Another point is that the performance of the G-DTR is worse than that C-DTR even if 8 pilot symbols per channel realization are utilized.

The last two simulations of this section finds out the performance of the receivers in higher order modulations. For the 8PSK modulation scheme, we use gray coding and choose the simulation parameters of the first simulation, i.e. L=9, T_m=0.25T_c, $N_p = 4$. The results can be seen in Figure 4.7. The gain of the GD-DTR compared to the C-DTR is about 0.4 dB at a bit error rate (BER) of 10^{-2}. At the same bit error rate

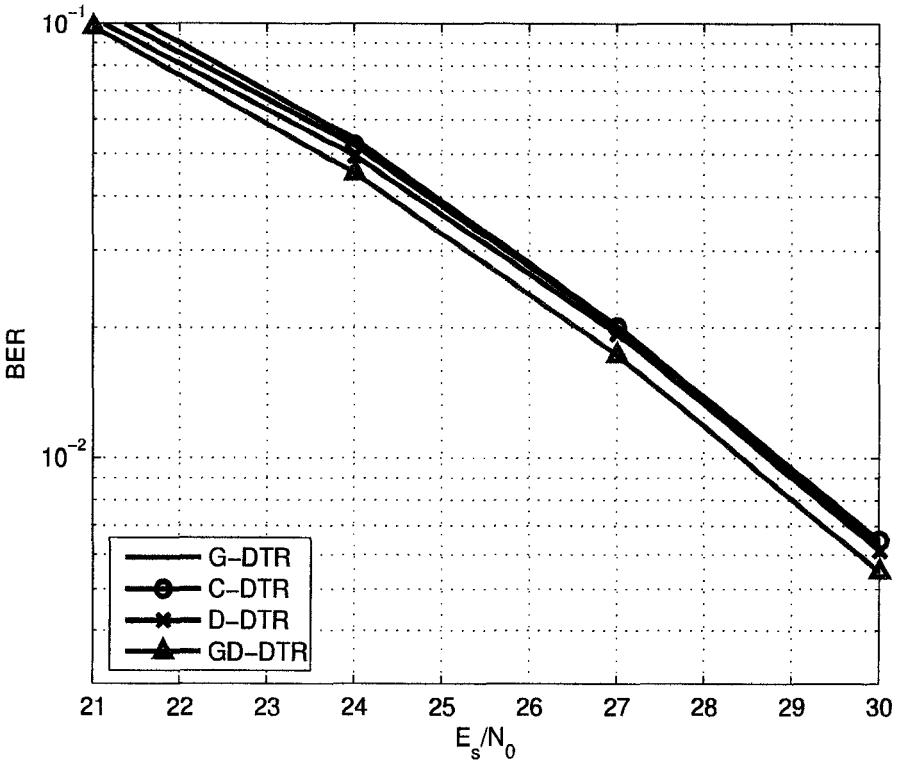

Figure 4.7: BER performances of (from top to bottom at 22dB SNR, in that order) G-DTR, C-DTR, D-DTR and GD-DTR with 8PSK modulation, where L=9, N_p=4, α=0.22, T_m=0.25T_c.

both the D-DTR and the G-DTR have gains around 0.1 dB compared to the C-DTR. Compared to QPSK results D-DTR and GD-DTR have less gain and G-DTR has no loss but gain. To understand those results we should keep in mind, that to achieve a specific BER, 8PSK requires more SNR than the QPSK and the pilot symbols in our simulations have the same energy with the data symbols. Therefore the quality of the channel estimates is higher for 8PSK than the QPSK at the same BER and we observe above results.

We finish this section, with the simulation of 16QAM modulation (Figure 4.8). The

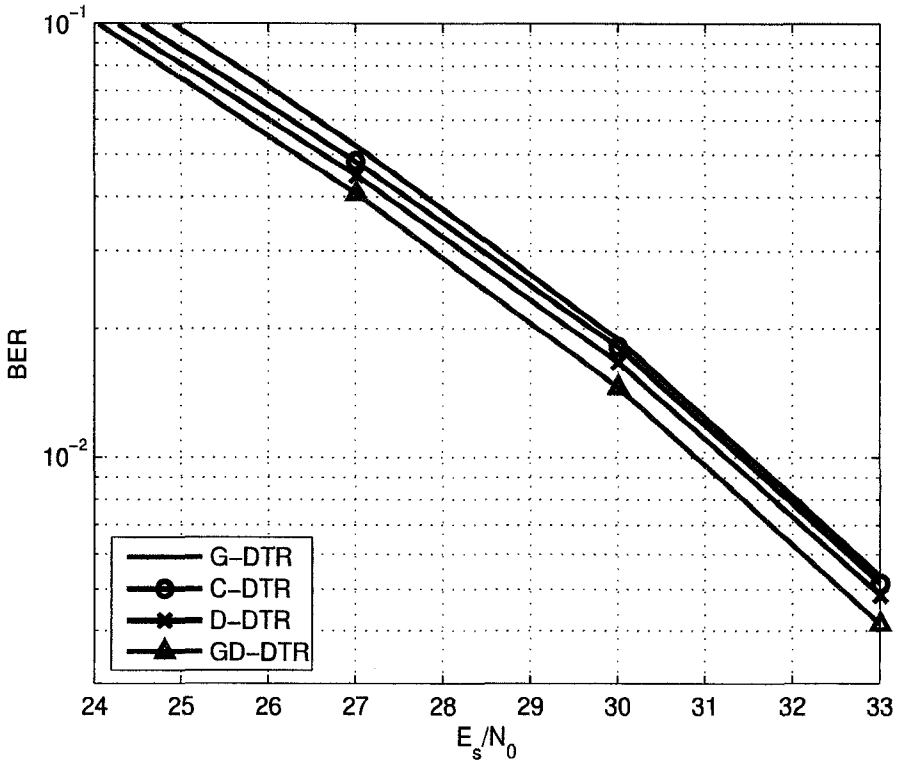

Figure 4.8: BER performances of (from top to bottom in that order) G-DTR, C-DTR, D-DTR and GD-DTR with 16QAM modulation, where L=9, N_p=4, α=0.22, T_m=0.25T_c.

simulation parameters are unchanged. At a BER of 10^{-2}, we observe that the gain of the GD-DTR compared to the C-DTR is about 0.5 dB. Unlike the 8PSK we observe a loss for G-DTR and a 0.2 dB gain for D-DTR compared to the C-DTR, which could be explained with the increase of the sensitivity to channel estimation errors due to the increase of the modulation order.

The next section will be about the estimated channel and noise statistics.

4.3 Simulations with Estimated Channel and Noise Statistics

We start our simulations with the KLT algorithm, in which first the covariance matrices are estimated and then eigenvalues and eigenvectors are obtained by the use of the KLT transform. About the obtained eigenvalues, in [4] all of them are used to set the weights. However our simulations show that due to the nature of the estimation, the estimated covariance matrices could be ill-conditioned and have negative eigenvalues. Therefore setting the weights of the negative eigenvalues equal to 0, will improve the performance of the D-DTR and GD-DTR.

During the simulations, we generate channel realizations 10ms/15 apart, since in UMTS/FDD systems the pilot symbols are put in time slots of 10ms/15 duration. The channel has the Doppler spread corresponding to a speed of 120 km/h at a carrier frequency of 2 GHz (f_d=222Hz). In Figure 4.9, we present the performance of the conventional discrete-time RAKE receiver and the D-DTR for the case of uncorrelated noise, i.e noise rise coefficient is equal to η=1. The simulation parameters are: the rms delay spread, which is equal to T_m=0.25T_c, the number of correlators, L=9, and the SNR E_s/N_0=14dB.

The important result of the simulation is that if only positive eigenvalues are used, the performance of the D-DTR is better than the C-DTR at all ε values up to ε=1. But if all eigenvalues (including the negative ones) are employed, the performance of the D-DTR is worse than the C-DTR if ε is larger than 0.04. At ε=0.1 we observe the worst performance of the D-DTR. After ε=0.1 the performance improves and at ε=1 it is almost equal to the performance of the C-DTR.

In Figure 4.10, we present the simulation results of the GD-DTR. We set η=10, to have maximum noise correlation for stable system operation. The rest of the simulation

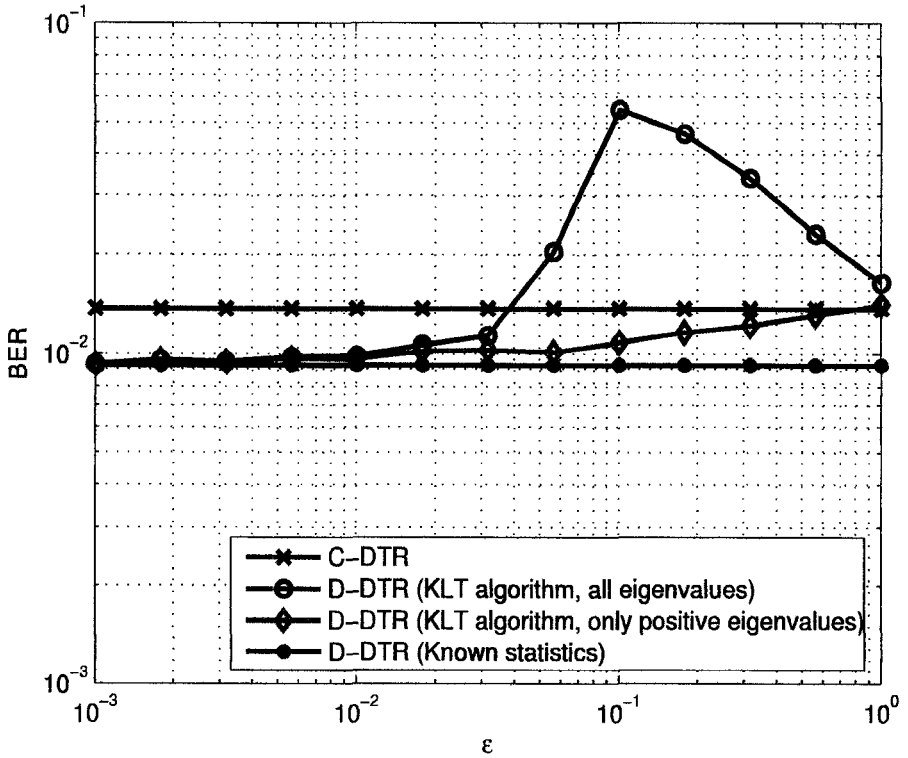

Figure 4.9: The BER performances of C-DTR, D-DTR with estimated statistics (KLT algorithm), D-DTR with estimated statistics employing only positive eigenvalues (KLT algorithm) and D-DTR with known statistics where E_s/N_0=14dB, L=9, N_p=4, T_m=0.25T_c.

parameters are the same with the previous simulation, except for E_s/N_0, which is equal to 23dB.

As seen in Figure 4.10 there is a monotonic decrease in the performance of the GD-DTR with positive eigenvalues with the increase of ε and after ε=0.01 its performance is worse than the C-DTR. However if all the eigenvalues are employed we observe a local maximum for the bit error rate at ε=0.01 and the global maximum is at ε=1. The reason behind the poor performance of the GD-DTR at large values of ε, is the

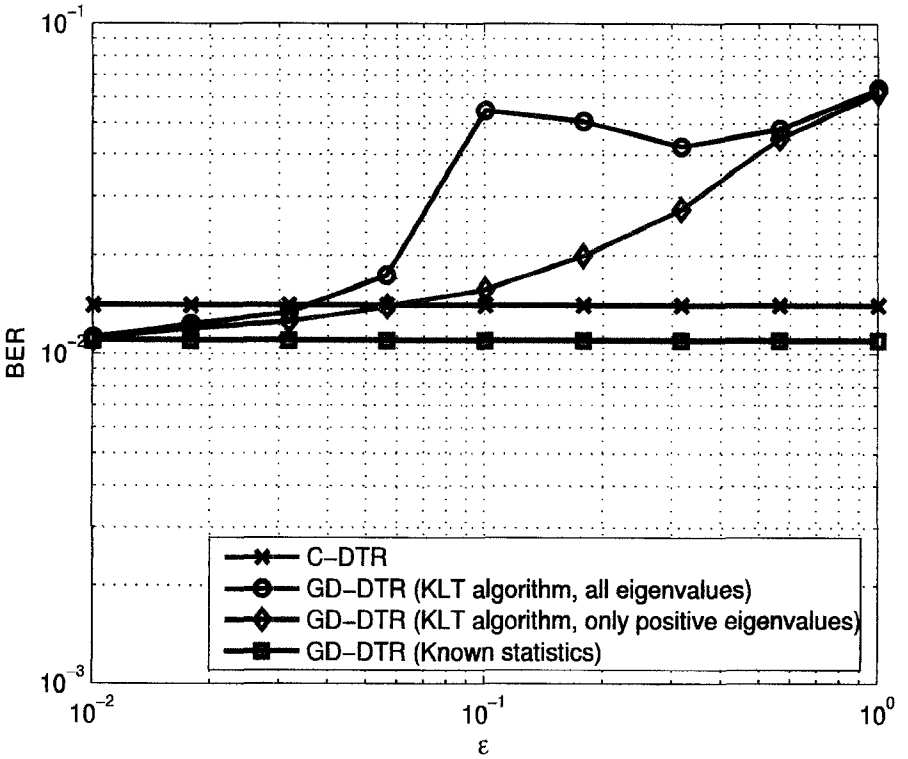

Figure 4.10: BER performances of C-DTR, GD-DTR with estimated statistics (KLT algorithm), GD-DTR with estimated statistics employing only positive eigenvalues (KLT algorithm) and GD-DTR with known statistics, where L=9, N_p=4, T_m=0.25T_c

inaccurate estimation of the $\mathbf{R_u}$, which affects the performance.

In the last simulation with the KLT algorithm, we show the performance of the D-DTR, GD-DTR, G-DTR and C-DTR with the above simulation parameters for comparison purpose. The estimation of $\mathbf{R_u}$ affects the performance of both the GD-DTR and G-DTR. As seen in Figure 4.11 after ε=0.1 the D-DTR has the best performance since it is not affected by the estimation of $\mathbf{R_u}$. Nevertheless ε=0.1 is equivalent to a very short distance for statistics estimation. In [4] the mean averaging time corresponding to ε=0.01 is given as 2.2 meters for 120 km/h mobile speed (99 time slots). Typically

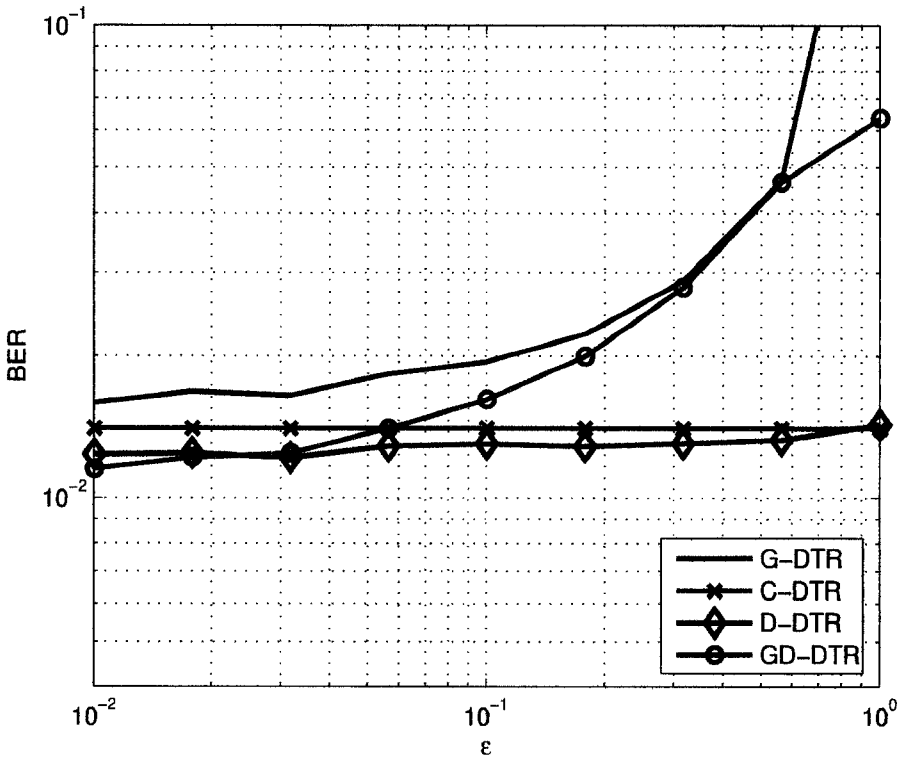

Figure 4.11: The BER performances of G-DTR, D-DTR, GD-DTR with estimated statistics (KLT algorithm) and C-DTR, where L=9, N_p=4, T_m=0.25T_c

in such a short distance neither the medium scale channel effects nor the average power of interference changes and for ε=0.01 the GD-DTR has the best performance among all the systems. This ends the simulation results with the KLT algorithm.

Our simulations with the update algorithm begin with the performance of the D-DTR. In Figure 4.12, we present the performance of the conventional discrete-time RAKE receiver and the D-DTR with known and estimated statistics. The simulation parameters are the rms delay spread is equal to T_m=0.25T_c, number of correlators L=9, mobile speed 120km/h and $\varepsilon = 0.01$.

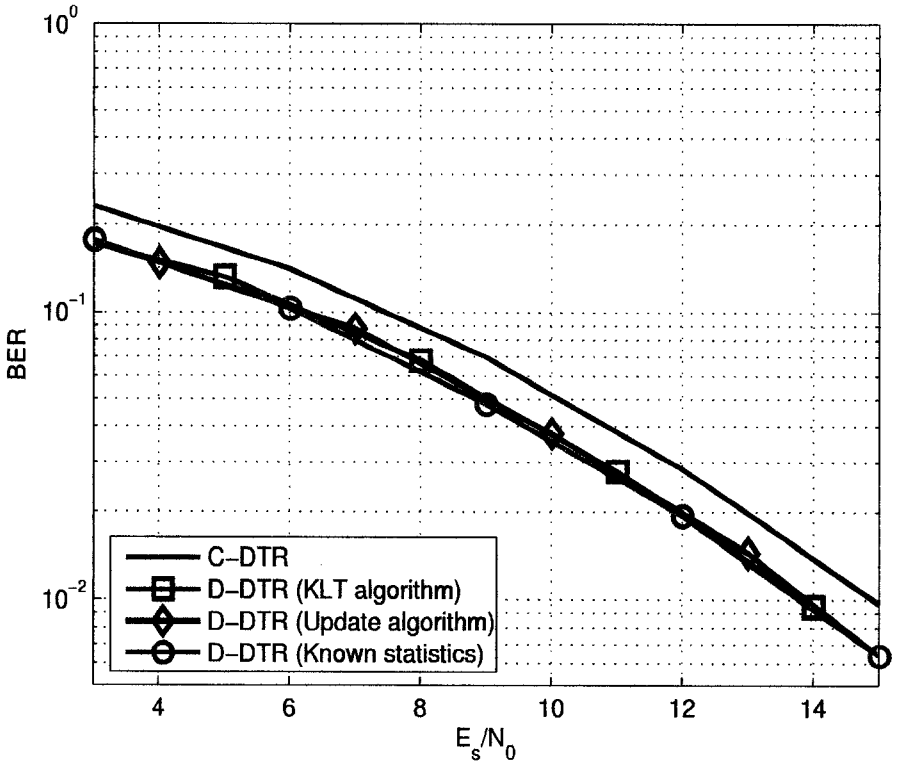

Figure 4.12: The BER performances of C-DTR, D-DTR with the update algorithm, D-DTR with the KLT algorithm and D-DTR with known statistics, where L=9, N_p=4, T_m=0.25T_c, η=1 and ε=0.01.

In Figure 4.12 the performance difference between the estimated and known statistics is very small. Since the update algorithm is less complex than the KLT algorithm, it can be efficiently used to update the eigenvalues and the eigenvectors.

In the next simulation we observe the performance of the update algorithm at different values of ε. The simulation parameters are the same as the previous simulation, except that E_s/N_0 is fixed to 14 dB.

According to the results shown in Figure 4.13, the update algorithm is more sensitive to the value of the ε than the KLT algorithm. However we observe again that at

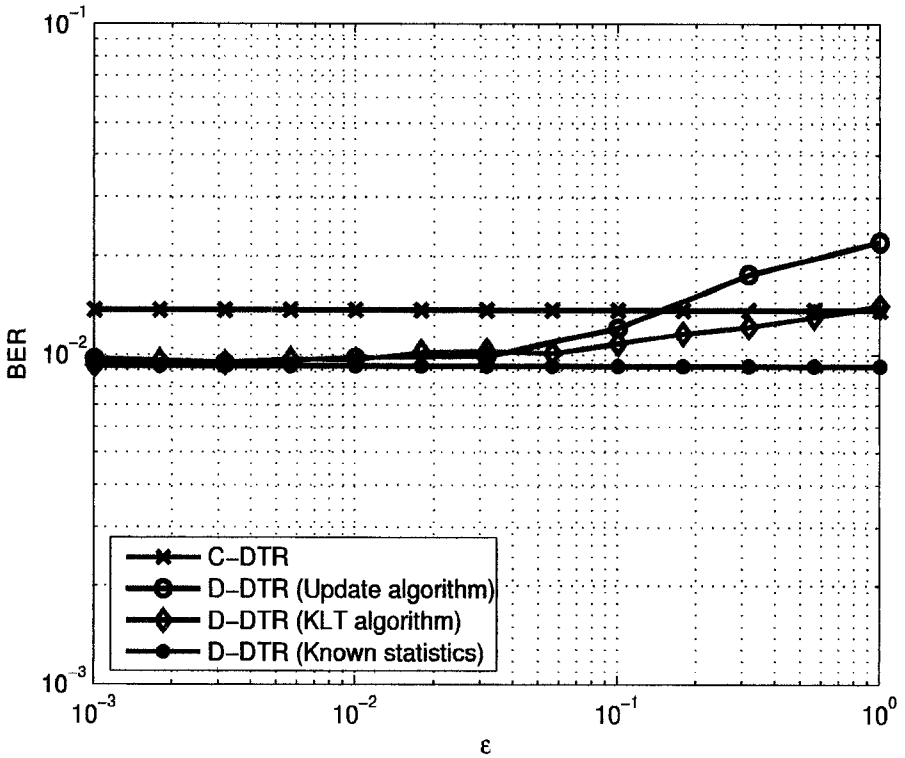

Figure 4.13: The BER performances of C-DTR, D-DTR with the update algorithm, D-DTR with the KLT algorithm, D-DTR with known statistics, where L=9, N_p=4, T_m=0.25T_c, E_s/N_0=14dB.

$\varepsilon = 0.01$, the update algorithm can follow the eigenvalues and the eigenvectors.

The update algorithm performs well with the GD-DTR receiver too. In Figure 4.14, we present the performance of the conventional discrete-time RAKE receiver and the GD-DTR with known and estimated statistics with the update algorithm. The simulation parameters are: the rms delay spread, which is equal to T_m=0.25T_c, number of correlators L=9, η=10 and $\varepsilon = 0.001$. Number of pilot symbols is set to 4 to show the performance gain of the GD-DTR.

In Figure 4.14 the performance difference between the estimated and known statis-

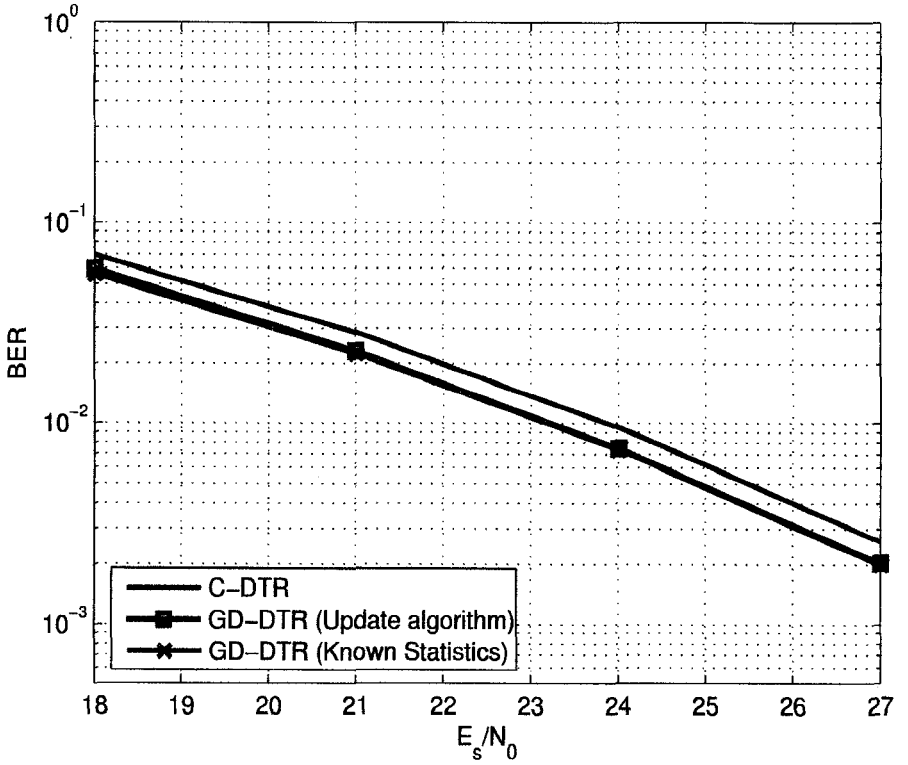

Figure 4.14: BER performances of C-DTR, GD-DTR with the update algorithm, GD-DTR with known statistics, where L=9, N_p=4, T_m=0.25T_c, η=10 and ε=0.001.

tics is very small. In the next simulation we observe the performance of the update algorithm at different values of ε. The simulation parameters are the same with the previous simulation except that the E_s/N_0 is fixed to 23 dB.

The results shown in Figure 4.15 proves one more time, that the update algorithm is sensitive to the value of the ε more than the KLT algorithm. We observe that if the values of ε is higher than 0.003, the update algorithm cannot follow the eigenvalues and the eigenvectors. In [4] the mean averaging time corresponding to ε=0.003 is given as 7.5 meters for 120 km/h mobile speed (333 time slots), which is still a small value

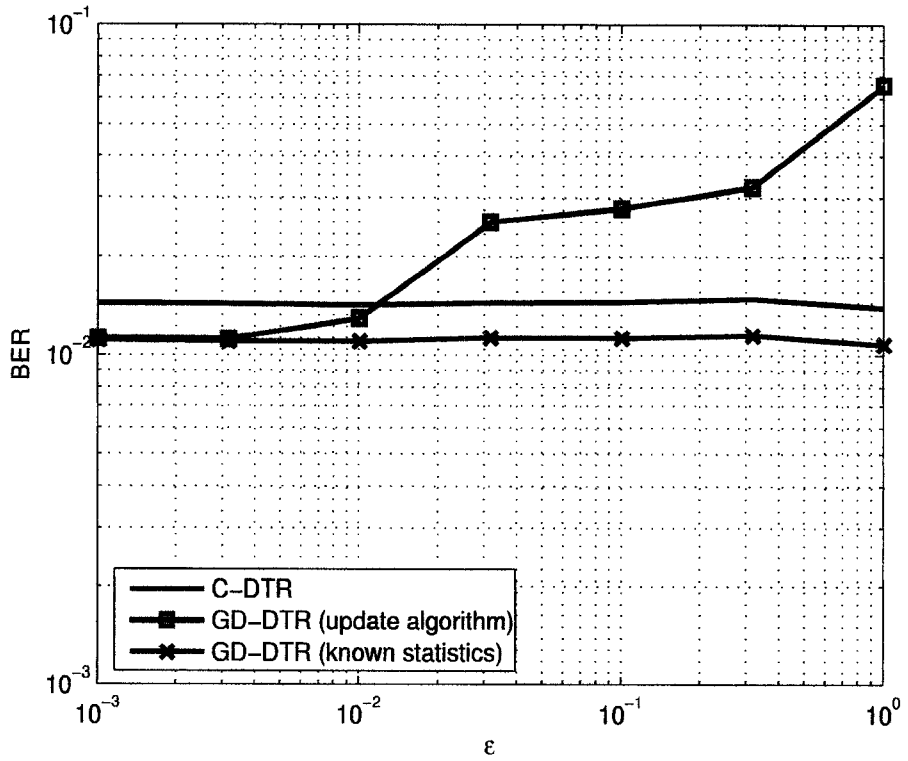

Figure 4.15: BER performances of C-DTR, G-DTR with the update algorithm, G-DTR with known statistics, where L=9, N_p=4, T_m=0.25T_c, η=10 and E_s/N_0=23dB.

for the change of the channel and interference characteristics. In conclusion, we can say that the system can work in real life scenarios. In the next section we revisit the modeling of interference based on UMTS downlink.

4.4 Simulations in UMTS downlink

The focus of this section is remodeling the interference according to UMTS downlink. Bottomley *et al.* showed how the weights can be computed for the downlink of UMTS

in [2]. We will go through their example and then provide the performance of both G-RAKE and GD-RAKE. We will call the systems G-RAKE and GD-RAKE in this section, since the simulations are done for chip spaced sampling. In the downlink of the UMTS system, the base station spreads each user's symbol with a user and symbol specific spreading waveform.We assume that there are K users in the system and that the ith symbol of user k is spread using the spreading waveform $a_{k,i}(t)$. The transmitted signal for the user k can be written as:

$$x_k(t) = \sqrt{E_k} \sum_{i=-\infty}^{\infty} s_{k,i} a_{k,i}(t - iT_k), \tag{4.5}$$

where E_k is the symbol energy and T_k is the symbol duration for user k. The spreading waveform $a_{k,i}(t)$ consists of a complex chip sequence convolved with the chip pulse shape $g(t)$

$$a_{k,i}(t) = \frac{1}{\sqrt{N}} \sum_{n=0}^{N-1} c_{k,i,n} g(t - nT_c), \tag{4.6}$$

where $c_{k,i,n}$ is the nth chip of the complex chip sequence, which is obtained by the multiplication of the user specific orthogonal spreading code with the complex base station and symbol specific scrambling code. Both codes have unit energy. Orthogonal spreading codes provide the transmission of different users data simultaneously without interference, whereas scrambling codes improve the multipath performance and reduce intracell interference. For $g(t)$, a root raised cosine pulse shaping is used. After the spreading operation, the signals are added synchronously and transmitted through the multipath channel, whose model was given previously. To explain the system, we will take the 0th symbol of the user 0 as the desired symbol. We can write the received signal at the receiver of user 0 as:

$$r(t) = \sum_{j=0}^{J-1} h_j x_0(\tau - \tau_l) + \sum_{k=1}^{K-1} \sum_{j=0}^{J-1} h_j x_k(\tau - \tau_j) + n_T(t) \tag{4.7}$$

where $n_T(t)$ denotes the thermal noise with one sided power spectral density N_0. At the mobile receiver, each RAKE finger despreads the received signal with the spreading waveform $a_{0,0}(t)$. The output of a RAKE finger with delay t can be expressed as

$$y(t) = \int_0^{T_s} r(\tau + t) a_{0,0}(\tau) d\tau \tag{4.8}$$

which is equal to

$$y(t) = \sum_{k=0}^{K-1} \sum_{j=0}^{J-1} \sum_{i=-\infty}^{\infty} \sqrt{E_k} h_j s_k(i) R_{k,i}(t - iT - \tau_j) + \sqrt{N_0} n'(t) \tag{4.9}$$

In the above equation $\sqrt{N_0} n'(t)$ denotes the noise after despreading, and $R_{k,i}(t)$ is the crosscorrelation function between the waveform of the ith symbol of the kth user and the desired symbol (0th symbol of the 0th user). This function, which is important to find the covariance matrix of noise plus interference, is equal to,

$$R_{k,i}(t) = \int_{-\infty}^{\infty} a_{k,i}(t + \tau) a^*_{0,0}(\tau) d\tau. \tag{4.10}$$

In [2], it is given by

$$R_{k,i}(t) = \frac{1}{N} \sum_{m=1-N}^{N-1} C_{k,i}(m) R_g(t + mT_c) \tag{4.11}$$

where $R_g(t) = \int_{-\infty}^{\infty} g(t+\tau) g^*(\tau) d\tau$ is the autocorrelation function of the chip pulse shape and $C_{k,i}(m)$ is the crosscorrelation function between complex spreading sequence of the kth user's ith symbol and the desired symbol. For the assumed spreading sequences (complex random scrambling codes and user specific spreading sequences) $C_{k,0}(0) =$

$0, k \neq 0$, $C_{0,0}(0) = N$ and

$$E[C_{k,i}(m)C^*_{k,i}(n)] = 0, m \neq n \tag{4.12}$$

$$E[|C_{k,i}(m)|^2] = \begin{cases} 0, & i = m = 0, k \neq 0 \\ N^2 & i = m = k = 0 \\ N - |m| & \text{otherwise} \end{cases} \tag{4.13}$$

From (4.9), we can split the RAKE filter output to four terms: the desired component $y_d(t)$, the self interference component $y_{ISI}(t)$, the multiuser interference component $y_{MUI}(t)$, and the thermal noise component $n'(t)$. That is,

$$y(t) = \sqrt{E_0}\, y_d(t)s_{0,0} + \sqrt{E_0}\, y_{ISI}(t) + \sqrt{E_I}\, y_{MUI}(t) + \sqrt{N_0}\, n'(t) \tag{4.14}$$

where

$$y_d(t) = \sum_{j=0}^{J-1} h_j R_{0,0}(t - \tau_l) \tag{4.15}$$

$$y_{ISI}(t) = \sum_{j=0}^{J-1} \sum_{\substack{i=-\infty \\ i\neq 0}}^{\infty} h_j s_0(i) R_{0,i}(t - iT - \tau_j) \tag{4.16}$$

$$y_{MUI}(t) = \frac{1}{\sqrt{E_I}} \sum_{k=1}^{K-1} \sqrt{E_k} \sum_{j=0}^{J-1} \sum_{i=-\infty}^{\infty} h_j s_k(i) R_{k,i}(t - iT - \tau_j) \tag{4.17}$$

and $E_I = \sum_{k=1}^{K} E_k$ is the total symbol energy of intracell interference. From (4.14) the output vector of the RAKE fingers $\mathbf{y}$ can be written as

$$\mathbf{y} = \sqrt{E_0}\,\mathbf{y}_d s_{0,0} + \sqrt{E_0}\,\mathbf{y}_{ISI} + \sqrt{E_I}\,\mathbf{y}_{MUI} + \sqrt{N_0}\,\mathbf{n}' \tag{4.18}$$

If we compare (4.18) and (2.10), $\mathbf{h}$ in (2.10) corresponds to;

$$\mathbf{h} = \sqrt{E_0}\mathbf{y}_d \tag{4.19}$$

and $\mathbf{u}$ in (2.10) corresponds to;

$$\mathbf{u} = \sqrt{E_0}\,\mathbf{y}_{ISI} + \sqrt{E_I}\,\mathbf{y}_{MUI} + \sqrt{N_0}\,\mathbf{n}' \tag{4.20}$$

Assuming $\mathbf{y}_{ISI}, \mathbf{y}_{MUI}$ and $\mathbf{n}'$ are uncorrelated, the covariance matrix $\mathbf{R_u}$ is equal to:

$$\mathbf{R_u} = E_0\,\mathbf{R}_{ISI} + E_I\,\mathbf{R}_{MUI} + N_0\,\mathbf{R}'_{\mathbf{n}} \tag{4.21}$$

where $\mathbf{R}_{ISI} = E[\mathbf{y}_{ISI}\mathbf{y}_{ISI}^{\dagger}]$. As an example, consider the RAKE finger $l = 1$ with delay d_1 and $l = 2$ with delay d_2; we can compute their corresponding element in the matrix $\mathbf{R}_{ISI}$ by

$$R_{ISI}(d_1, d_2) = \sum_{j=0}^{J-1}\sum_{q=0}^{J-1}\sum_{\substack{i=-\infty \\ i\neq 0}}^{\infty} h_j h_q^* E[R_{0,i}(d_1 - iT - \tau_j)R_{0,i}^*(d_2 - iT - \tau_q)] \tag{4.22}$$

Expanding the above equation with (4.11) and (4.13) gives,

$$\begin{aligned} R_{ISI}(d1, d2) = \; & \tfrac{1}{N^2}\textstyle\sum_{j=0}^{J-1}\sum_{q=0}^{J-1}\sum_{\substack{i=-\infty \\ i\neq 0}}^{\infty} h_j h_q^* \sum_{m=1-N}^{N-1}(N - |m|) \\ & \times R_g(d_1 + mT_c - iT - \tau_j)R_g^*(d_2 + mT_c - iT - \tau_q) \end{aligned} \tag{4.23}$$

In (4.21) $\mathbf{R}_{MUI} = E[\mathbf{y}_{MUI}\mathbf{y}_{MUI}^{\dagger}]$ and similar to the above equation, the elements of $\mathbf{R}_{MUI}$ can be computed as

$$\begin{aligned} R_{MUI}(d_1, d_2) = \; & \tfrac{1}{N^2} \textstyle\sum_{j=0}^{J-1} \sum_{q=0}^{J-1} \sum_{i=-\infty}^{\infty} h_q h_j^* \sum_{m=1-N}^{N-1} (N - |m|) \\ & \times R_g(d_1 + mT_c - iT - \tau_q) R_g^*(d_2 + mT_c - iT - \tau_j)(1 - \delta(m)\delta(i)) \end{aligned} \tag{4.24}$$

In (4.21) $\mathbf{R}'_{\mathbf{n}} = E[\mathbf{n}'\mathbf{n}'^{\dagger}]$ and

$$R_{n'}(d_1, d_2) = \frac{1}{N} \sum_{m=1-N}^{N-1} C_{0,0}(m) R_g(d_1 - d_2 + mT_c) \tag{4.25}$$

For the elements of $\mathbf{y}_d$, we have

$$y_d(d_1) = \frac{1}{N} \sum_{j=0}^{J-1} h_j \sum_{m=1-N}^{N-1} C_{0,0}(m) R_g(d_1 - \tau_j + mT_c). \tag{4.26}$$

Using the above equations and appropriate delay values, all the elements of $\mathbf{y}_d$ and $\mathbf{R}_{\mathbf{u}}$ can be found. $y_d(d_1)$ and $\mathbf{R}'_{\mathbf{n}}$ are functions of the desired signals spreading code autocorrelation function $C_{0,0}(m)$. We can use the average of the autocorrelation functions as an approximation, which is equal to

$$E[C_{0,0}(m)] = N\delta(m) \tag{4.27}$$

Replacing $C_{0,0}(m)$ with the above equation in (4.25) and (4.26), we obtain $\bar{\mathbf{R}}_{n'}$ an approximation of $\mathbf{R}_{n'}$, and $\bar{y}_d(d_1)$ an approximation of $y_d(d_1)$ such that,

$$\bar{R}_{n'}(d_1, d_2) = R_g(d_1 - d_2) \tag{4.28}$$

$$\tilde{y}_d(d_1) = \sum_{j=0}^{J-1} h_j R_g(d_1 - \tau_j) \tag{4.29}$$

With the last two equations, we have all the elements needed to calculate $\mathbf{R_u}$, $\mathbf{h}$ and consequently $\mathbf{w}$ in the downlink system.

To compare with the results available in the literature, we have chosen a specular rather than a diffuse channel with 3 chip spaced multipaths as in [2]. The paths have the relative average power of 0, -0.75, -1.5 dB. The simulated system resembles the downlink of WCDMA. Every user's data are spread first by a user specific Walsh-Hadamard orthogonal code then multiplied by the base station specific scrambling code. The number of users is 24. The spreading gain is 128. The modulation scheme is QPSK. The number of pilot symbols is 4. The finger locations are aligned with the paths for conventional RAKE receiver, i.e the delays are [0 -1 -2] chip periods. We set the delay of the first path to zero as a reference. The results are shown in Figure 4.16. In contrast to all previous simulations, the GD-RAKE has the worst performance among all the receivers. The performance of the G-RAKE is very close to GD-RAKE. The D-RAKE and the conventional RAKE receivers have 1.5 dB advantage at a BER of 10^{-2} and have a smaller error floor. Although it can not be seen in the Figure, the D-RAKE has a minuscule gain compared to the conventional RAKE. Why did we observe such results? There are several explanations, firstly, the three paths are close to have a uniformly distributed delay spread. The third path have 70% as much energy as the first path. Secondly, since the paths are separated by a chip period, the interference is less correlated then the half chip spaced version. However the main performance loss of the G-RAKE and GD-RAKE is due to the miscalculation of $\mathbf{R_u}$. Since the $\mathbf{R_u}$ is a function of $\mathbf{h}$, the calculation with the estimated $\mathbf{h}$ leads to poor performance.

In Figure 4.17, we show the performance of the same systems with an extra finger

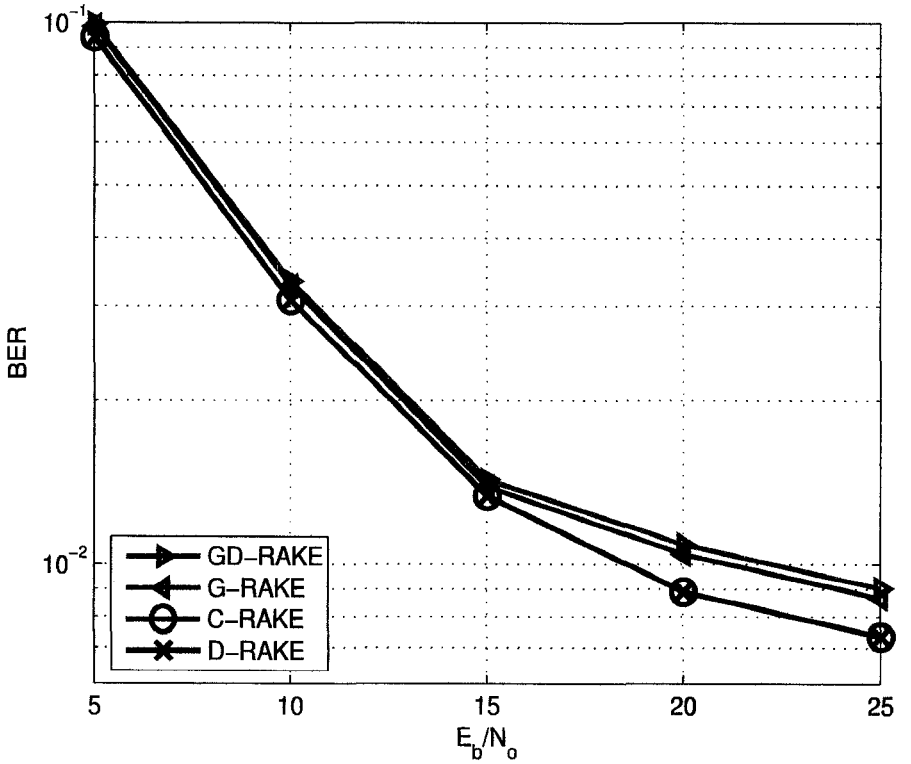

Figure 4.16: Bit error rate curves for (from top to bottom at 25dB) GD-RAKE, G-RAKE, C-RAKE, D-RAKE receivers with relative finger delays of [0 -1 -2] chip periods. The paths in the simulation have the relative delays of [0 -1 -2] chip periods and they have the relative average powers of [0 -0.75 -1.5] dB.

located on chip period before of the first finger of the previous simulation, i.e. finger locations are [1 0 -1 -2]. For both RAKE and D-RAKE receivers, such a selection is illogical since it cannot improve the performance. There is no channel gain at the new finger location but only noise plus interference. The reason we have simulated them is to show the amount of performance loss of them compared to previous simulation. Comparing Figure 4.16 with Figure 4.17 shows that there is no loss in the case of the D-DTR and more than 6 dB for the conventional RAKE receiver. In the case of the

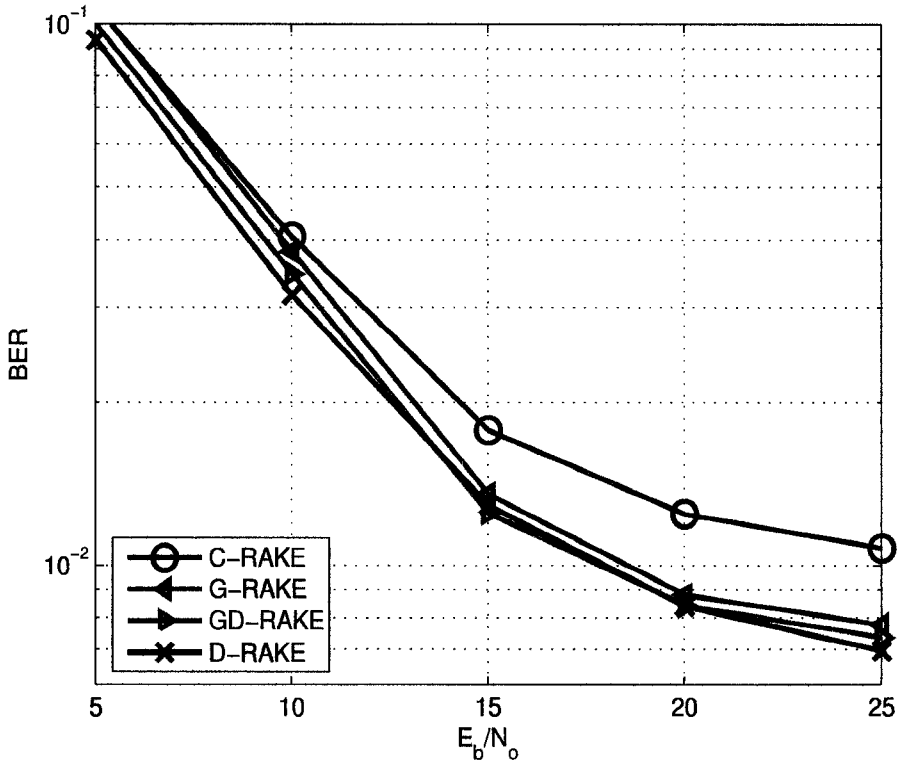

Figure 4.17: Bit error rate curves for (from top to bottom at 25dB) RAKE, G-RAKE, GD-RAKE, D-RAKE receivers with finger delays [1 0 -1 -2]. The paths in the simulation have the relative delays of [0 -1 -2] chip periods and they have the relative average powers of [0 -0.75 -1.5] dB.

GD-RAKE and G-RAKE, although adding a finger improves their performances, they are still worse than the D-RAKE. Therefore we believe employing the GD-RAKE and G-RAKE in systems, where $\mathbf{R}_u$ depends on the channel is not a clever choice. In the next chapter, we return to the discrete-time systems and introduce the MIMO versions of the receivers.

4.5 Chapter Summary

In this chapter we presented simulation results of the receivers for different scenarios. According to the simulation results, where we assumed perfect spreading codes and known statistics, the gain of GD-DTR compared to C-DTR increases with the decrease of the delay spread and the number of pilot symbols and the increase of roll off factor and the number of RAKE fingers. Our simulations show that the G-DTR is very sensitive to channel estimation errors and could have the worst performance among the RAKE receiver at low SNR's. The D-DTR guarantees a better performance than the C-DTR in all considered situations, but its gain with respect to the C-DTR is very limited. Our simulations with 8PSK and 16QAM modulations show that the gain of GD-DTR compared to C-DTR is less compared to QPSK modulation at the same bit error rate, with the main reason of higher SNR's required for the same bit error rates by 8PSK and 16QAM. We did simulations with the statistics estimation algorithms (KLT and update algorithms), introduced in the previous chapter. Both algorithms could trace the statistics, if the forgetting factor is small enough. Since the update algorithm has a slight complexity advantage, it can be more advantageous for estimation of the statistics, however the KLT algorithm is less sensitive to forgetting factor and for D-DTR it guarantees a better or the same performance of C-DTR. The last part of the chapter was dedicated to downlink DS-CDMA simulations in which, noise plus interference statistics are a function of the channel realizations. Since channel estimation errors affect the quality of statistics estimation, both GD-RAKE and G-RAKE perform worse than the D-DTR. Therefore our suggestion is to use the GD-DTR system only in uplink scenarios.

Chapter 5

RAKE Receivers in MIMO Systems

5.1 Introduction

MIMO systems have become popular in wireless communication standards because of their high capacity. Due to this popularity, single antenna systems are generalized to MIMO systems in literature. For the generalized RAKE receiver, this is done by Grant *et al.*. In [8], Grant *et al.* have proposed two methods: the JD-GRAKE and the MMSE-GRAKE . The JD-GRAKE jointly decodes the symbols spread by the same spreading code and transmitted from different antennas. The MMSE-GRAKE is an alternative system which is less complex than the JD-GRAKE. In the MMSE-GRAKE the symbols are decoded one by one, by treating the rest of the symbols as interference. Such a decoding decreases the complexity at the price of a decrease in performance. The extension of the D-DTR to MIMO systems is done in this chapter. We derive the equations, which take into account the channel estimation errors in MIMO systems. Afterward we combine one of the discrete-time version of the JD-GRAKE system with the MIMO D-DTR to obtain the MIMO GD-DTR system. We start this chapter with the explanation of the MIMO G-RAKE systems.

5.2 MIMO G-RAKE

Grant *et al.* applied generalized RAKE reception method to MIMO systems in [8]. They assume a DS-CDMA system with N_T transmit antennas and the number of available spreading waveforms is K. To maximize the spectral efficiency, every waveform is used in all transmit antennas as shown in Figure 5.1. At the receiver site, there are N_R

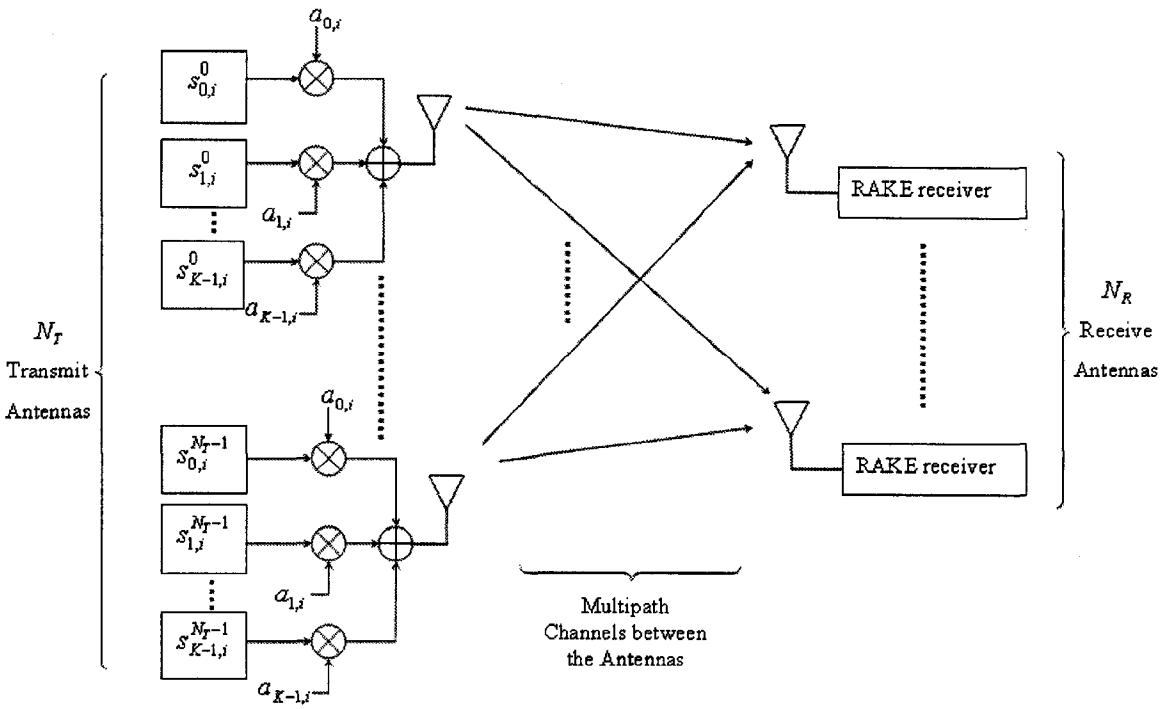

Figure 5.1: MIMO RAKE reception model at the ith symbol period with N_T transmit and N_R receive antennas. Every receive antenna feeds to an L finger RAKE receiver.

receive antennas. Suppose the desired symbols are the symbols during the 0th symbol period that share the spreading waveform $a_{0,0}$. The received vector after despreading can be written as:

$$\mathbf{y} = \mathbf{H}\mathbf{s}_{0,0} + \mathbf{u}_{0,0} \tag{5.1}$$

where the vector $\mathbf{s}_{0,0} = [s^0_{0,0}, s^1_{0,0}, \cdots, s^{N_T-1}_{0,0}]^T$ contains the desired symbols. Assume that there are L fingers per RAKE receiver (i.e. per receive antenna), the size of the MIMO channel matrix $\mathbf{H}$ is $(N_r L) \times N_T$. The vector $\mathbf{u}_{0,0}$ denotes the noise plus interference with respect to $\mathbf{s}_{0,0}$. We denote the covariance matrix of $\mathbf{u}_{0,0}$ with $\mathbf{R_u} = E[\mathbf{u}_{0,0}(\mathbf{u}_{0,0})^H]$.

Grant *et al.* propose two methods for the MIMO G-RAKE reception, the joint-detection G-RAKE (JD-GRAKE) and the MMSE-GRAKE. The JD-GRAKE decodes jointly the same code symbols from different antennas $\mathbf{s}_{0,0}$. Using such a decoding strategy, the JD-GRAKE eliminates most of the interference in the system since the same waveform symbols are main source of interference. The interference from symbols spread by other waveforms was diminished in the despreading symbols. To detect all the symbols sent during a symbol period, the JD-GRAKE should compute $K|C|^{N_T}$ metrics, where $|C|$ is the size of the signal constellation.

The MMSE-GRAKE is an alternative system which is less complex than the JD-GRAKE. In the JD-GRAKE the symbols are decoded jointly, whereas in the MMSE-GRAKE the symbols are decoded one by one, by treating the rest of the symbols as interference. For the MMSE-GRAKE, assuming the symbol $s^0_{0,0}$ is the desired symbol, the received vector can be written as:

$$\mathbf{y} = \mathbf{h_0} s^0_{0,0} + \mathbf{u}^0_{0,0} \tag{5.2}$$

where $\mathbf{h_0}$ is the channel vector from the 0th transmit antenna and $\mathbf{u}^0_{0,0}$ is equal to

$$\mathbf{u}_{0,0}^{0} = \mathbf{u}_{0,0} + \sum_{m=1}^{N_t-1} \mathbf{h_m} s_{0,0}^{m}, \tag{5.3}$$

where $\mathbf{u}_{0,0}^{0}$ is the noise plus interference vector for $s_{0,0}^{0}$. It includes not only $\mathbf{u}_{0,0}$, the noise plus interference from thermal noise and symbols with different codes, but also the rest of the symbols with spreading waveform $a_{0,0}$. Since the symbols are decoded one by one, this system has the total metric computations $KN_T|C|$ and therefore is less complex.

The authors of [8] claim that if the channels are dispersive and/or the number of receive antennas is larger than the number of transmit antennas, then the performance of the MMSE-GRAKE is acceptable, but the JD-GRAKE performs well in light dispersion cases too.

This ends the introduction of MIMO G-RAKE systems. In the next subsection, we introduce the MIMO D-DTR.

5.3 MIMO D-DTR

The decorrelating discrete-time RAKE receiver was proposed for RAKE reception system with channel estimation errors. We explained the system in Chapter 3. The assumptions of the system were that the channel is estimated at the receiver and the only noise source in the system is AWGN.

For the MIMO D-DTR, we kept these assumptions. The system model of the MIMO D-DTR is shown in Figure 5.2. In the system, there are N_T transmit and N_R receive antennas. Each receive antenna employs a RAKE receiver with L fingers. At the transmitter site, we take only one spreading waveform into consideration to eliminate interference from different waveforms. Therefore, for a given time instant all the trans-

mit antennas use the same spreading waveform to spread the symbols. During the transmission, the signals are chip synchronized.

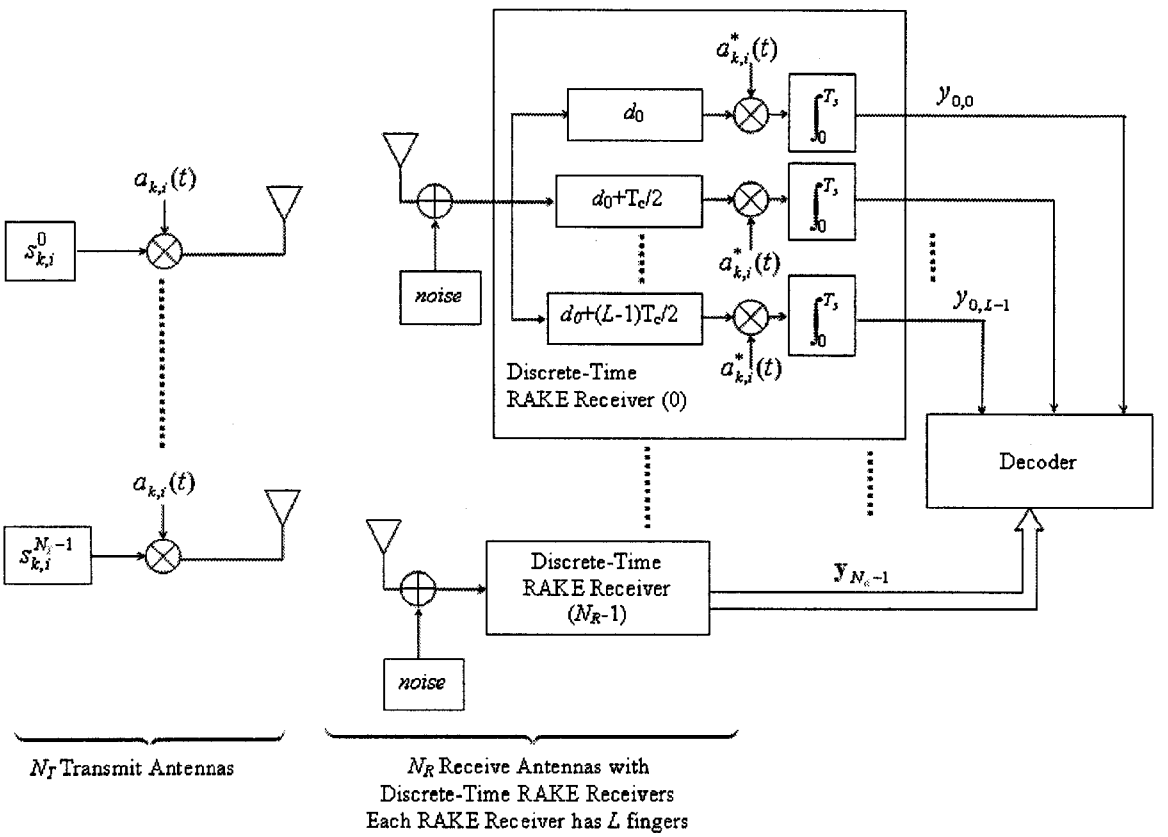

Figure 5.2: MIMO D-DTR reception model with N_T transmit and N_R receive antennas. Every receive antenna employs an L finger D-DTR.

The channels between the transmit and receive antennas are independent and have the same delay profile and therefore the same $\mathbf{R_h}$. The received signal vector after despreading at the nth receive antenna is equal to

$$\mathbf{y}_n = \mathbf{H}_n\mathbf{s} + \mathbf{u}_n, \tag{5.4}$$

where $\mathbf{H}_n$ is the channel matrix between the transmit antennas and nth receive antenna, and $\mathbf{s}$ consists of the symbols from transmit antennas. The MIMO D-DTR follows the decoding method of the D-DTR. First, the channels in $\mathbf{y}_n$ are decorrelated using $\mathbf{U}$, the eigenvector matrix of $\mathbf{R_h}$, such that

$$\mathbf{y'}_n = \mathbf{U}^H \mathbf{y}_n. \tag{5.5}$$

Like in the D-DTR, we assume that the channels are estimated in the MIMO D-DTR. The number of pilot symbols per transmit antenna is denoted by N_p. The pilot symbols are sent simultaneously on all transmit antennas using orthogonal pilot sequences such as those of Walsh-Hadamard. The estimate of $\mathbf{H}_n$ is denoted by $\hat{\mathbf{H}}_n$. The MIMO D-DTR applies the decorrelating process to the $\hat{\mathbf{H}}_n$ too, such that,

$$\hat{\mathbf{H}}'_n = \mathbf{U}^H \hat{\mathbf{H}}_n. \tag{5.6}$$

At this point we have decorrelated channels and we can start the derivation process. Since all transmit-receive antenna pairs have the same covariance matrix $\mathbf{R_h}$, corresponding to decorrelated channels ($\mathbf{h'}$'s) with the pdf:

$$p(\mathbf{h'}) = \prod_{l=0}^{L-1} \frac{1}{\pi\, \Gamma_l} \exp\Big(-\frac{|h'_l|^2}{\Gamma_l}\Big). \tag{5.7}$$

The estimate, $\hat{\mathbf{h}}'$, of $\mathbf{h}'$ has the conditional pdf,

$$p(\hat{\mathbf{h}}'|\mathbf{h}') = \prod_{l=0}^{L-1} \frac{1}{\pi\sigma^2} \exp\Big(\frac{|h'_l - \hat{h}'_l|^2}{\sigma^2}\Big), \tag{5.8}$$

conditional on the vector $\mathbf{h}'$ [4]. In the above equation σ^2 is equal to $2N_0/(T_c E_s N_p)$. The estimate $\hat{\mathbf{h}}'$ is gaussian distributed and has the pdf

$$p(\hat{\mathbf{h}}') = \prod_{l=0}^{L-1} \frac{1}{\pi(\sigma^2 + \Gamma_l)} \exp\Big(-\frac{|\hat{h}'_l|^2}{\sigma^2 + \Gamma_l}\Big). \tag{5.9}$$

From the Bayes rule, we can write

$$p(\mathbf{h}'|\hat{\mathbf{h}}') = \prod_{l=0}^{L-1} \frac{1}{\pi}\Big(\frac{1}{\sigma^2} + \frac{1}{\Gamma^2}\Big) \exp\Big(-\frac{|h'_l - \hat{h}'_l|^2}{\sigma^2} - \frac{|h'_l|^2}{\Gamma_l} + \frac{|\hat{h}'_l|^2}{\sigma^2 + \Gamma_l}\Big). \tag{5.10}$$

Now we focus on the pdf's of $p(\mathbf{y}_n|\mathbf{s}, \hat{\mathbf{H}}'_n)$ and $p(\mathbf{y}_n|\mathbf{s}, \mathbf{H}'_n)$, where $\mathbf{H}'_n$ and $\hat{\mathbf{H}}'_n$ denote respectively the decorrelated channel matrix between all transmit antennas and the nth receive antenna and the estimate of $\mathbf{H}'_n$. The mth column of $\mathbf{H}'_n$, the decorrelated channel vector from the mth transmit antenna, is denoted by $\mathbf{h}'_{nm}$. The pdf $p(\mathbf{y}_n|\mathbf{s}, \mathbf{H}'_\mathbf{n})$ is equal to

$$p(\mathbf{y}_n|\mathbf{s}, \mathbf{H}'_\mathbf{n}) = \prod_{l=0}^{L-1} \frac{1}{\pi\Sigma^2} \exp\Big(-\frac{|\mathbf{y}_n - (s_0\mathbf{h}'_{n0l} + \cdots + s_{N_T-1}\mathbf{h}'_{n(N_T-1)l})|^2}{\Sigma^2}\Big). \tag{5.11}$$

From the theory of probability we can write the pdf $p(\mathbf{y}_n|\mathbf{s}, \hat{\mathbf{H}}'_\mathbf{n})$ as

$$\begin{aligned} p(\mathbf{y}_n|\mathbf{s}, \hat{\mathbf{H}}'_\mathbf{n}) \;=\; & \int_{\mathbf{h}'_{n0}} \cdots \int_{\mathbf{h}'_{nN_T-1}} p(\mathbf{y}_n|\mathbf{s}, \mathbf{H}'_\mathbf{n}) p(\mathbf{h}'_{nN_T-1}|\hat{\mathbf{h}}'_{nN_T-1}) d\hat{\mathbf{h}}'_{nN_T-1} \cdots \\ & p(\mathbf{h}'_{n0}|\hat{\mathbf{h}}'_{n0}) d\hat{\mathbf{h}}'_{n0} \end{aligned} \tag{5.12}$$

We solve (5.12) using (5.10) and (5.11), starting with the innermost integral. We obtain

$$p(\mathbf{y}_n|\mathbf{s}, \hat{\mathbf{H}}'_\mathbf{n}) \;=\; \prod_{l=0}^{L-1} \int_{\mathbf{h}'_{n0}} \cdots \int_{\mathbf{h}'_{nN_T-2}} \frac{1}{\pi\Sigma^2 A} \exp\Big(\frac{1}{\Sigma^2 A}|\mathbf{y}_n - (s_0\mathbf{h}'_{n0l} + \cdots$$

$$+s_{N_T-2}\mathbf{h'}_{n(N_T-2)l}+\frac{s_{N_T-1}\hat{\mathbf{h}}'_{n(N_T-1)l}}{1+\sigma^2/\Gamma_l}|^2\Big)\times \tag{5.13}$$
$$p(\mathbf{h'}_{nN_T-2}|\hat{\mathbf{h}}'_{nN_T-2})d\hat{\mathbf{h}}'_{nN_T-2}\cdots p(\mathbf{h'}_{n0}|\hat{\mathbf{h}}'_{n0})d\hat{\mathbf{h}}'_{n0},$$

where $1/A$ is equal to:

$$\frac{1}{A}=\frac{(1+\frac{\sigma^2}{\Gamma_l})}{1+\sigma^2(\frac{|s|^2}{\Sigma^2}+\frac{\sigma^2)}{\Gamma_l})}. \tag{5.14}$$

After solving the second innermost integral, we obtain

$$\begin{aligned} p(\mathbf{y}_n|\mathbf{s},\hat{\mathbf{H}}'_{\mathbf{n}}) &= \prod_{l=0}^{L-1}\int_{\mathbf{h'}_{n0}}\cdots\int_{\mathbf{h'}_{nN_T-3}}\frac{1}{\pi\Sigma^2A^2}\times\exp\Big(-\frac{1}{\Sigma^2A^2}|\mathbf{y}_n-(s_0\mathbf{h'}_{n0l}+\cdots \\ &+\frac{s_{N_T-2}\hat{\mathbf{h}}'_{n(N_T-2)l}}{1+\sigma^2/\Gamma_l}+\frac{s_{N_T-1}\hat{\mathbf{h}}'_{n(N_T-1)l}}{1+\sigma^2/\Gamma_l}|^2\Big)\times \\ &p(\mathbf{h'}_{nN_T-3}|\hat{\mathbf{h}}'_{nN_T-3})d\hat{\mathbf{h}}'_{nN_T-3}\cdots p(\mathbf{h'}_{n0}|\hat{\mathbf{h}}'_{n0})d\hat{\mathbf{h}}'_{n0}. \end{aligned} \tag{5.15}$$

After solving all the integrals, we obtain,

$$p(\mathbf{y}_n|\mathbf{s},\hat{\mathbf{H}}'_{\mathbf{n}})=\prod_{l=0}^{L-1}\frac{1}{\pi\Sigma^2A^{N_T}}\exp\Big(-\frac{1}{\Sigma^2A^{N_T}}|\mathbf{y}_n-(\frac{s_0\hat{\mathbf{h}}'_{n0l}}{1+\sigma^2/\Gamma_l}+\cdots+\frac{s_{N_T-1}\hat{\mathbf{h}}'_{n(N_T-1)l}}{1+\sigma^2/\Gamma_l})|^2\Big). \tag{5.16}$$

The MIMO D-DTR chooses the symbol vector $\bar{\mathbf{s}}$ which maximizes the following quantity among all possible symbol vectors:

$$\prod_{n=0}^{N_R-1}p(\mathbf{y'}_n|\bar{\mathbf{s}},\hat{\mathbf{H}}'_n). \tag{5.17}$$

The simulation results for the MIMO C-DTR and the MIMO D-DTR are shown in Figure 5.3. The properties of the multipath channel are taken from the simulations in chapter 5 ($T_m = 0.25T_c$, L=9, η=1, N_p=4). To reduce the overall complexity we used BPSK as the modulation scheme. As it can be seen from Figure 5.3, the gain of the MIMO D-DTR is about 2 dB at a bit error rate of 10^{-2}.

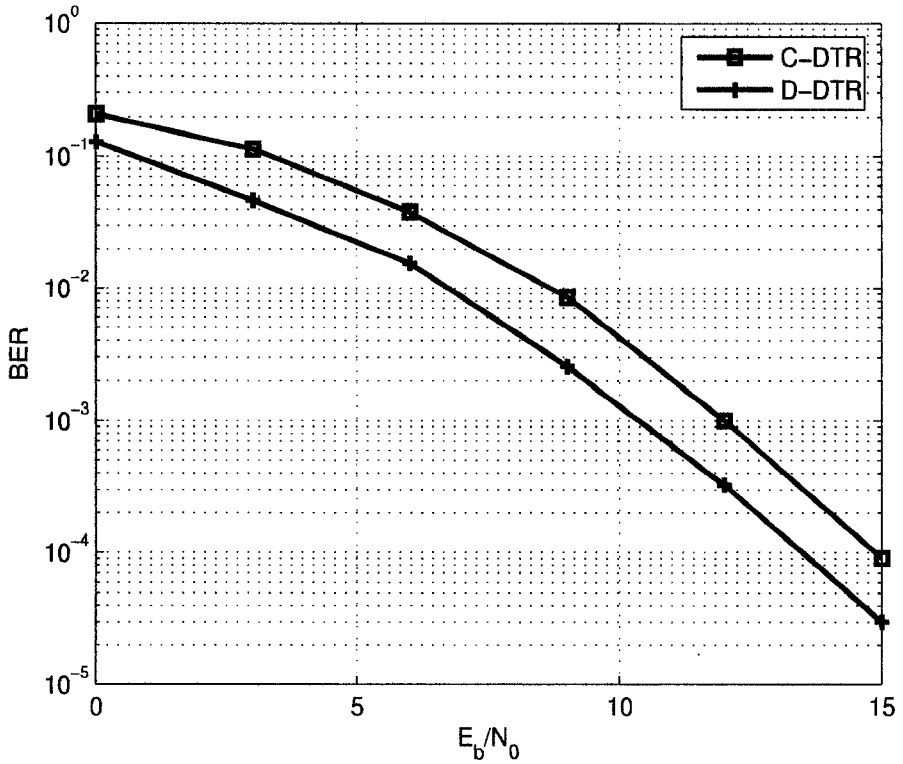

Figure 5.3: The BER performances of the MIMO conventional DTR and the MIMO D-DTR for a 2×2 system, where $L = 9$, T_m=$0.25T_c$, N_p=4.

In this section, we introduced the MIMO D-DTR system. In the next section we will combine it with the discrete-time version of the JD-RAKE to obtain the MIMO GD-DTR.

5.4 MIMO GD-DTR

The MIMO GD-DTR jointly decodes the incoming symbols and takes into consideration the noise plus interference matrix $\mathbf{R_u}$ like the JD-RAKE. However it is a discrete-time receiver and the weights of the receiver depend on the channel estimation errors as well. The MIMO GD-DTR follows the steps of the GD-DTR. It starts with the decorrelation process of the noise plus interference using the matrices Λ and Ω resulting from the decomposition of the covariance matrix $\mathbf{R_u}$, such that,

$$\mathbf{z}_n = \Lambda\Omega^H\mathbf{y}_n = \Lambda\Omega^H(\mathbf{H}_n\mathbf{s}_k + \mathbf{u}_n), \tag{5.18}$$

and $\hat{\mathbf{F}}_n$=$\Lambda\Omega^H\hat{\mathbf{H}}_n$, where $\hat{\mathbf{H}}$ is the estimation of $\mathbf{H}$. After the decorrelating process of the channels are applied to $\mathbf{z}_n$, as:

$$\mathbf{z'}_n = \mathbf{U'}^H\mathbf{z}_n, \tag{5.19}$$

and to $\hat{\mathbf{F}}_n$, such that

$$\hat{\mathbf{H}}'_n = \mathbf{U'}^H\hat{\mathbf{F}}_n, \tag{5.20}$$

where $\mathbf{U'}$ is the eigenvector matrix of $\mathbf{R'_h} = \Lambda\Omega^H\mathbf{R_h}\Omega\Lambda$, as explained in Chapter 2. Since $\mathbf{z'}_n$ above has the same distribution with $\mathbf{y'}_n$ in (5.5), the derivation in the previous section is valid for the GD-DTR case as well. However for the GD-DTR system, due to the noise decorrelating process, Σ^2=1 and σ^2=$1/N_pE_s$. The MIMO GD-DTR chooses the symbol vector $\bar{\mathbf{s}}$ which maximizes the following quantity:

$$\prod_{n=0}^{N-1} p(\mathbf{z'}_n|\mathbf{s} = \bar{\mathbf{s}}, \hat{\mathbf{H}}'_n), \tag{5.21}$$

with respect to all possible s vectors. The soft output of the bit from the mth transmit antenna, Λ_m, can be obtained from the above equation, such that:

$$\Lambda_m = \log \frac{\prod_{n=0}^{N-1} p(\mathbf{z'}_n | s_m = -1, \hat{\mathbf{H}}'_n)}{\prod_{n=0}^{N-1} p(\mathbf{z'}_n | s_m = 1, \hat{\mathbf{H}}'_n)}. \tag{5.22}$$

Up to this point, we assumed that there is no correlation between the receive antennas. If it exists, then we should process the signal at different antennas together such that,

$$\mathbf{y} = \mathbf{H}\mathbf{s}_k + \mathbf{u}, \tag{5.23}$$

where $\mathbf{y}$ and $\mathbf{u}$ consist of all received signals and noise plus interference values respectively and the matrix $\mathbf{H}$ is $N_R L$ by N_T channel matrix. Since, we assumed correlation between the receive antennas the interference values at different antennas will be correlated as well, thus the $\mathbf{R_u}$ will be changed. Let us remind that, now the size of the covariance matrices both $\mathbf{R_u}$ and $\mathbf{R_f}$ will be $N_R L$ by $N_R L$. Like the uncorrelated MIMO system, we apply first the noise plus interference decorrelation process

$$\mathbf{z} = \Lambda \Omega^H \mathbf{y} = \Lambda \Omega^H (\mathbf{F}\mathbf{s}_k + \mathbf{u}), \tag{5.24}$$

and $\hat{\mathbf{F}}$=$\Lambda\Omega^H\hat{\mathbf{H}}$, where $\hat{\mathbf{H}}$ is the estimation of $\mathbf{H}$. Afterward the decorrelating process of the channels is applied to $\mathbf{z}$,

$$\mathbf{z}' = \mathbf{U}'^H \mathbf{z}, \tag{5.25}$$

and to $\hat{\mathbf{F}}$, such that

$$\hat{\mathbf{H}}' = \mathbf{U}'^H \hat{\mathbf{F}}. \tag{5.26}$$

The probability of receiving $\mathbf{z}'$, given the transmitted symbol vector $\mathbf{s}_k$ and $\hat{\mathbf{H}}'$, is equal to:

$$p(\mathbf{z}'|\mathbf{s}_k, \hat{\mathbf{H}}') = \prod_{n=0}^{N_R-1} \prod_{l=0}^{L-1} \frac{1}{\pi} \Big(\frac{1 + \frac{1/N_p E_s}{\Gamma'_{nL+l+1}}}{w'_{nL+l+1}} \Big)^{N_T} \exp(-X_{nL+l+1}) \tag{5.27}$$

where corresponding X_{nL+l+1} is equal to

$$X_{nL+l+1} = \Big(\frac{1 + \frac{1/N_p E_s}{\Gamma'_{nL+l+1}}}{w'_{nL+l+1}} \Big)^{N_T} \Big| \mathbf{z}_{n,l} - \sum_{m=0}^{M-1} \frac{\hat{h}'_{m,n,l} s_{m,k}}{1 + \frac{1/N_p E_s}{\Gamma'_{nL+l+1}}} \Big|^2. \tag{5.28}$$

In the above equations Γ'_{nL+l+1} and w'_{nL+l+1} are obtained using the new covariance matrices. Since the complexity of singular value decomposition exponentially increases with matrix size, this system could be too complex for practical purposes. Albeit we will give some examples of performance in our simulations.

To show the performance of the MIMO GD-DTR, we first choose a 2 transmit and 2 receive antenna (2×2) system. Like the MIMO D-DTR simulation, the modulation scheme is BPSK. The channel connecting one transmit antenna to one receive antenna has an exponential delay profile with rms delay spread of T_m=$0.25T_c$. The number of correlators, L, is equal to 5. This system collects %95 of the average received signal energy, according to [4]. The number of pilot symbols per transmit antenna, N_p, is equal to 2. The noise rise coefficient is η=10. The simulation results are shown in Figure 5.4. As it can be seen from Figure 5.4, the gain of the MIMO GD-DTR is about 0.65 dB at a BER of 10^{-2}, compared to the MIMO C-DTR. Employing the MIMO G-DTR actually causes a performance loss, whereas the MIMO D-DTR has a very limited gain compared to the MIMO C-DTR. The loss of the MIMO G-DTR is attributed to the poor channel estimation and the limited gain of the MIMO D-DTR is due to the highly correlated noise.

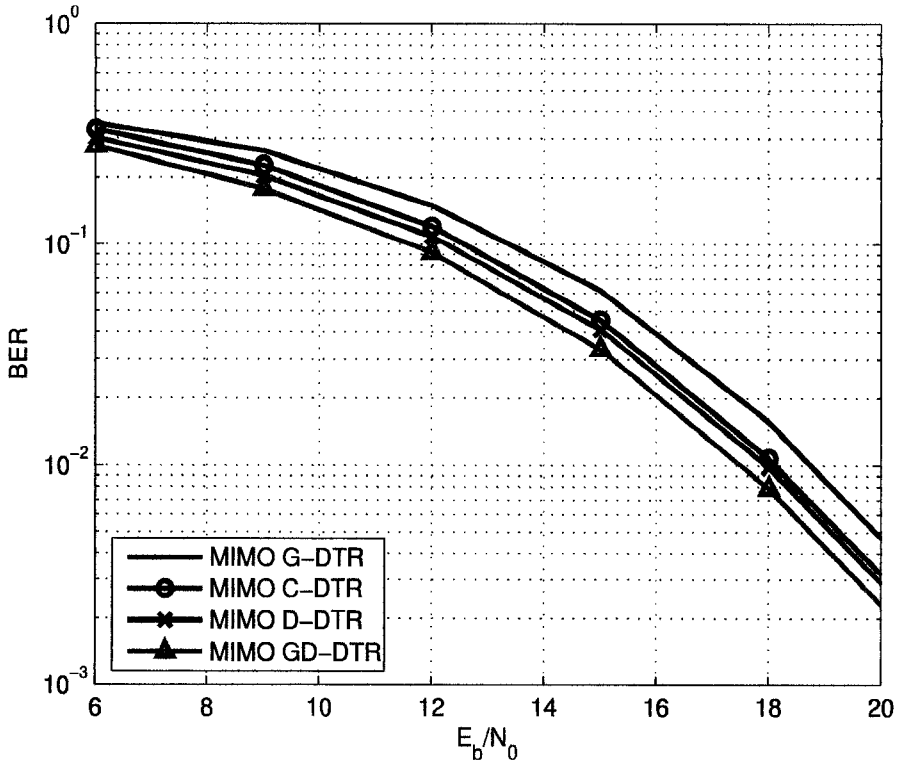

Figure 5.4: BER performances of the MIMO C-DTR, the MIMO D-DTR, the MIMO G-DTR and the MIMO GD-DTR for a 2 × 2 system, where L=5, N_p=2, α=0.22, T_m=0.25T_c, η=10.

In the next simulation, we increase the number of correlators from 5 to 9 so as to increase the average received signal energy collected from %95 to %99. The results are shown in Figure 5.5. In this case, the gain of the MIMO GD-DTR compared to MIMO C-DTR is increased to about 1.4 dB at a BER of 10^{-2}. Figure 5.5 shows that as the number of Rake fingers increase, the performance of the MIMO D-DTR and GD-DTR are improved while the performance of the MIMO C-DTR and G-DTR are degraded. Here, additional correlators correspond to weak path gains where channel estimation errors has greater impact, and since the MIMO C-DTR and G-DTR do not combine

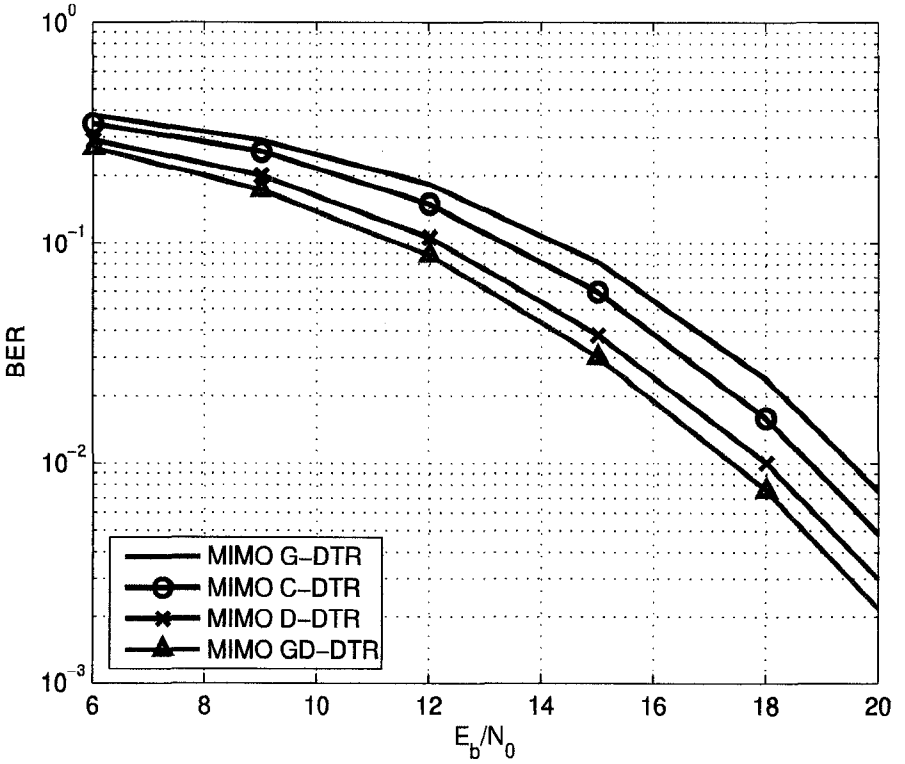

Figure 5.5: BER performances of the MIMO C-DTR, the MIMO D-DTR, the MIMO G-DTR and the MIMO GD-DTR for a 2 × 2 system, where L=9, N_p=2, α=0.22, T_m=0.25T_c, η=10.

the channel gains optimally, their overall noises increase and their performances drop.

The last set of simulations for the 2×2 MIMO system is done with perfect channel state information at the receiver, to quantify maximum gain available from the MIMO G-DTR receiver. The performances are shown in Figure 5.6. According to this figure, the gain of the MIMO G-DTR is limited to 0.25 dB at a BER of 10^{-2} compared to MIMO C-DTR. Although not shown in the figure, the MIMO GD-DTR has the same performance as the MIMO G-DTR and the MIMO D-DTR has the same performance as the MIMO C-DTR as expected.

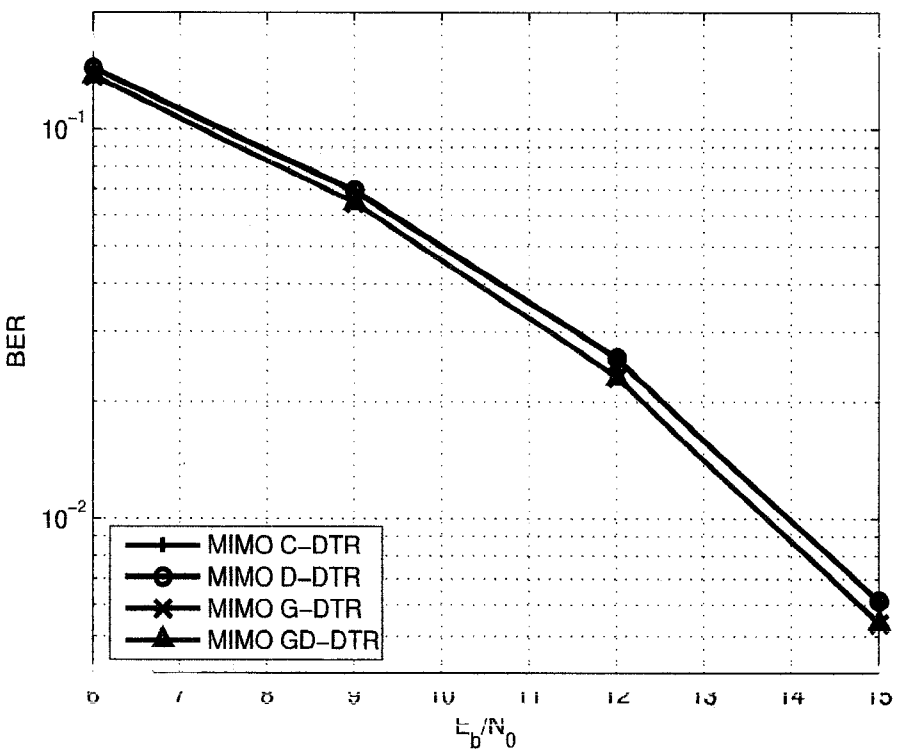

Figure 5.6: BER performances of the MIMO C-DTR, the MIMO D-DTR, the MIMO G-DTR and the MIMO GD-DTR for a 2×2 system, where the receiver have the perfect channel state information and L=9, α=0.22, T_m=0.25T_c,

In our simulations with a 3×3 MIMO system, we observe a slight increase in the gain of the MIMO GD-DTR with respect to the MIMO C-DTR. For example, in Figure 5.7, which shows the performance with N_p=2 and L=9, the gain of the MIMO GD-DTR is around 1.7 dB at a BER of 10^{-2}, compared to the MIMO C-DTR.

To see the effect of the channel delay spread on the performance, we set T_m=T_c and present the corresponding performance in Figure 5.8. The overall performance of all the systems is increased in Figure 5.8 compared to Figure 5.7, whereas the SNR gain of the MIMO GD-DTR decreased compared to the MIMO C-DTR.

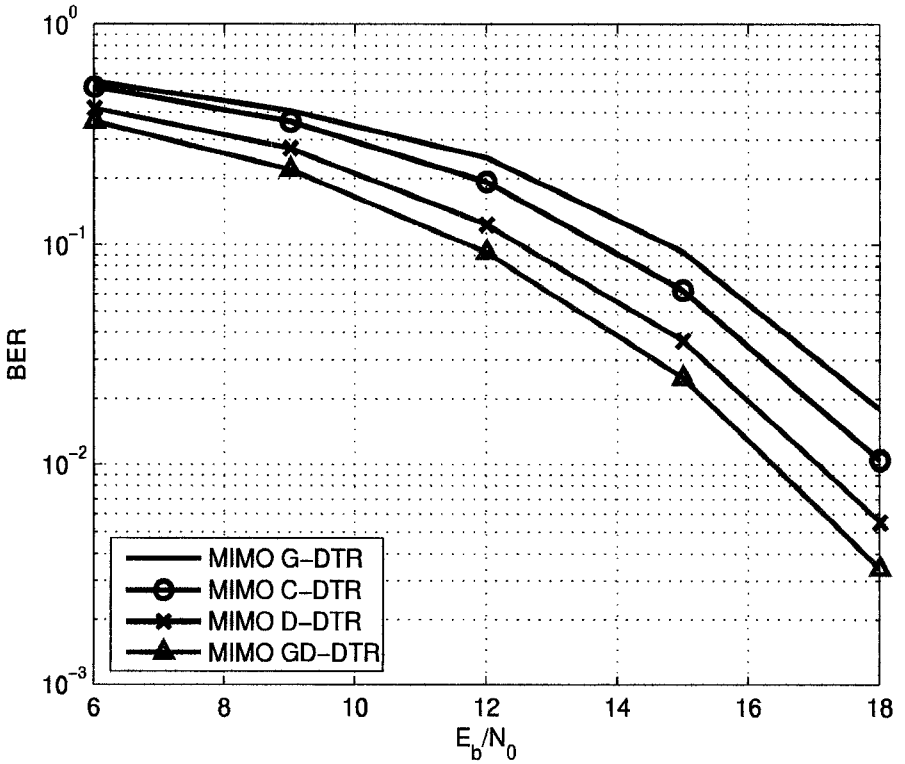

Figure 5.7: BER performances of the MIMO C-DTR, the MIMO D-DTR, the MIMO G-DTR and the MIMO GD-DTR for a 3 × 3 system, where L=9, N_p=2, α=0.22, T_m=0.25T_c

The last simulation set considers, that there is correlation between the receive antennas. For example assuming 90% correlation between adjacent antennas, we obtain the covariance matrix of

$$\mathbf{R_r} = \begin{bmatrix} 1 & 0.9 & 0.81 \\ 0.9 & 1 & 0.9 \\ 0.81 & 0.9 & 1 \end{bmatrix} \tag{5.29}$$

for 3 receive antennas. Other parameters are set to be L=5, N_p=2, η=10 and T_m=0.25T_c.

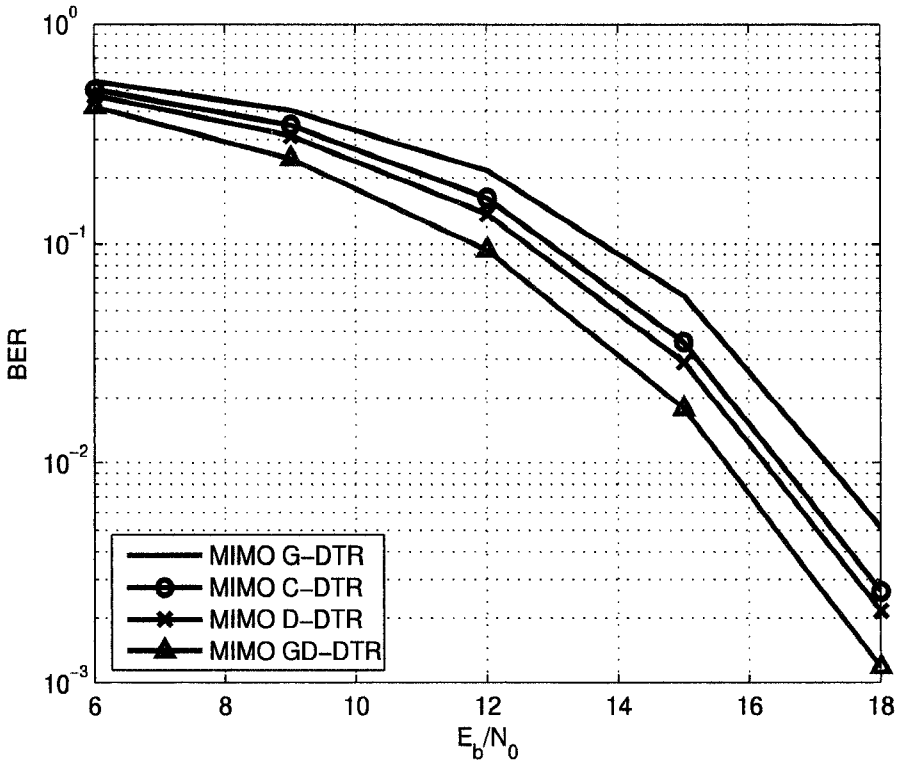

Figure 5.8: BER performances of the MIMO C-DTR, the MIMO D-DTR, the MIMO G-DTR and the MIMO GD-DTR for a 3×3 system, where L=9, N_p=2, α=0.22, T_m=T_c

All the advanced RAKE receivers take into account the correlation between the receive antennas. The simulation results are shown in Figure 5.9. We observe that the MIMO GD-DTR has 3.4 dB gain compared to the MIMO C-DTR receiver at a BER of 10^{-2}. The MIMO D-DTR system has almost the same performance of the MIMO D-DTR. The MIMO G-DTR has the second best performance for all E_b/N_0 values, which can be explained by the high correlation coefficients between the receive antennas.

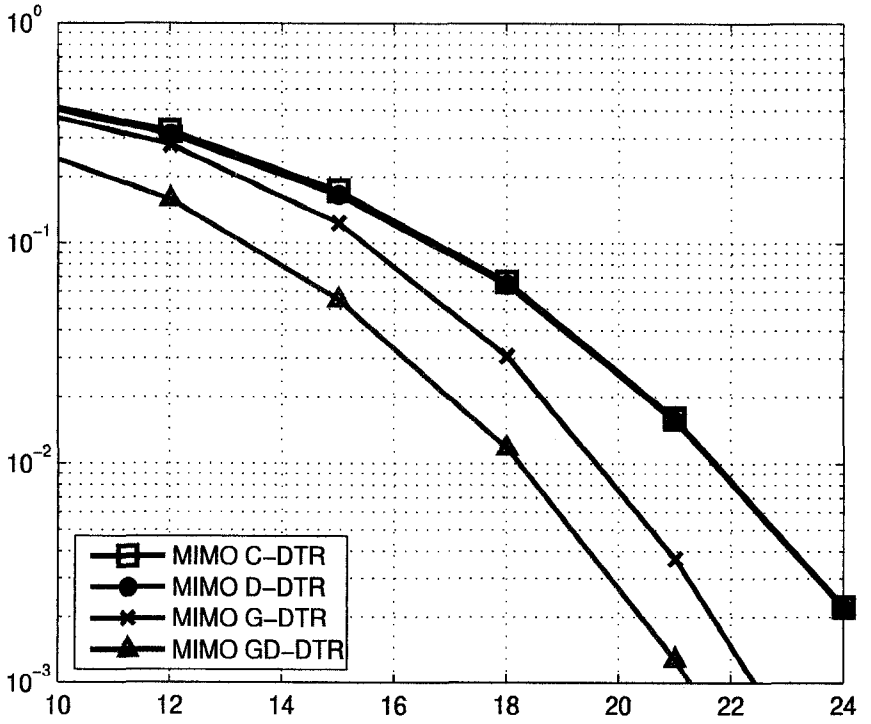

Figure 5.9: BER performances of the MIMO C-DTR, the MIMO D-DTR, the MIMO G-DTR and the MIMO GD-DTR for the case of correlated receive antennas (3×3 system), where L=5, N_p=2, α=0.22, T_m=0.25T_c, η=10

5.5 Chapter Summary

We can conclude from our simulations that the gain of the MIMO GD-DTR with respect to the MIMO C-DTR increases with a decrease of the delay spread and with an increase of the number of RAKE fingers and the number of antennas. The MIMO G-DTR system gives the worst results in all simulations with channel estimation errors but the one with correlated receive antennas. Even if the perfect channel state information is available, the gain of the MIMO G-DTR is very limited. The performance of the MIMO D-DTR

receiver is always between the MIMO GD-DTR and the MIMO C-DTR. This ends our simulations with MIMO GD-DTR receiver.

Chapter 6

Conclusions

In this thesis, we have introduced the GD-DTR, a new RAKE reception method. It combines two complementary advanced RAKE receivers the D-DTR and the G-RAKE. GD-DTR requires the estimation of channel and noise plus interference statistics. We came up with a statistics estimation method, which does not require KLT transform. Our simulations show that the statistic estimation methods work efficiently enough for GD-DTR to have a gain compared to a normal RAKE receiver.

We did several simulations to see the effect of different parameters. Among those parameters, the increase in the roll off factor and number of RAKE fingers and the decrease in the delay spread and number of pilot symbols cause an increase in the gain of GD-DTR compared to C-DTR. Another important result of our simulations is the indication of G-DTR's sensitivity to channel estimation errors. Interestingly the G-DTR could have the worst performance among the RAKE receiver at low SNR's. Our simulations with 8PSK and 16QAM modulations show that the gain of GD-DTR compared to C-DTR is less when compared to its gain in QPSK modulation. The simulations in downlink DS-CDMA simulations resulted with poor performance of GD-DTR, due to the high effect of channel estimation errors to the estimation of noise plus

interference statistics. Therefore our suggestion is to use the GD-DTR system only in uplink scenarios. The thesis include a chapter dedicated to the RAKE receivers in MIMO systems. The MIMO GD-DTR system, which we have introduced, show that, the increase in the number of antennas of the MIMO GD-DTR system increase the gain of the receiver as well. MIMO G-DTR system performed poorly in all of the simulations except when there correlation between the receiver antennas. The MIMO D-DTR system has a performance always better than the MIMO C-DTR.

As a future research, we would suggest to focus on optimization of system performance if the covariance matrix of noise plus interference is a function of channel coefficients. Our simulations showed that the GD-DTR is sensitive to the estimation of noise plus interference covariance matrix, it is a good idea to investigate possible ways to reduce this sensitivity. Appendix of this thesis include simulation results of a G-RAKE receiver in UWB systems. We believe that the performance of the GD-RAKE should be tested in UWB systems as well.

Appendix A

G-RAKE in UWB DS-CDMA systems

In this part we will give the definition of the ultra wideband systems and state some of their characteristics to be used in wireless personal area networks. Afterward we will mention the properties of UWB channels, including high number of multipaths, which enables RAKE reception. As an advanced RAKE reception method we simulated G-RAKE in UWB channel and present our initial results here.

The FCC defines ultra-wideband as any signal that occupies more than 500 MHz bandwidth in the 3.1 to 10.6 GHz band and that meets the spectrum mask specified in [21].

UWB systems have some features, which are well suited to wireless personal area networks WPANs. WPANs are intended for small number of people in a small radius. Basically any wireless data communication in a room could be in the focus of WPANs. The first generation of WPAN's is the Bluetooth system, but its data rate is very low for some applications such as high speed connection between a router and a laptop. The advantage of UWB systems comes from the well known capacity formula of Shannon:

$$\text{Capacity} = \text{Bandwidth} \times \log(1 + \text{SNR}) \tag{A.1}$$

Although the power of UWB systems is limited by FCC, since the bandwidth of UWB systems is very large, they can support very high data rates especially in short distances. Using these high rates, applications such as video transfer, multimedia shows, data backup can be supported without any need of wires. The restriction of transmit power in UWB systems could be an advantage for them, since those systems wouldn't need high power amplifiers and their battery life will be longer.

There are many papers in literature related to the modeling of UWB channels, such as [22, 23, 24]. IEEE standardization committee for WPANS came up with a channel model based on the Saleh-Valenzuela indoor model [1]. Saleh-Valenzuela model assumes that the multipath signals come in clusters, the arrival rate of clusters and the arrival rate of the rays in a cluster are both Poisson distributed. The energy of clusters decay exponentially. The energy of the rays in a cluster decays exponentially as well. The gain magnitude of the rays for a specific time is Rayleigh distributed. In Figure A.1 we show a representation of the model.

In IEEE 802.15 WPAN ultra wideband channel specifications 4 channel models are specified. **CM1** is based on line of sight (LOS) measurements (0-4m). **CM2** is based on no line of sight (NLOS) measurements (0-4m). **CM3** is based on LOS measurements (4-10m). **CM4** is generated for a 25 ns rms delay spread to represent an extreme NLOS multipath channel. The details of these models is given in Appendix B. The Matlab functions to generate those channels are included in the IEEE channel report [1]. For example Figure A.2 depicts one of the channel realizations of **CM1**. As seen in Figure A.2, the channel values span a long time. We cannot see directly the clustering but at the 8^{th} ns a strong ray could be seen and that ray can be accepted as a first ray of a

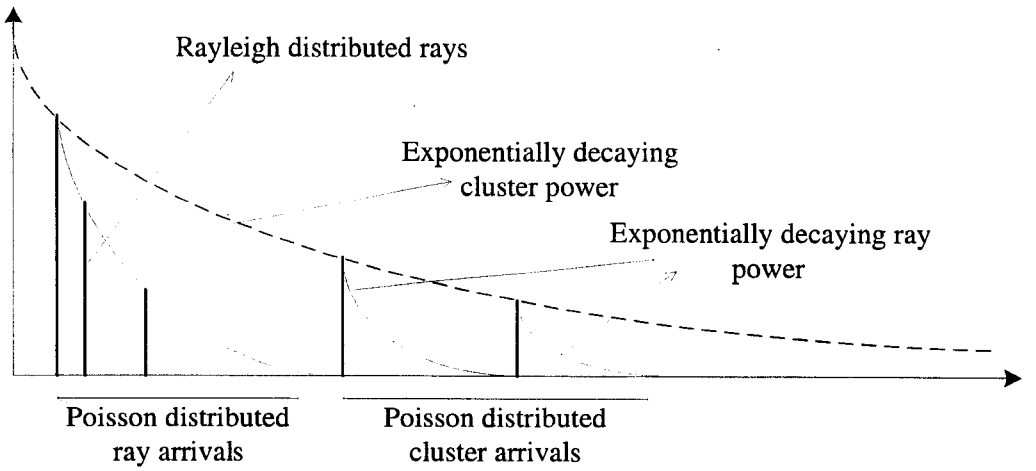

Figure A.1: Saleh-Valenzuela model representation.

cluster. To see the effect of pulse shaping we convolved this channel with the square root raised cosine filter with roll-off factor α=0.5. The results are presented in Figure A.3. As we can see, different multipath components are still resolvable but in clusters. For example at the 5^{th} ns we see a cluster with 4 elements, 2 with magnitudes around -0.6 and the other two around -0.2.

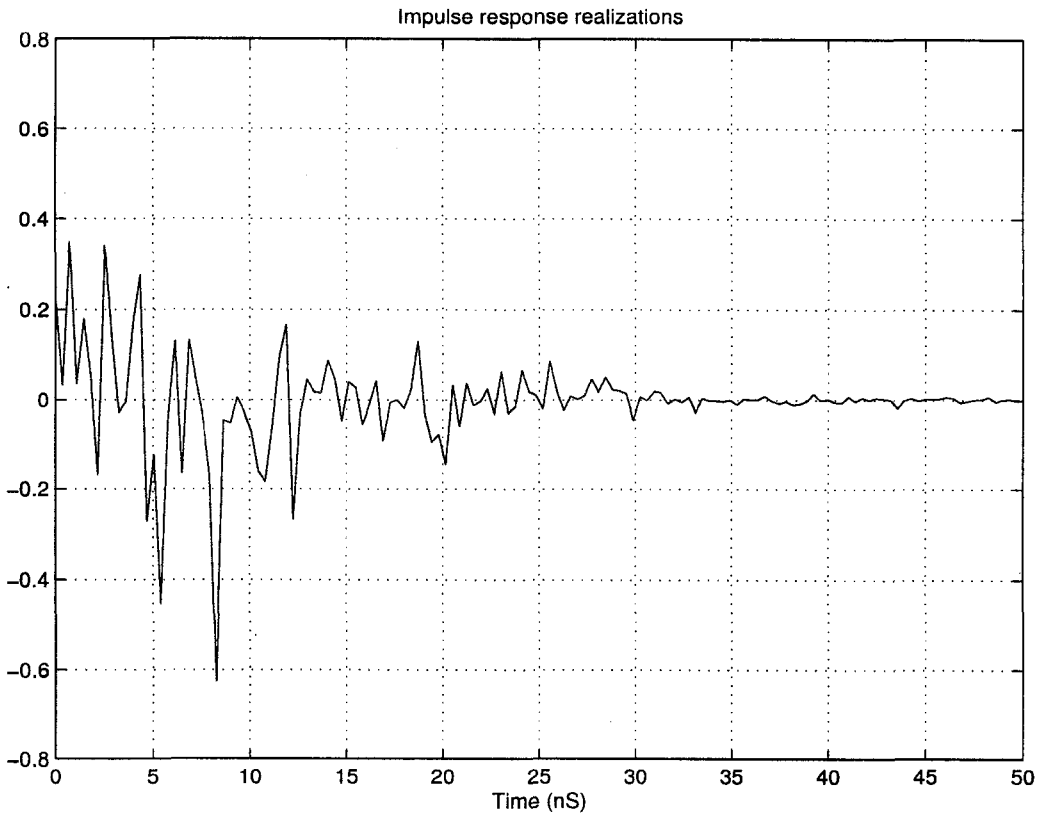

Figure A.2: A UWB channel realization of the **CM1** type.

We have explained the properties of UWB channels. In the next section we explain our simulations with the UWB channels

A.1 Use of the RAKE receivers in UWB systems

The first RAKE reception analysis with the accepted IEEE 802.15 standard channel is made by Rajeswaran *et. al* in [25]. However there were also some papers with other channel models such as, [26]. In [25] and [27] no interference from other users or other systems is assumed. We will assume both realistic ISI and multiuser interference in our

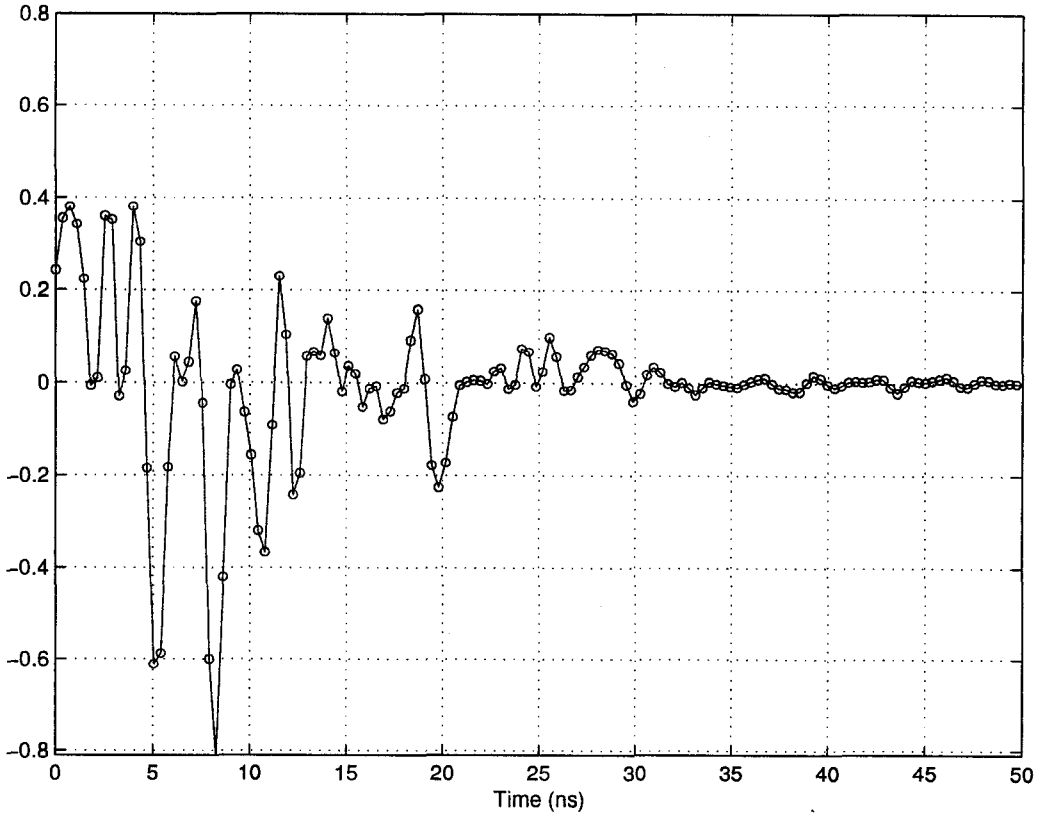

Figure A.3: A UWB channel realization of the **CM1** type convolved with square root raised cosine filter with roll off factor 0.5 (with the sampling instants).

simulations.

A.1.1 Simulations with G-RAKE Reception

In this section we present some of our simulation results done with a UWB system proposals, namely DS-UWB. The DS-UWB system is developed by OKI communications and Communications Research Lab of Japan and supported by Motorola. DS-UWB can be seen as an impulse radio since it uses direct sequence spreading of a binary phase shift keyed UWB pulses. Therefore one symbol is sent using a pulse (chip) sequence. To

support different data rates in the system, authors proposed variable sequence lengths and also different coding rates. The difference from an impulse radio is that DS-UWB divides the allocated spectrum into two bands, one band nominally occupying the spectrum from 3.1 to 4.85 GHz (the low band), and the second band occupying the spectrum from 6.2 to 9.7 GHz (the high band). The main advantages of DS-UWB is that it requires very simple transmitters since it sends baseband pulses. It is good for short ranging applications due to larger bandwidths of UWB pulses and the silicon chips of DS-UWB are ready for implementation. The main problems of DS-UWB are in the reception part. Due to multipath there is intersymbol interference, hence equalization is necessary. Also to collect energy from the channel RAKE reception is needed. A 16 finger RAKE is used in the proposal to show the system performance. We don't have the new version but in the early DS-UWB proposals two decision feedback equalizers (DFE) are mentioned. The first one has 5 symbol span and the second one has 10 symbol span. Both have 2 feed forward coefficients.

The equalization system is the classical one, where the outputs of the RAKE receiver are combined and then symbol by symbol equalization is done, as shown in Figure A.4 for a 3 finger system.

In the simulations, the channels between the transmitter and receiver are the standard channels of IEEE (having no phase information) for 4-10 meter distance and no line of sight case. Before presenting the results, let us list the properties of the simulations:

1. The channels for the interferer is generated randomly from the other standard UWB channels (NLOS 4-10 meter distance).

2. We initially assume that the power of the interferer is equal to half of the desired signal power.

3. BPSK modulation is used.

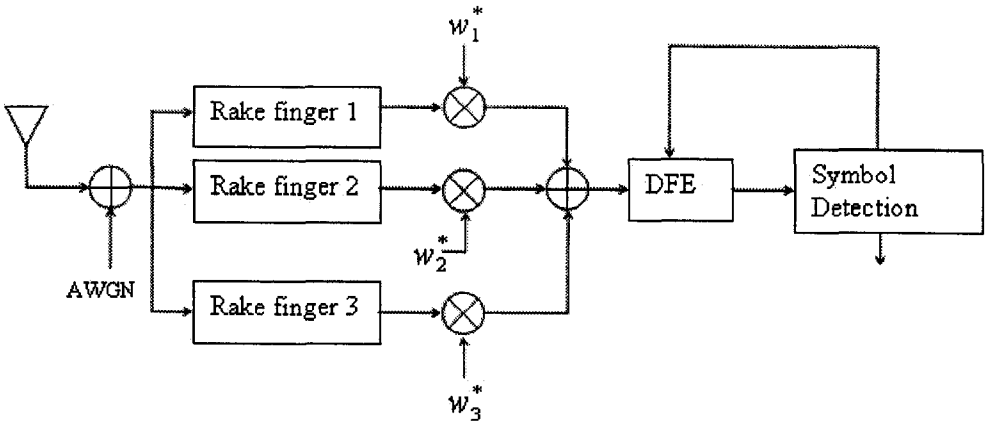

Figure A.4: Decision feedback equalization for UWB systems.

4. The chip sequences are chosen from the proposal of DS-UWB with chip duration of 0.36 ns.

5. The sequence length is 24 and every chip sequence has 2 zeros in it. Length 24 is still the longest chip sequence length of DS-UWB. The desired chip sequence is equal to [-1 1 -1 -1 1 -1 -1 1 -1 0 1 0 -1 -1 1 1 1 -1 1 1 1 -1 -1 -1].

6. Equalizer coefficients are calculated assuming perfect channel knowledge.

7. As in the case of the IEEE standard proposals [28], the average of the best 90 performances out of 100 channel realizations is shown.

The simulation results are depicted in Figure A.5. In this first simulation results, the number of fingers is equal to 5.

As seen in Figure A.5, G-RAKE outperforms RAKE by 3 dB at a bit error rate of 5×10^{-3} and have a lower error floor of 5×10^{-4}. Another simulation is done for 10 finger receivers. Figure A.6 shows the results. As expected, the performances of both the G-RAKE and RAKE improve with increasing number of fingers. Comparing Figure

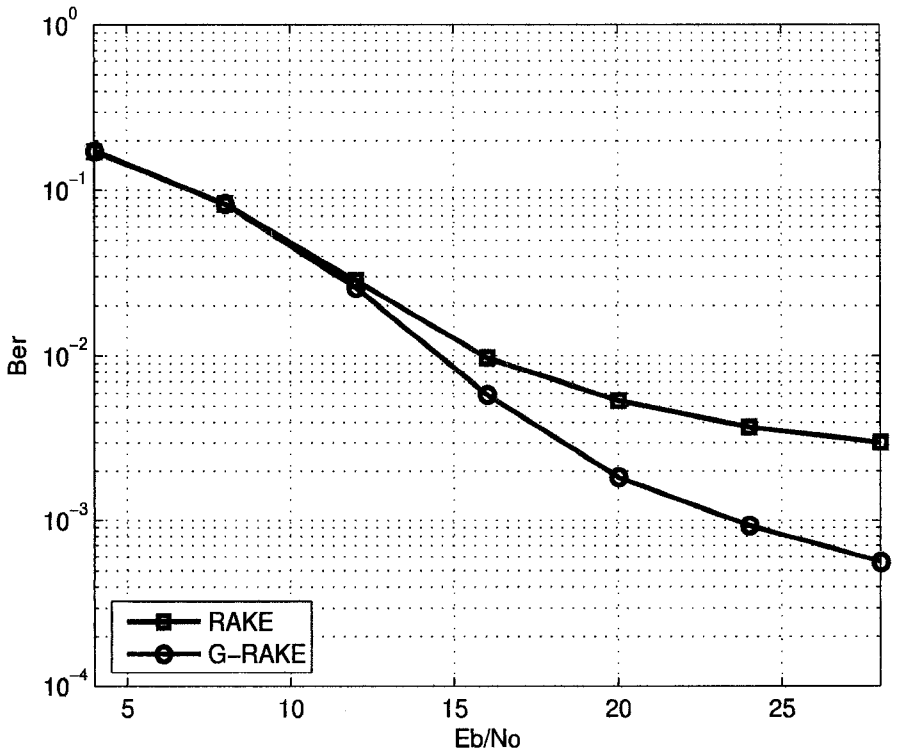

Figure A.5: Bit error rate curves of the 5 finger receivers, where interference power is half of the desired signal power.

A.5 and A.6 shows that the improvement is about 2 dB at a bit error rate of 5×10^{-3} for the G-RAKE receiver. The performance improvement of the RAKE receiver is higher then the G-RAKE, therefore the SNR gain of the G-RAKE decreases to 0.5 dB at a bit error rate of 5×10^{-3} compared to the RAKE receiver. Nevertheless, the G-RAKE has a lower error floor than the RAKE receiver.

In the final simulation results of the section, we increased the interference power to the level of the desired signal power. Figure A.7 shows the performance results. As expected, the performances of both receivers are degraded. In this case the bit error

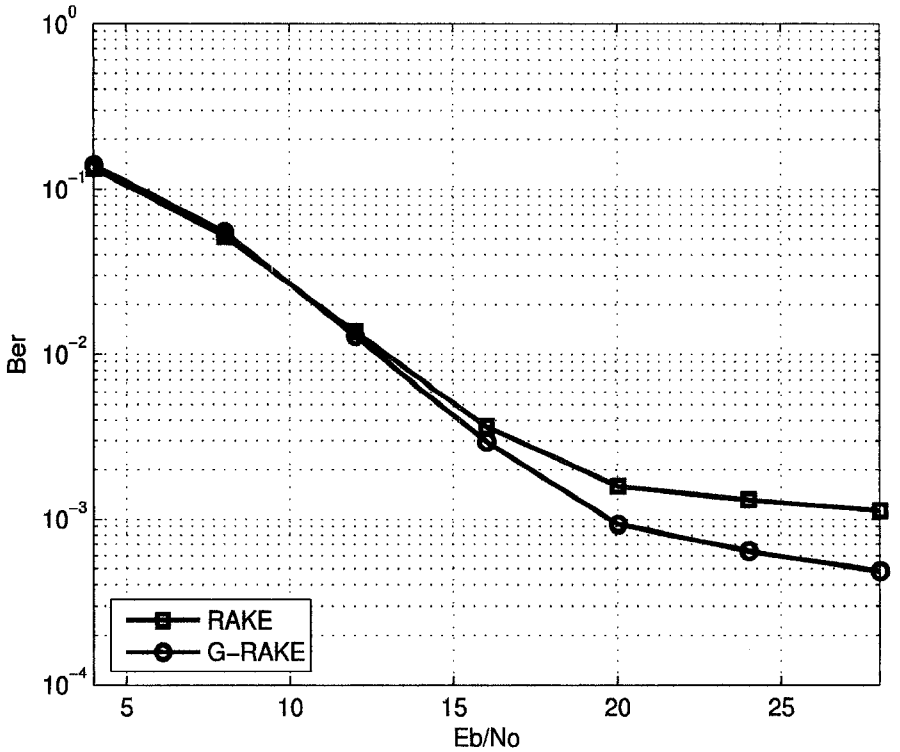

Figure A.6: Bit error rate curves of the 10 finger receivers, where interference power is half of the desired signal power.

rate of 5×10^{-3} is actually below the error floor of RAKE receiver and G-RAKE not only achieves that bit error rate at 23 dB SNR, its error floor is beyond 28 dB SNR.

A.2 Summary

We have shown that G-RAKE system can improve the DS-UWB system performance. We believe intensive research could reveal more advantages of G-RAKE reception in UWB systems.

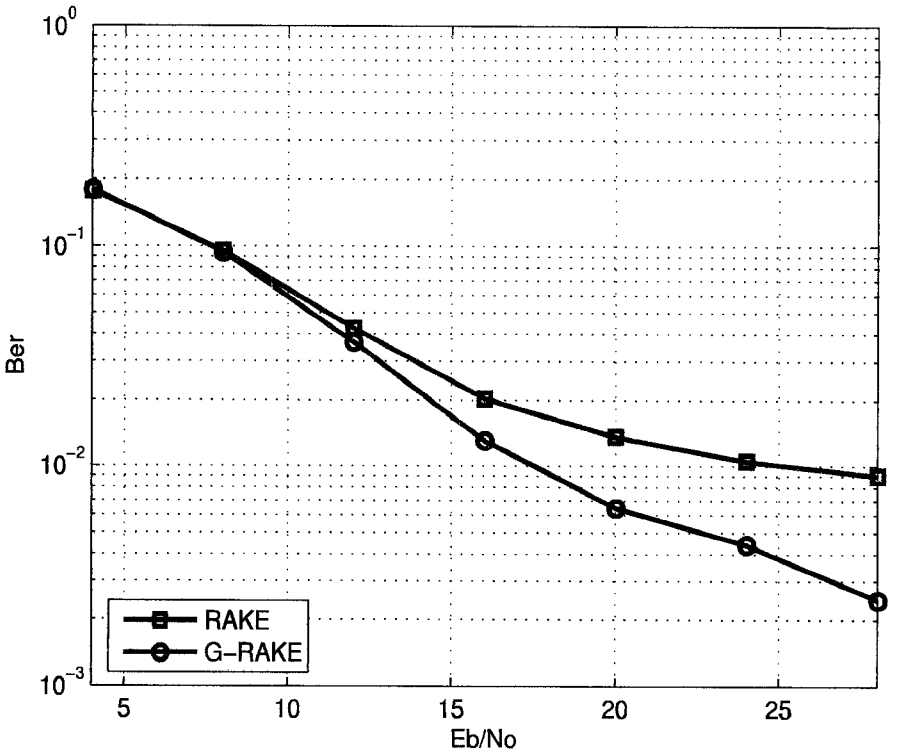

Figure A.7: Bit error rate curves of the 5 finger receivers, where interference power is equal to the desired signal power.

Appendix B

IEEE WPAN System Specifications and UWB Channel Model

The IEEE 802.15 High Rate Alternative PHY Task Group (TG3a) for Wireless Personal Area Networks (WPANs) was established to define a standard in ultra wideband spectrum. The specifications of IEEE are listed in the Table B.1.

Table B.1: IEEE Specifications for WPAN System.

Data rates	55 Mbps,110Mbps (10 meter),220 Mbps(4 meter) 480 Mbps(optional)
EIRP	FCC regulations
Power Consumption	100 mW (Cmos tech.)
Co-located piconets	4
PER (1024 byte packets)	$< 8\%$
Interference	Robust against IEEE 802.11,Bluetooth,etc
Cost	Similar to Bluetooth
Scalability	Compatibility with 802.15
Signal Acquisition	$<$ 20 microsecond Preamble
Location awareness	Location information to be propagated
Antenna practicality	Size and form consistent

The demands of IEEE perfectly fits the properties of UWB systems, low power, high

data rate, location awareness. Since UWB systems are very low power, interference may degrade the performance and IEEE demands that the standard should be robust to at least to other IEEE standards. Although IEEE Task group managed to decide on a Channel Model and reduce 23 standard proposal to 2 proposals, none of the last 2 proposals (Multiband OFDM and DS-UWB) could get enough vote to be selected. As January 2006 the task group is dissolved. Nevertheless first consumer products will be on the market in year 2006. Regarding the UWB channel, the following excerpt is from the final report of the channel committee [1] and explains the basics of the UWB channels of IEEE:

'Based on this clustering phenomenon observed in several channel measurements, we propose an UWB channel model derived from the Saleh Valenzuela model with a couple of slight modifications. We recommend using a lognormal distribution rather than a Rayleigh distribution for the multipath gain magnitude, since our observations show that the lognormal distribution seems to better fit the measurement data. In addition, independent fading is assumed for each cluster as well as each ray within the cluster. Therefore, the multipath model consists of the following, discrete time impulse response:

$$h_i(t) = X_i \sum_{l=0}^{L} \sum_{k=0}^{K} h_{k,l}^{i} \delta(t - T_l^i - \tau_{k,l}^i) \tag{B.1}$$

where $h_{k,l}^i$ are the multipath gain coefficients, T_l^i is the delay of the l^{th} cluster, $\tau_{k,l}^i$ is the delay of the k^{th} multipath component relative to the l^{th} cluster arrival time T_l^i,X_i represents the log-normal shadowing, and i refers to the i^{th} realization. Finally, the proposed model uses the following definitions:

T_l = the arrival time of the first path of the l^{th} cluster;

k, l = the delay of the k^{th} path within the l^{th}cluster relative to the first path arrival

time, T_l;

Λ= cluster arrival rate;

λ= ray arrival rate, i.e., the arrival rate of path within each cluster.

By definition, we have $\tau_{0,l} = 0$. The distribution of cluster arrival time and the ray arrival time are given by

$$p(T_l|T_{l-1}) = \Lambda \exp[-\Lambda(T_l - T_{l-1})] p(\tau_{k,l}|\tau_{(k-1),l}) = \lambda \exp[-\lambda(\tau_{k,l} - \tau_{(k-1),l})] \quad \text{(B.2)}$$

The channel coefficients are defined as follows:

$$h_{k,l} = p_{k,l}\xi_l\beta_{k,l}, 20\log_{10}(\xi_l\beta_{k,l}) \propto \text{Normal}(\mu_{k,l}, \sigma_1^2 + \sigma_2^2) \quad \text{(B.3)}$$

where $n_1 \propto$ Normal(0,σ_1^2) and $n_2 \propto$ Normal(0,σ_2^2) are independent and correspond to the fading on each cluster and ray, respectively,

$$E[|\xi_l\beta_{k,l}|^2] = \Omega_0 \exp(-T_l/\Gamma) \exp(-\tau_{k,l}/\gamma) \quad \text{(B.4)}$$

where T_l is the excess delay of bin l and Ω_0 is the mean energy of the first path of the first cluster, and $p_{k,l}$ is equiprobable +/-1 to account for signal inversion due to reflections. The $\mu_{k,l}$ is given by

$$\mu_{k,l} = \frac{10\ln(\Omega_0) - 10T_l/\Gamma - 10\tau_{k,l}/\gamma}{\ln(10)} - \frac{(\sigma_1^2 + \sigma_2^2)\ln(10)}{20} \quad \text{(B.5)}$$

In the above equations, ξ_l reflects the fading associated with the l^{th} cluster, and $\beta_{k,l}$ corresponds to the fading associated with the k^{th} ray of the l^{th} cluster. Note that, a complex tap model was not adopted here. The complex baseband model is a natural fit for narrow band systems to capture channel behavior independently of carrier frequency,

but this motivation breaks down for UWB systems where a real-valued simulation at RF may be more natural. Finally, since the log-normal shadowing of the total multipath energy is captured by the term, X_i , the total energy contained in the terms $h_{k,l}^i$ is normalized to unity for each realization. This shadowing term is characterized by the following:

$$20\log_{10}(X_i) \propto \text{Normal}(0, \sigma_x^2) \tag{B.6}$$

According to above equations 4 different channel types are generated. Before giving the characteristics of these channel let us define the important parameters of the simulation model one more time.

Λ= cluster arrival rate

λ= ray arrival rate, i.e., the arrival rate of path within each cluster

Γ= cluster decay factor

γ= ray decay factor

σ_1= standard deviation of cluster lognormal fading term (dB)

σ_2= standard deviation of ray lognormal fading term (dB)

σ_x= standard deviation of lognormal shadowing term for total multipath realization (dB)

These parameters are found by trying to match important characteristics of the channel. Table B.2 lists some initial model parameters for a couple of different channel characteristics that were found through measurement data. In the table **CM1** is based on LOS measurements (0-4m). **CM2** is based on NLOS measurements (0-4m). **CM3** is based on LOS measurements (4-10m). **CM4** is generated for a 25 ns rms delay spread to represent an extreme NLOS multipath channel.'

Table B.2: IEEE Multipath channel characteristics and corresponding model parameters [1].

Target Channel Characteristics	**CM 1**	**CM 2**	**CM 3**	**CM 4**
Mean excess delay (ns) (τ_m)	5.05	10.38	14.18	
RMS delay (ns) (τ_{rms})	5.28	8.03	14.28	25
Number of Paths within 10 dB of strongest path, NP(10dB)			35	
Number of Paths to capture %85 of signal energy, NP(85%)	24	36.1	61.54	
Model Parameters				
Λ(1/ns)	0.0233	0.4	0.0667	0.0667
λ(1/ns)	2.5	0.5	2.1	2.1
Γ	7.1	5.5	14.00	24.00
γ	4.3	6.7	7.9	12
σ_1(dB)	3.3941	3.3941	3.3941	3.3941
σ_2(dB)	3.3941	3.3941	3.3941	3.3941
σ_x(dB)	3	3	3	3
Model Characteristics				
Mean excess delay (ns) (τ_m)	4.9	9.4	13.8	26.8
RMS delay (ns) (τ_{rms})	5	8	14	26
NP(10dB)	13.3	18.2	25.3	41.4
NP (85%)	21.4	37.2	62.7	122.8
Channel energy mean (dB)	-0.5	0.1	0.2	0.1
Channel energy std (dB)	2.9	3.3	3.4	3.2

Bibliography

[1] L. Foerster *et al.*, "IEEE P802.15 Working Group for Wireless Personal Area Networks (WPANs) Channel Modeling Sub-committee Report Final," Tech. Rep., Dec. 2001.

[2] G. E. Bottomley, T. Ottosson, and Y. E.Wang, "A generalized RAKE receiver for interference suppression," *IEEE J. Select. Areas Commun.*, vol. 18, pp. 1536–1545, Aug. 2000.

[3] A. Viterbi, *CDMA: Principles of Spread Spectrum Communication.* Addison-Wesley, 1995.

[4] M. Siala, "Maximum *a posteriori* decorrelating discrete-time RAKE receiver," *Annals of Telecommunications*, vol. 59, no. 3-4, pp. 374–411, Apr./Mar. 2004.

[5] Q. Zhang, J. Huang, and Y. Xie, "High Resolution Delay Estimation," in *TENCON'93*, 1993, pp. 579–583.

[6] R. V. Nee, "The Multipath Estimation Delay Lock Loop," in *Int. Sym. on Spread Spectrum Tech. and App.*, Dec. 1992, pp. 39–42.

[7] H. Boujemaa, O. Fratu, M. Siala, and P. Loubaton, "On the performance of a discrete-time RAKE," in *The 11th IEEE Int. Sym. on Personal, Indoor and Mobile Radio Com.*, vol. 2, Sept. 2000, pp. 949–953.

[8] S. Grant, K. Molnar, and G. Bottomley, "Generalized RAKE receivers for MIMO systems," in *Proc. IEEE 54th Vehicular Technology Conference, VTC Fall 2003*, vol. 1, Oct. 2003, pp. 424–428.

[9] J. G. Proakis, *Digital Communications.* New York: McGraw-Hill, 2001.

[10] B. Boujemaa and M. Siala, "Recepteurs en rateau pour les systemes a etalement de spectre par sequences directes," *Annales des Telecommunications*, vol. 56, no. 5-6, pp. 113–139, Apr./Mar. 2001.

[11] J. Winter, "Optimum Combining for Indoor Radio Systems with Multiple Users," *IEEE Trans. Commun.*, vol. 35, pp. 1222–1230, Nov. 1987.

[12] T. S. Rappaport, *Wireless Communications: Principles and Practice.* Prentice-Hall, 2002.

[13] B. Champagne, "Adaptive eigendecomposition of data covariance matrices based on first-order perturbations," *Signal Processing, IEEE Transactions on [see also Acoustics, Speech, and Signal Processing, IEEE Transactions on]*, vol. 42, no. 10, pp. 2758–2770, 1994.

[14] ——, "SVD-updating via constrained perturbations with application to subspace tracking," in *Signals, Systems and Computers, 1996. 1996 Conference Record of the Thirtieth Asilomar Conference on*, 1996, pp. 1379–1385 vol.2.

[15] B. Champagne and Q.-G. Liu, "A new family of EVD tracking algorithms using Givens rotations," in *Acoustics, Speech, and Signal Processing, 1996. ICASSP-96. Conference Proceedings., 1996 IEEE International Conference on*, vol. 5, 1996, pp. 2539–2542 vol. 5.

[16] T. J. Willink, "An efficient SVD update algorithm and applications to MIMO communications," in *Eusipco 2005*, Sept. 2005.

[17] W. H. Press, *Numerical Recipes in C: The Art of Scientific Computing.* Cambridge Univ. Press, 1992.

[18] H. Holma and A. Toskala, *WCDMA for UMTS: Radio Access for Third Generation Mobile Communications.* Wiley, 2004.

[19] S. Foo *et al.*, "Spatio-temporal Investigation of UTRA-FDD channels," in *Third Int. Conf. on 3G Mobile Com. Tech.*, May 2002, pp. 175–179.

[20] "UMTS Physical Layer Simulator," Nov. 2005. [Online]. Available: http://www.umtsprobe.com/downlink_physical_channels.htm

[21] "First report and order, revision of part 15 of the commission's rules regarding the ultra-wide band communications," FCC, Washington,DC, ET Docket 98-153, 2002.

[22] L. A. Rusch, C. Prettie, D. Cheung, Q. Li, and M. Ho, "Characterization of UWB Propagation from 2 to 8 GHz in a Residential Environment," *IEEE J. Select. Areas Commun.*, submitted for publication.

[23] S. Ghassemzadeh, L. Greenstein, T. Sveinsson, and V. Tarokh, "A multipath intensity profile model for residential environments," in *Proc. Wireless Communications and Networking*, vol. 1, Mar. 2003, pp. 150–155.

[24] S. Ghassemzadeh, R. Jana, C. Rice, W. Turin, and V. Tarokh, "A statistical path loss model for in-home UWB channels," in *Proc. IEEE Ultra Wideband Systems and Technologies*, Mar. 2002, p. 5964.

[25] A. Rajeswaran, V. Somayazulu, and J. Foerster, "RAKE performance for a pulse based UWB system in a realistic UWB indoor channel," in *IEEE International Conference on Communications, ICC '03.*, vol. 4, 2003, pp. 2879–2883 vol.4.

[26] D. Cassioli, M. Win, F. Vatalaro, and A. Molisch, "Performance of low-complexity RAKE reception in a realistic UWB channel," in *IEEE International Conference on Communications ICC'02.*, vol. 2, 2002, pp. 763–767 vol.2.

[27] B. Mielczarek, M. Wessman, and A. Svensson, "Performance of coherent UWB Rake receivers with channel estimators," in *Vehicular Technology Conference, VTC 2003-Fall.*, vol. 3, 2003, pp. 1880–1884 Vol.3.

[28] R.Fischer *et al.*, "DS-UWB Proposal Update, IEEE 802.15-04/0140r2," Tech. Rep., 2004.

List of Publications from the Thesis

- T. Baykas, M. Siala, and A. Yongacoglu, "Generalized decorrelating discrete-time RAKE receiver," to appear in *IEEE Tran. on Wireless Communication*

- T. Baykas, M. Siala, and A. Yongacoglu, "Generalized decorrelating discrete-time RAKE receiver," in *Proc. IEEE 57th Vehicular Technology Conference, VTC Spring 2005,* May 2005.

- T. Baykas, M. Siala, and A. Yongacoglu, "MIMO decorrelating discrete-time RAKE receiver," in *Proc. IEEE 57th Vehicular Technology Conference, VTC Spring 2005,* May 2005.

- T. Baykas, M. Siala, and A. Yongacoglu, "MIMO generalized decorrelating discrete-time RAKE receiver," in *Proc. 13th European Signal Processing Conference, Eusipco 2005,* Sep 2005.

- T. Baykas, A. Yongacoglu, "Performance of Advanced Discrete-Time RAKE Receivers," in *IEEE SIU 2006 Proc. Sinyal Isleme Uygulamalari Kurultayi,*Apr 2006.